Copper nanowires as alternative flexible transparent electrodes for organic solar cells

by

Nicholas William Hoy

submitted in accordance with the requirements for
the degree of

MASTER OF SCIENCE

In the subject

Physics

At the

UNIVERSITY OF SOUTH AFRICA

Supervisor: Prof. P.S. Mbule

(13 January 2023)

DECLARATION

Name: Nicholas William Hoy

Student number: 59842997

Degree: MSc Physics

Copper nanowires as alternative flexible transparent electrodes for organic solar cells.

I declare that the above dissertation is my own work and that all the sources that I have used or quoted have been indicated and acknowledged by means of complete references.

I further declare that I submitted the dissertation to originality checking software and that it falls within the accepted requirements for originality.

I further declare that I have not previously submitted this work, or part of it, for examination at Unisa for another qualification or at any other higher education institution.

13/01/2023

Signature Date

The universe is knowable.

- Ken Liu

Good, better, best. Never let it rest. 'Til your good is better and your better is best.

- St. Jerome

Acknowledgements

Firstly, I would like to thank God who helped to give me the strength that I needed to get through this study and to bring me here.

I'd like to thank my family and friends who were there and were willing to listen to me ramble on about my project as I tried to solve an issue I had come across while also offering an outside perspective.

I'd like to thank my supervisor Prof. Pontsho Mbule for her incredible and amazing support throughout this entire process, who constantly helped to push me to do my best and guided me through this endeavour.

I would also like to thank the University of South Africa (UNISA) and Physics department for giving me the opportunity to use their research infrastructure and resources to conduct and complete my project, and also for financially supporting my project with a bursary.

I would like to thank Dr Guy Kabongo for his continuous assistance with X-ray diffraction (XRD) measurements and fruitful discussions about my project.

Lastly, I would like to thank the annual conference of the South African Institute of Physics (SAIP2022) for allowing me to present part of my work at the 2022 conference.

Abstract

Copper nanowires (CuNWs) were synthesized using hydrothermal method and deposited onto flexible polymer substrates to make films acting as electrodes for organic solar cells (OSCs). Substrates used were polycarbonate (PC), polyethylene naphthalate (PEN), polyethersulfone (PES), and polyethylene terephthalate (PET). Aluminium and gallium doped ZnO nanoflakes (AZO and GZO-NFs) were coated onto CuNWs to act as a protective layer against oxidation.

X-ray diffraction (XRD) confirmed formation of CuNWs, AZO and GZO-NFs. Scanning electron microscope (SEM) showed long and smooth CuNWs with average diameter of 112.82 ± 1.2 nm and length of over 50 μm. PET substrate showed ~88.64% light transmittance, while PC showed ~87.93%, PES (~85.78%) and PEN (~81.78%). Upon coating CuNWs, transmittance was slightly low indicating minimum influence on the electrodes' light transmission. From atomic force microscopy (AFM) results, CuNWs on PEN substrate showed lower roughness value of ~46.35 nm. Tensile strength results showed that PET substrate would be the optimal choice due to better flexibility and mechanical strength.

Keywords

Copper nanowires; hydrothermal; aluminium-doped zinc oxide; gallium-doped zinc oxide; nanoflakes; mechanical properties; flexibility; organic solar cells; electrode; polymer substrate;

List of Acronyms and symbols

AFM	Atomic Force Microscopy
AZO-NFs	Aluminium-doped zinc oxide nanoflakes
CuNPs	Copper nanoparticles
CuNWs	Copper nanowires
ETL	Electron transport layer
GZO-NFs	Gallium-doped zinc oxide nanoflakes
HTL	Hole transport layer
ITO	Indium tin oxide
ODA	Octadecylamine
OSCs	Organic Solar Cells
PC	Polycarbonate
PCE	Power conversion efficiency
PEN	Polyethylene naphthalate
PES	Polyethersulfone
PET	Polyethylene terephthalate
SEM	Scanning Electron Microscopy
r-GO	Reduced graphene oxide
rpm	Revolutions per minute
UV-VIS	Ultraviolet – visible Spectroscopy
XRD	X-ray diffraction
D	Crystallite size
λ	Wavelength
β	Full width at half maximum
θ	Angle of diffraction
α	Absorption coefficient
hv	Incident photon energy
E_g	Optical bandgap of the film
n	Transition mode
A	Absorbance of the film

t	Thickness of the film
σ	Stress
F	Force
A	Cross-sectional area of the sample
ε	Strain
ΔL	Elongation of the sample
L_i	Initial length of the sample

Table of Contents

List of figures

List of tables

Chapter 1. Introduction

1.1 Overview

The need for energy is a pressing matter in most parts of the world as previously used methods that relied on fossil fuels are being phased out and completely removed from the grid due to the impact they have on society and the environment. One of the alternative avenues that is currently being explored to resolve this is solar energy. In comparison to other renewable methods to obtain energy (hydro- and wind power), solar energy can be used in a range of situations and areas and is not reliant on a constant water source or strong wind source and thus can be comfortably used in both urban and rural areas. Over the years, various types of solar cells have been developed, such as; single-crystalline silicon solar cells (c-Si cells) [1], thin film silicon solar cells [2], dye-sensitized solar cells [3], quantum dot-sensitized solar cells [4], and perovskite solar cells (PSC) or organic solar cells (OSCs) [5] to list a few.

With advanced electronics being rapidly developed the demand for handheld and portable electronics has increased which in turn requires further study to improve and aid in the development. Transparent flexible solar cells have since received more attention and focus, as several properties of such devices are favorable, such as its flexibility, portability, light weight, durability, and the usage it finds with curved surfaces [6]. This is in comparison to the standard solar cells, 90% of which are crystalline silicon solar cells [7], which are rigid, thicker, and heavier which results in the storage and transportation of such devices being more costly than the flexible devices. These devices which are flexible and lightweight also allows them to be utilized in other diverse situations where the rigid ones are simply not compatible (i.e., on backpacks or for flight and space applications).

There are, however, draw backs to the transparent flexible solar cells. They do not yet have the same power conversion efficiency (PCE) as the rigid solar cells. Some flexible devices are costly to produce, have a short lifespan, and can be sensitive to the environmental impacts [8]. Not all of the various types of flexible solar cells share these drawbacks and it is thus important to decide which to focus on and then to attempt to improve them. Due to the abundance of the precursors required for OSCs and its relatively high PCE, OSCs are an ideal candidate to study and thus improve

flexible solar cells. There are five main aspects to OSCs that need to be examined and improved upon to better the device - the electron transport layer (ETL), the hole transport layer (HTL), the substrate used, the electrode, and the organic layer. Of these, the electrode and the substrate used have been lacking in further detailed research thus holding the devices back.

The choice of material for the substrate of the solar cell is very important as the substrate is the part of the device that determines the flexibility of the entire device. The substrate also has an impact on the mechanical and environmental stability usually dictating what temperatures the solar cell can withstand and how permeable it is to oxygen and water [9]. This is due to the fact that both oxygen and water often result in serious degradation of performance for the solar cell, thus the substrate should be a barrier that prevents the penetration of oxygen and water. Another important property that certain substrates have is that they are transparent which can then be used to develop transparent solar cells which require excellent optical properties to be efficient and able to transmit light in the visible-light spectrum. The substates will also be exposed to various chemicals (gasses and solvents) during the fabrication of the solar cells and thus needs to be stable to these various chemicals. Furthermore, during the synthesis process the various other layers of the solar cell potentially require high temperatures to complete, thus ideally the substrate needs to be able to withstand these temperatures or the synthesis methods for the other layers need to be carefully considered and chosen. For this reason, it is important to carefully choose a suitable substrate that meets the above criteria and select a method to produce the rest of the solar cell which will not damage or harm the chosen substrate.

For the bottom electrode the choice of material is again important, as it will impact the transparency and overall stability of the device. The conductivity (and sheet resistance) of the electrode also plays an important role for the device and impacts the figure of merit of the device. Currently one of the more widely used electrodes is indium tin oxide (ITO) due to their low resistance, high work function, and high transmittance [10]. However, ITOs have been found to be brittle and not ideal for flexible solar cells [11], unstable, and expensive to produce [12]. The electrode layer also has a further impact on the flexibility of the device. One of the more promising choices for the electrode is metal nanowires as they can be easily synthesized, have excellent flexibility, low sheet resistances, and high transparencies. A problem that metal-nanowires face is that they

are sensitive to oxygen and water, and certain synthesis processes can be quite expensive and thus needs to be reexamined and improved upon for future usage. Furthermore, the nanowires may not remain on the substrate after undergoing bending and/or stretching which degrades the performance of the solar cell. If metal nanowires are to be used, then a layer of protection needs to be placed over them that does not reduce the nanowires' positive properties while also keeping them in place and protecting them against possible oxidation.

1.2 Problem statement

There are several critical issues which are associated with the chemical, thermal and mechanical stability of ITO. The rarity of indium and its high prices are additional factors that makes ITO undesirable in transparent flexible electrode applications. Again, ITO materials are brittle resulting in devices containing ITO to be unusable in situations where stretching, twisting, folding, or bending are required. Thus, there has been effort devoted to developing alternatives to ITO such as, metal films, Al-doped ZnO and conducting polymers. For the usage of transparent flexible electrodes in solar cells, it is important that both the substrate and the electrode layer are transparent, flexible, and can withstand certain amounts of stresses that might be applied to it in its everyday use on a device. As the substrate and bottom electrode material are on top of each other in solar cells and impact each other, studying both simultaneously will have more meaningful and impactful results in the long term. Thus, both will be examined in order to produce a transparent flexible perovskite based solar cell. Additionally, a protective layer for the nanowire layer as the electrode, is necessary and will need to have the same criteria as the substrate and nanowire films.

1.3 Aim of the study

To successfully prepare long and smooth CuNWs with no impurities as well as AZO and GZO-NFs onto polymer substrates and subsequently; (i) evaluate the structure, morphology, optical, surface and mechanical (tensile strength) properties for possible application in organic solar cells; (ii) compare the protective capabilities of the NF layer and (iii) analyse the effects of the various layers and their potential impact on future device performance.

1.4 Objectives of the study

- Synthesis of thin, long, and smooth CuNWs via a hydrothermal route and successfully separate the CuNWs from any copper nanoparticles using a water-hydrophobic system.
- Synthesis of AZO and GZO-NFs via a wet-chemical route for the protection of the CuNWs
- Deposition of the CuNWs and AZO/GZO-NFs layers onto different polymer substrates via drop-casting and spin-coating methods
- Characterise the prepared thin films/electrodes to evaluate:
    - Crystallite size, morphology, surface roughness, transmittance and, bandgap energy
    - Yield strength, ultimate strength, strain hardening exponent, Young's modulus and resilience

1.5 Dissertation layout

- **Chapter 1:** This chapter covered the introduction for the dissertation.
- **Chapter 2:** This chapter covers the literature review of transparent flexible electrodes. It also covers the information regarding the types of substrates that have been used, the types of metal nanowires used and, the protective layer materials used over the metal nanowires layer.
- **Chapter 3:** This chapter provides the theory behind the characterization and synthesis techniques used in this study.
- **Chapter 4:** This chapter covers the hydrothermal synthesis of the CuNWs as well as various characterisation techniques used to analyse the prepared samples.
- **Chapter 5:** This chapter covers the detailed mechanical properties of the prepared electrodes

Chapter 6: This chapter covers the summary and conclusion of the study.

References

1. Liu X, Jia L, Fan G, Gou J, Liu SF, Yan B (2016) Au nanoparticle enhanced thin-film silicon solar cells. Solar Energy Materials and Solar Cells 147:225–234
2. Banerjee A, Su T, Beglau D, Pietka G, Liu FS, Almutawalli S, Yang J, Guha S (2012) High-Efficiency, Multijunction nc-Si:H-Based Solar Cells at High Deposition Rate. IEEE J Photovolt 2:99–103
3. Sharma K, Sharma V, Sharma SS (2018) Dye-Sensitized Solar Cells: Fundamentals and Current Status. Nanoscale Res Lett 13:1–46
4. Sahu A, Garg A, Dixit A (2020) A review on quantum dot sensitized solar cells: Past, present and future towards carrier multiplication with a possibility for higher efficiency. Solar Energy 203:210–239
5. Green MA, Ho-Baillie A, Snaith HJ (2014) The emergence of perovskite solar cells. Nat Photonics 8:506–514
6. Yang D, Yang R, Priya S, Liu S (Frank) (2019) Recent Advances in Flexible Perovskite Solar Cells: Fabrication and Applications. Angewandte Chemie International Edition 58:4466–4483
7. Battaglia C, Cuevas A, de Wolf S (2016) High-efficiency crystalline silicon solar cells: status and perspectives. Energy Environ Sci 9:1552–1576
8. Zhang J, Zhang W, Cheng H-M, Silva SRP (2020) Critical review of recent progress of flexible perovskite solar cells. Materials Today 39:66–88
9. Uddin A, Upama M, Yi H, Duan L (2019) Encapsulation of Organic and Perovskite Solar Cells: A Review. Coatings 9:1–17
10. Wang Y, Liu P, Wang H, Zeng B, Wang J, Chi F (2019) Flexible organic light-emitting devices with copper nanowire composite transparent conductive electrode. J Mater Sci 54:2343–2350
11. Ye S, Rathmell AR, Chen Z, Stewart IE, Wiley BJ (2014) Metal Nanowire Networks: The Next Generation of Transparent Conductors. Advanced Materials 26:6670–6687
12. Li X, Wang Y, Yin C, Yin Z (2020) Copper nanowires in recent electronic applications: progress and perspectives. J Mater Chem C Mater 8:849–872

Chapter 2. Literature Review

2.1 Transparent flexible electrodes

Transparent flexible electrodes offer a unique and promising avenue for research owing to the large number of applications in devices such as solar cells [1, 2], touch screens [3], infrared detectors [4], and organic light emitting diodes [5]. Additionally, the flexibility of the electrode will allow it to be moulded and shaped into whatever shape or size its specific application will require; allowing for more widespread usage of such a device in different fields and applications. In the application of solar cells, the requirement of the electrode being transparent requires the trade-off and the usage of a wide bandgap. While a wide bandgap material cannot absorb energy using lower-energy photons, a smaller bandgap can. However, energy absorbed from high-energy photons from the smaller bandgaps results in these photogenerated charges to lose most of the energy which is caused by the thermalization that takes place for the electrons to travel out of a material. Regardless of which bandgap is used a large portion of any potential solar energy is lost [6]. Additionally, energy loss as a result of series resistance can be reduced due to the higher voltage that can be reached with wide bandgap materials [7]. The usage of wide bandgaps also encourages the use and study of multijunction cells have the potential to be far more efficient than other commercially used solar cells.

2.2 Substrates

When considering an electrode, the substrate is an important aspect to think about as it is one of the fundamental building blocks of the device. It is, therefore important to select a suitable substrate that will have minimal negative impacts while offering suitable protection. For that purpose, some of the more widely used materials will be briefly looked at and examined in this section. These are metal, ceramic, and polymer substrates.

2.2.1 Metal substrates

Thin metal foils have been found to be flexible due to the high ductility of metals allowing for the usage of these foils in flexible electrodes [8]. Of these, stainless-steel

foil is the most commonly used metal substrate due to its excellent thermal and chemical stability as well as its low cost. It has been used in flexible solar cells since the 1980's [9]. Metal foils initially seem to be a promising candidate also due to their good electrical conductivity which results in a lower resistance as well as fast ion and electron transmission [10]. Due to the excellent thermal stability of the metal substrates, it allows them to be able to undergo higher processing temperatures allowing for various different deposition methods for later stages of the electrode synthesis process.

The metal foils do however, present several drawbacks such as the reduced capability of the portability of any device that uses it. This is due to the higher density that metals possess resulting in an increase in weight for any device that utilizes one. Furthermore, while there has been progress made with optimising the transparency of metal foil substrates by reducing their thickness, which results in an increase of the resistivity of the film, any potential gain that had been made with using such a substrate is negated [11]. Stainless-steel, one of the more widely used metals in industries, has a reflectance in the range of 60-70% across the visible spectrum range and is thus not optically transparent which further supports the previous statement [12].

2.2.2 Ceramic substrates

Glass is the most commonly used material for ceramic substrates. Glass substrates possess excellent thermal stability and resistance to chemical and environmental stability; preventing moisture from passing through it. With thinner films of glass the thermal stability decreases [13]. The transmittance of the glass is also excellent allowing visible light through and absorbing minimal wavelengths. Furthermore, the poor ductility of the glass results in a lowered flexibility which in turn results in a much smaller bending radius and reduced stretching capabilities [8]. However, using thin glass substrates (below 100 µm) the substrate can become flexible and has previously been used already in the fabrication of solar cells [14]. Though as previously stated, the reduction in thickness of the film reduces the working temperature which reduces any potential gain it would have made.

2.2.3 Polymer substrates

Polymer substrates come with various qualities and characteristics that all depend on the type of polymer used. Generally, polymers possess excellent optical transmittance as well as flexibility which makes them attractive for transparent flexible electrodes. This superior flexibility comes from the Young's modulus parameter of the material which describes material's resistance to elastic deformation. Both ceramics and metals have a much higher Young's modulus than polymers which allows polymers to be more easily stretched and bent [15]. When comparing the yield strength of materials, which is the stress at which permanent deformation occurs, stainless steel has a yield strength of 200 MPa [16] and PET polymer only a yield strength of 40 MPa [17], the PET has an elongation of 70% [18] while stainless steel has one of 33% [19] thus indicating that the polymer has better formability than the steel.

These mechanical properties of the films can be studied by using a stress-strain curve (Figure 2.1) where various important properties of films and other materials can be tested. These properties include the Young's Modulus, yield strength, strain hardening exponent, and the modulus of resilience. Knowing these key properties would allow for the interpretation of the strength a film would possess, the elasticity of the film, and how much of a load the film can withstand before becoming damaged. It is thus important to study these properties for any potential substrate as it dictates what the completed films can be used for.

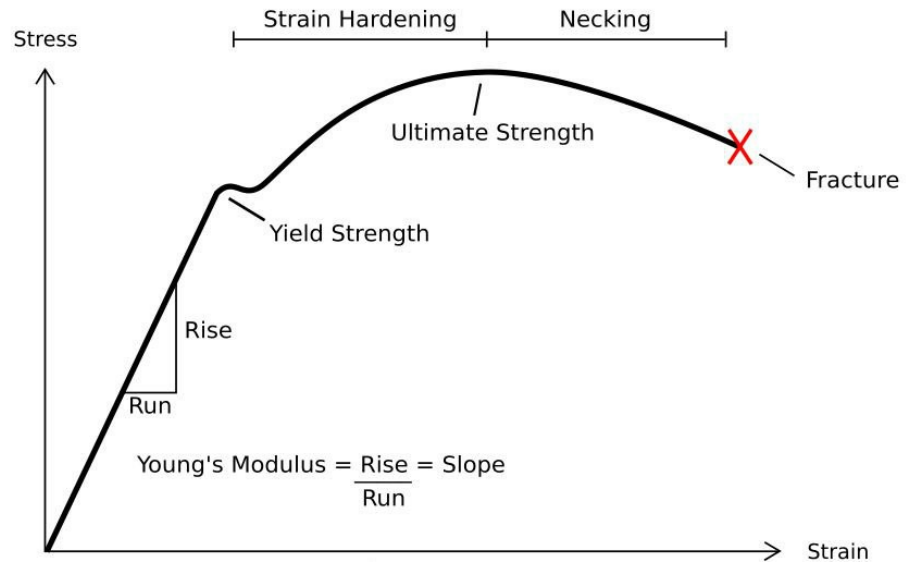

Figure 2. 1: Example illustration of a stress-strain graph [20]

Polymer substrates are also found to be more portable, having a smaller density resulting in them being light-weight as well as being low cost; allowing for relatively easy implementation in various applications [21]. The wide range of polymers also offers the potential for varied possible applications for the different types of polymer substrates.

Despite the polymers excellent robustness, many have a low glass transition temperature resulting in them being unable to withstand high-temperature annealing processes that are usually required with metal oxide layers that are used in solar cells [22]. However, this can be worked around by only using these polymer substrates in devices that use low process temperatures such as organic solar cells which will allow the polymers and other substrates to be better utilised. The permeability of polymer substrates is also an issue as both oxygen and water could potentially be detrimental to the rest of the electrode and fabricated device [23]. This can be overcome however, by using a barrier layer on either side of the polymer substrate which would allow it to maintain its flexibility while now having better permeability.

Due to their potential use, polymer substrates will be further examined in this study by comparing four different types of substrates and observing their properties.

2.3 The electrode material

The electrode is another aspect that needs to be carefully considered as it must not reduce the transmittance of the device too much but must also have excellent conductivity to allow it to operate more efficiently. Indium tin oxide (ITO) is one of the more commercially used transparent conducting electrodes due to its low sheet resistance and high transmittance [24]. However, ITO has certain properties that are less than desirable; such as its high toxicity [25], intrinsic brittleness [26], and its high cost due to minimal availability [27]. It is due to these reasons that alternative transparent conductors must be sought and developed to further improve and advance the field.

Various alternatives have been studied thus far including carbon nanotubes [28–31], graphene [32–35], metal nanogrids [36–38], and conductive polymers such as PEDOT:PSS [39, 40]. While carbon-based transparent conducting electrodes (TCEs) have been investigated thanks to their durability, production at low cost, and solution

processability, there are drawbacks to their use due to their high sheet resistance at high transmittance which would be required in the use of flexible transparent solar cells [31, 41]. While PEDOT:PSS has been used as the hole transporting layer (HTL), it also has very poor sheet resistance as well as poor optical transmittance properties [40]. For metal meshes a specific structure design is needed which leads to a tedious manufacturing process which increases the production cost and development time [42]. The properties of most of these alternatives are shown in Figure 2.2. One of the more promising alternatives is metal nanowires due to their high conductivity and excellent optical transmittance. Metal nanowires have already been proven to be suitable and efficient materials to produce transparent flexible electrodes which are equivalent to ITO produced electrodes [43]. There are three metals which are potential candidates for this particular method namely: gold, silver, and copper, due to their high conductivity and low sheet resistance. However, due to gold's exceptionally high market price compared to silver and copper, it is unsuitable for such uses as it would significantly increase the production cost of the solar cell. For that reason, only silver and copper have been considered and will be briefly examined here.

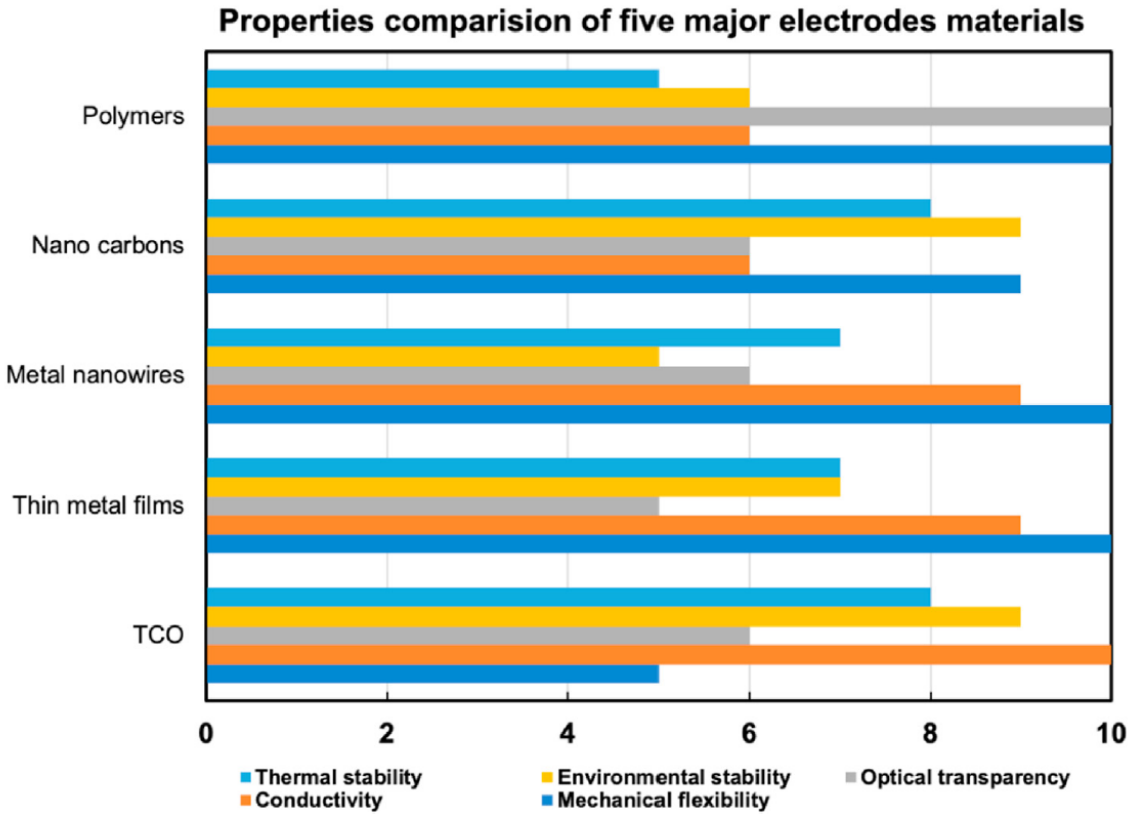

Figure 2. 2: Comparison of various electrodes physical properties [15]

2.3.1 Silver nanowires

Silver nanowires (AgNWs) have been extensively examined over the years as the bottom electrode for solar cells due to the excellent properties they possess such as its high electrical ($6.3 \times 10^7\ Sm^{-1}$), thermal ($429\ W\ m^{-1}K^{-1}$) [44] conductivities, and low electric resistivity (1.59×10^{-8} Ωm) [45]. Recent developments with silver nanowires will be briefly looked at in this section.

While the electrical resistance of silver is favourable, in order to make its implementation into solar cells as an electrode, the sheet resistance of the AgNWs layer needs to be as low as possible. Various post deposition methods have been examined in an attempt to improve this. Of the different methods used, thermal annealing is a relatively straightforward method to decrease the sheet resistance but has been reported to result in deformities at high temperatures which results in an increase of the sheet resistance [46]. To solve this problem, along with their poor adhesion to substrates that AgNWs tend to have, Yu *et al.* [47] used a hot lamination method in order to negate these drawbacks. This method is scalable, simple, and cost-effective for large-scale production and has seen some success with the transfer of graphene [48, 49]. This method was also able to use a polycarbonate substrate despite the high temperature required for the hot lamination due to the process only taking 2 minutes at 2×10^5 Pa. This heated lamination process also improved the adhesion of the nanowires to the film as a consequence of the nanowires being partially embedded in the film. [50] . The final substrate also had a sheet resistance of 12.5 Ω/sq which is even more superior to ITO.

However, a major drawback to utilizing AgNWs is both the scarcity of the metal [51] and the high cost of silver, which is currently at R11 095.82/kg as of writing this dissertation (16 November 2022), and due to the amount of silver that would be required for any form of mass production of solar panels the cost of the entire process is thus also increased. This makes the usage of such methods of harvesting energy unfeasible for most countries and places in the world that would most benefit from such forms of energy.

2.3.2 Copper nanowires

Another alternative to silver nanowires is copper nanowires (CuNWs), although they have lower electrical (59.6×10^6 Sm^{-1}) [52] and thermal conductivity (386 $Wm^{-1}K^{-1}$) [53] and also higher resistivity (1.67×10^{-8} Ωm) [54] the price of copper (at the time of writing this dissertation) is R144.14/kg (16 November 2022) which is almost 80 times less than the price of silver, making it much more feasible for implementation for energy harvesting.

Various studies have synthesized CuNWs using different techniques with varying ratios of capping agents, copper salts, and temperatures which in turn have lead to different diameters for the CuNWs. This is important to control and maintain as not all diameters are ideal for the usage in flexible transparent conductors in solar cells. For this reason, it is important to study and to understand these factors which will in turn help to produce the ideal CuNWs. A study done by Huang *et al.* [55] looked into this to better find a way of successfully synthesizing high-quality CuNWs and to examine these factors. It was found that two different copper salts, $CuCl_2$ and $CuCl_2{\cdot}H_2O$, impacted the diameter of the CuNWs which doubled while using $CuCl_2{\cdot}H_2O$ while also remaining pure, indicating that high quality CuNWs with varying diameters can be made by altering the type of copper salt. These excess chemicals and Cl^- are removed by washing with deionized water and ethanol. Furthermore, a study by Wang *et al* [56] found that the amount of time the hydrothermal process took impacted the final length of the CuNWs with longer CuNWs being observed with a longer hydrothermal process. These are both important to control throughout the synthesis process as the aspect ratio of the nanowires has been found to impact the electrical conductivity and transmittance. The nanowire films with higher aspect ratios achieve higher electrical conductivity and better transmittance [57]. However, nanowires that are too long are also undesirable as they have been observed to bundle together and not very well dispersed as films[58].

There are various methods that have been used in the past to synthesize high quality CuNWs in order to better utilize them in electrodes. The first method that will briefly be examined in this section is the normal aqueous phase reduction which was first demonstrated in 2005 by Zeng *et al.* [59] when synthesizing CuNWs with hydrazine and ethylenediamine as the two key components. In this particular reaction sodium hydroxide prevents Cu^{2+} from forming $Cu(OH)_2$ while the hydrazine reduces the Cu^{2+}

to Cu^0 and produces CuNWs with the ethylenediamine ensuring the proper morphology is formed. This was done in under an hour and with a low temperature of under 50 ^oC. However, hydrazine is not ideal to be used due to its high toxicity it presents environmental and biological risks [60]. Furthermore, chronic toxicity and carcinogenicity has been observed in mice and rats exposed to the chemical [61].

Another method is the hydrothermal method which involves chemical reactions taking place in a sealed and heated environment, usually a stainless-steel autoclave sealed in an oven. During this process the temperature of the system is controlled in order to encourage the particle growth of the solution. The capping agent used in hydrothermal method dictates the size and shape of the formed nanoparticles with ODA being commonly used to ensure the formation of CuNWs. In a reaction that has $CuCl_2{\cdot}H_2O$, ascorbic acid and, ODA, when the temperature of the reaction solution reaches 80 ^oC, the ODA reacts with hydrogen and releases ammonia. The $CuCl_2{\cdot}H_2O$ is then dissolved within the ammonia water and the products from this react with the ascorbic acid to form the copper atoms which in turn form the CuNWs [62]. This method is reliable and repeatable which is important for further developments within the field.

An issue that all CuNWs synthesis methods have, is that unwanted nanoparticles are also formed in these methods as well as other by-products with the remaining reactants. These are usually produced due to the non-instantaneous nucleation which results in the growth of particles along multiple pathways which results in a decrease to the film transparency thanks to their strong light scattering properties [63]. While there have been several separation techniques reported to obtain pure nanowires, these reports mostly focus on AgNWs and AuNWs [64–67] and rarely on CuNWs which is the focus of this study. One of the more common methods is to centrifuge the CuNWs solution although this does not achieve a high purity of CuNWs [59]. Another suggested method, which has been previously used in protein separation, is cross-flow separation by a hollow fiber membrane which separates the CuNWs and copper nanoparticles (CuNPs) [63]. As the membrane can only be reused a few times the high cost that is required in this process has prevented it from being more widely used.

In a study done by Kang *et al.* [68] an efficient and minimal-toxicity separation method to obtain pure CuNWs synthesized in a hydrothermal method using ODA as a capping agent was developed. After the synthesis of the CuNWs (with some CuNPs

inadvertently produced as well) they were added to deionized water with excess ODA and then to a nonpolar organic solvent of n-hexane which was then vortexed for 10 seconds. This solution was allowed to settle for 30 minutes and was observed that the water and n-hexane separated with the CuNW settling at the bottom of n-hexane and CuNPs settling at the bottom of the water (Figure 2.3 (a-b)). This was repeated for three cycles to completely purify the CuNWs. Testing with an XRD technique afterwards found that the process had indeed purified the CuNWs, furthermore, it was found that the CuNWs were still coated in an organic layer (the ODA) while the CuNPs had a minimal amount of the organic layer on the surface. The latter of these findings resulted in the proposal of a possible mechanism to explain these findings. Previous studies have found that the ODA molecule is amphiphilic which is a result of it having a long hydrophobic tail and a hydrophilic amino head [69, 70].

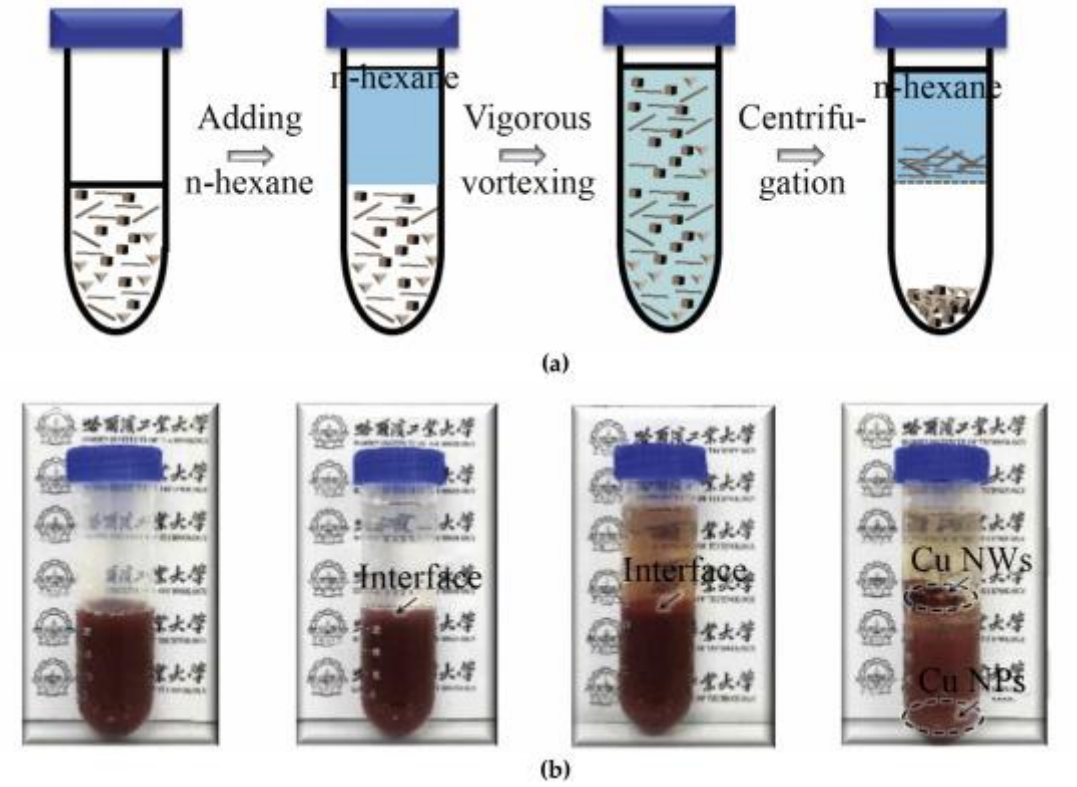

Figure 2. 3: (a) Illustration and (b) photographs of the CuNWs separation process [71]

During the synthesis process [68] the amino heads are absorbed into the surface of the copper nanostructures with the tails being exposed to the solution [72]. The copper nanostructures covered by the ODA are then inclined to stay in the n-hexane during the separation process due to the strong attraction between the hydrophobic tails and n-hexane molecules. Due to the weak absorption of the CuNPs to the organic materials, during the vortex stage the organic materials are removed from the CuNPs. When the n-hexane and water separate once more it is the force between the n-hexane and the organic materials on the CuNWs that pull them into the n-hexane which is consistent with previous reports on similar separation processes [73]. The CuNPs, now lacking the organic materials, then settle at the bottom of the water and are not attracted to the n-hexane layer. To verify this, other hydrophobic organic solvents were used (toluene and dichloromethane) with both yielding similar results of separating the CuNWs and CuNPs. This demonstrates that it is not the difference of density of these nanostructures, but the molecule polarity of organics that results in the separation and purification of CuNWs. The transparency of the purified CuNWs was improved by around 3% while under the same resistance. Better understanding of the reasons behind the separation, opens future endeavors to purify CuNWs and make the process even more efficient.

2.4 Copper nanowires protective layer

A negative aspect that has held back the wider usage of CuNWs is how easily they oxidize when they come into contact with oxygen and water. Despite this, coating the CuNWs could potentially prevent this from happening while also improving the attributes of the film (transmittance, flexibility, conductivity etc.). In this section, different protective methods will be briefly discussed.

2.4.1 Metal coatings

One method to prevent oxidation and provide the CuNWs with stability, is to coat them with another metal, creating a core-shell structure with the CuNWs being the core of the structure. Nickel (Ni) is one such metal that has been previously reported for this method. Rathmell *et al.* [74] completed a study using Ni as a protective shell for the CuNWs with the added Ni only resulting in a slight decrease in the films transmittance.

Films with a transmittance of 85-87% were treated in an oven at 85 °C and their sheet resistance was measured at regular intervals to observe the effects of oxidation. It took only 1 day for the bare CuNWs to increase and 5 to increase by an order of magnitude. For the Cu@Ni NWs, with only 10% nickel relative to the copper, was found to remain stable for 30 days only increasing by 10 Ω/sq and anything over 34% nickel had almost no change in the same period. However, this method required the use of hydrazine, which as stated before is an extremely toxic chemical. Similar methods have also been studied however, they also required the use of toxic chemicals making the reaction unsuitable [75, 76].

Other metals that have been used in the past to coat CuNWs have been silver and gold. Silver has shown promise with its lower electrical resistivity than that of copper [77] and have been found to create NWs with rough surfaces [78, 79] which could increase the light trapping capabilities if the electrode is used in a solar cell device [80]. Zhang *et al.* [81] examined utilizing silver as a protective shell for CuNWs via a facile adsorption and decomposition method while avoid galvanic replacement reactions. This shell managed to protect the CuNW from oxidation in system with a relative humidity of 85% as well as at high temperatures of up to 140 ^{o}C demonstrating its excellent stability. A schematic of this Cu@AgNW shell is given in Figure 2.4.

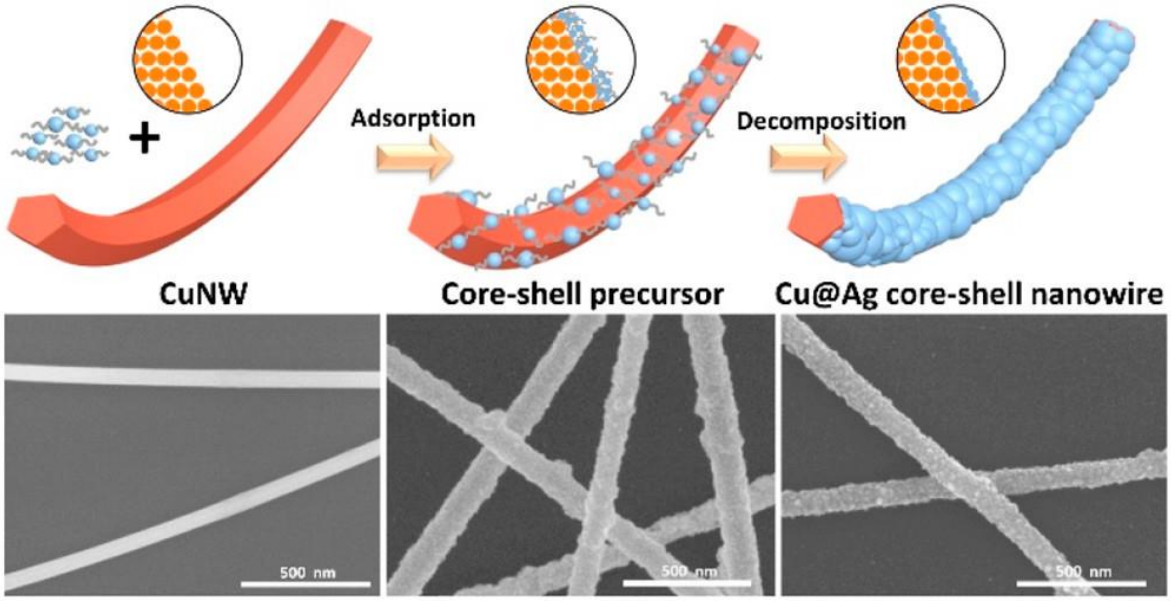

Figure 2. 4: Schematic diagram of the formation of Cu@Ag core–shell nanowires. [81]

Niu *et al.* [82] investigated using gold despite its higher cost when compared to silver. It was observed that CuNWs needed to be coated in thick shells of metals in order to completely protect them from humid conditions which in turn deteriorates the optical performance of the device. It was suggested by Niu *et al.* that the imperfect coverage of the shells could play a critical role in this regard and that the issue could be addressed by using the epitaxial growth of an evenly produced shell of metal with only a few atomic layers on the CuNWs. This was done using the gold to produce a thin gold shell around the CuNWs that managed to protect the CuNWs as well as outperform the similarly coated CuNWs with silver. While offering new techniques, these methods are still unsuitable for any large-scale production due to the high cost of the metal coatings used.

2.4.2 Metal oxide coatings

Another type of protection that has been used to stabilize and improve CuNWs is the usage of metal oxides coating the nanowires or creating a shell around them. The first method that will be examined is titanium dioxide (TiO_2) which is used in dye-sensitized solar cells and has been found to have excellent physicochemical properties as well as low toxicity and cost [83]. Several studies have been done in the past that managed to successfully coat the CuNWs with TiO_2 [84–86] using different techniques, however all of the processes required annealing at high temperatures (<400^{o}C) which is not ideal in the usage of flexible plastic substrates, for solar devices, which don't have a high temperature threshold, and the fact that annealing at such high temperatures are not suitable for large-scale fabrication of flexible electrodes.

Another type of oxide that has been studied and used to protect CuNWs from oxidation is zinc oxide (ZnO). With zinc being one of the more commonly used and found metals makes it ideal in the usage of a protective layer. A study done by Chen *et al.* [87] looked at using ZnO to protect from oxidation without degrading the performance of the films. This was done via electroplating the zinc onto the surface of the CuNWs and then oxidizing the metal coating to create a transparent ZnO shell. This ZnO shell was found to protect the CuNW in the short-term, but long-term tests yielded poor results with the resistivity of the film eventually reaching unsuitable levels. This could be potentially linked to the zinc vacancy defect sites that are formed with wet-chemically

prepared ZnO solutions which have also reportedly reduced the power conversion efficiency (PCE) of the films [88]. These vacancy sites can be filled with metal cation dopants, with aluminum ions being more widely used as they have smaller radii than Zn^{2+} ions [89].

Aluminium-doped zinc oxide (AZO) has since been examined and has been found to offer protection to the CuNWs from oxidation. A study by Won *et al*. [90] developed a method to synthesize an AZO/CuNW/AZO film without annealing as it decomposes the organic residues which results in them forming into the metallic copper phase which is not ideal for flexible substrates. The films that were then fabricated had sheet resistances that remained nearly unchanged while stored for 5 months at room temperature. Also, while stored in an environment at 80 ℃ the sheet resistance only doubled (while still being usable) after 166 hours of storage while a bare CuNW became unusable after 8 hours in the same conditions. The flexibility of the device was also tested and the sheet resistance was found to be nearly constant after 1280 bending cycles which is attributed to the CuNWs being embedded between the AZO films keeping the structure secure. Not only does the AZO layer then protect the CuNWs from oxidation, but it also drastically improves the adhesion to the film which is an issue with nanowire films. Similar studies with AZO as a protective layer yielded similar results with an improved protection for the CuNW against oxidation while also improving the adhesion to the film [91, 92].

With AZO, the bandgaps of the AZO layers can also be adjusted by varying the composition of Zn/Al. By doing this and layering the different AZO layers on top of one another it is possible to improve the electron extraction of the material by creating a favorable band alignment between the electron transport layer (ETL) and the electrode [93].

2.4.3 Graphene Material

Another method of coating and protecting CuNWs is by using graphene in various forms. Graphene is an atomically thin layer of carbon atoms (sp^2-bonded) which are arranged in a lattice structure with honeycomb shapes, which have various unique properties such as mechanical flexibility, high electrical conductivity, chemical stability, and excellent optical transparency, which are ideal properties for optoelectronic

applications [32, 35, 94]. It is for these reasons that graphene has been used in thin transparent conductive electrodes.

By depositing reduced graphene oxide (r-GO) films onto the CuNW film via dry transfer method [95], hybrid films are produced where the resistance is improved from bare CuNWs and r-GO film due to the nanowires connecting the r-GO platelets together while the r-GO platelets also help to fill in any gaps between the unconnected CuNWs as well improving the conductivity of the film. A drawback to this procedure was that the hybrid films were produced in a complicated way with multiple steps which is unideal for future scalable production which is the case with many graphene depositing processes.

A study done by Zhang *et al.* [96] utilized a solvothermal method that was done by only using a single step (called one-pot) for high performance flexible electrodes to produce r-GO CuNW which did not require any excessively high temperatures for the process and made the synthesis protocol simpler compared to the previous studies. It was again found that the CuNW helped to connect r-GO 'islands', improving the overall connectivity of the electrode. This however, resulted in the CuNWs not being completely covered by the r-GO layer which is unideal as the exposed parts of the CuNWs would be able to oxidate and negatively impact the rest of the film.

While coating with graphene offers potential new aspects that can be explored and better utilized, the cost of the synthesis of the films prevents any large-scale productions from happening as well as the reduced transmittance films with graphene (lower than 85% which is usually not ideal for transparent solar cells).

Of these protective methods that have been examined, using doped ZnO offers the best choice in terms of protecting the CuNWs, improving its attributes, and reducing any potential negative impact on the completed device.

2.5 Flexible organic solar cell device

Organic solar cells (OSCs) are an attractive alternative to current more rigid solar cells due to their relatively lower cost, light weight, flexibility, and with the possibility to surpass other solar cells PCEs [97–99]. OSCs utilize an organic semiconductor as the

photoactive layer to generate electricity from sunlight from a simple cathode/anode configuration similar to other devices.

The potential at fabricating a flexible OSC has many advantages which would allow such a cell to be applied to portable and wearable devices allowing them to generate power throughout the day with their normal usage. Compared to the more common rigid solar cells, the flexible OSCs have the potential to be more widely used in this regard. Figure 2.5 demonstrates some of these potential uses. In order to achieve this the bottom electrode with a flexible substrate is required to successfully develop and manufacture such a device.

Over recent years there have been a handful of studies that have examined such flexible transparent electrodes. Such a study was done by Kaltenbrunner *et al*. [100] where an ultrathin PET substrate of 1.4 μm was used in a perovskite-based solar cell. The final solar cell showed excellent stability maintaining a power output with a PCE of 12% on the polymer based substrate. Another study by Kang *et al*. [101] also utilized a polymer-based substrate though focused on PEN foil instead along with a AgNW transparent electrode. A reason for the choice of PEN is that it has a high-temperature tolerance of up to 155 ^{O}C with a relatively low thermal expansion coefficient. This results in any thermal expansion mismatch between the layers and the polymer substrate being minimized [102]. The final solar cell achieved a PCE of 12.85% with the cells maintaining 80% of their initial PCE after 1000 bending cycles which shows excellent stability.

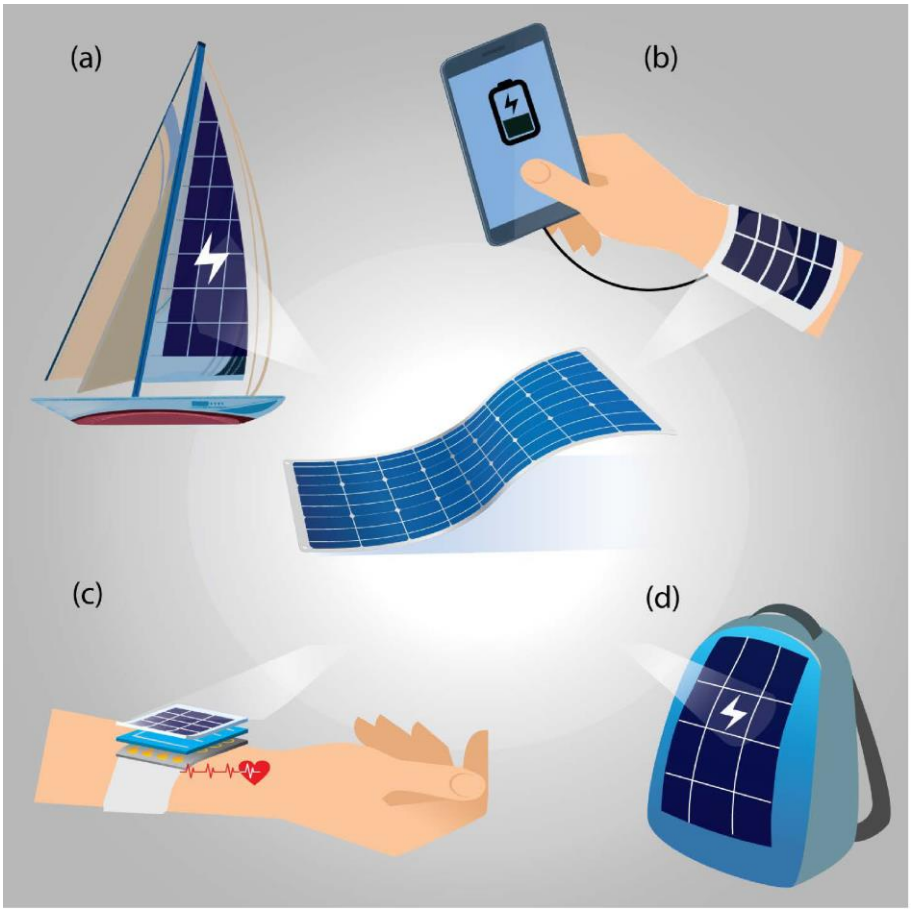

Figure 2. 5: Possible application of a flexible solar cell as a) textile (eg. Sail for a boat), b) power source for other wearable electronics, c) self-powered electronics for monitoring health, and d) light-weight wearable power supply for backpacks [103].

References

1. Günes S, Neugebauer H, Sariciftci NS (2007) Conjugated Polymer-Based Organic Solar Cells. Chem Rev 107:1324–1338
2. Wang X, Zhi L, Müllen K (2008) Transparent, Conductive Graphene Electrodes for Dye-Sensitized Solar Cells. Nano Lett 8:323–327
3. Wang J, Liang M, Fang Y, Qiu T, Zhang J, Zhi L (2012) Rod-Coating: Towards Large-Area Fabrication of Uniform Reduced Graphene Oxide Films for Flexible Touch Screens. Advanced Materials 24:2874–2878
4. Xu W, Gong Y, Liu L, Qin H, Shi Y (2011) Can graphene make better HgCdTe infrared detectors? Nanoscale Res Lett 6:1–4
5. Wu J, Agrawal M, Becerril HA, Bao Z, Liu Z, Chen Y, Peumans P (2010) Organic Light-Emitting Diodes on Solution-Processed Graphene Transparent Electrodes. ACS Nano 4:43–48
6. DeMeo D, MacNaughton S, Sonkusale S, Vandervelde T (2011) Electrodeposited Copper Oxide and Zinc Oxide Core-Shell Nanowire Photovoltaic Cells. In: Hashim A (ed) Nanowires - Implementations and Applications. InTech, pp 141–156
7. Siebentritt S (2002) Wide gap chalcopyrites: material properties and solar cells. Thin Solid Films 403–404:1–8
8. Erlat AG, Yan M, Duggal AR (2009) Substrates and Thin-Film Barrier Technology for Flexible Electronics. In: Wong W, Salleo A (eds) Flexible Electronics: Materials and Applications. Springer Science & Business Media, pp 413–449
9. Carlson DE (1989) Amorphous-silicon solar cells. IEEE Trans Electron Devices 36:2775–2780
10. Shang K, Gao J, Yin X, Ding Y, Wen Z (2021) An Overview of Flexible Electrode Materials/Substrates for Flexible Electrochemical Energy Storage/Conversion Devices. Eur J Inorg Chem 2021:606–619
11. Wang Q, Raglione M, Li B, Jin X, Toor F, Arnold M, Ding H (2019) High Throughput Laser Process of Transparent Conducting Surfaces for Terahertz Bandpass Ultrathin Metamaterials. Sci Rep 9:1–13
12. Karlsson T, Roos A (1984) Optical properties and spectral selectivity of copper oxide on stainless steel. Solar Energy Materials 10:105–119
13. Zhang Y, Woods CN, Alvarez M, Jin Y, Riggleman RA, Fakhraai Z (2018) Effect of substrate interactions on the glass transition and length-scale of correlated dynamics in ultra-thin molecular glass films. J Chem Phys 149:1–8
14. Dou B, Miller EM, Christians JA, et al (2017) High-Performance Flexible Perovskite Solar Cells on Ultrathin Glass: Implications of the TCO. J Phys Chem Lett 8:4960–4966

15. Li X, Li P, Wu Z, Luo D, Yu H-Y, Lu Z-H (2021) Review and perspective of materials for flexible solar cells. Materials Reports: Energy 1:1–24

16. van den Berg GJ (2000) The effect of the non-linear stress–strain behaviour of stainless steels on member capacity. J Constr Steel Res 54:135–160

17. Aref-Azar A, Biddlestone F, Hay JN, Haward RN (1983) The effect of physical ageing on the properties of poly(ethylene terephthalate). Polymer (Guildf) 24:1245–1251

18. Amborski LE, Flierl DW (1953) Physical Properties of Polyethylene Terephthalate Films. Ind Eng Chem 45:2290–2295

19. Alizadeh-Sh M, Marashi SPH, Pouranvari M (2014) Resistance spot welding of AISI 430 ferritic stainless steel: Phase transformations and mechanical properties. Materials & Design (1980-2015) 56:258–263

20. (2022) Instructables workshop . In: https://www.instructables.com/Steps-to-Analyzing-a-Materials-Properties-from-its/.

21. Mishra S, Ghosh S, Singh T (2021) Progress in Materials Development for Flexible Perovskite Solar Cells and Future Prospects. ChemSusChem 14:512–538

22. Higashioji T, Tsunekawa T, Bhushan B (2003) Mechanical property and dimensional stability of substrates for magnetic tapes. Tribol Int 36:437–445

23. Hanada T, Negishi T, Shiroishi I, Shiro T (2010) Plastic substrate with gas barrier layer and transparent conductive oxide thin film for flexible displays. Thin Solid Films 518:3089–3092

24. Ye S, Rathmell AR, Chen Z, Stewart IE, Wiley BJ (2014) Metal Nanowire Networks: The Next Generation of Transparent Conductors. Advanced Materials 26:6670–6687

25. Bomhard EM (2016) The toxicology of indium tin oxide. Environ Toxicol Pharmacol 45:282–294

26. Yang S, Su B, Bitar G, Lu N (2014) Stretchability of indium tin oxide (ITO) serpentine thin films supported by Kapton substrates. Int J Fract 190:99–110

27. Mohl M, Dombovari A, Vajtai R, Ajayan PM, Kordas K (2015) Self-assembled large scale metal alloy grid patterns as flexible transparent conductive layers. Sci Rep 5:1–8

28. Jeon I, Cui K, Chiba T, Anisimov A, Nasibulin AG, Kauppinen EI, Maruyama S, Matsuo Y (2015) Direct and Dry Deposited Single-Walled Carbon Nanotube Films Doped with MoO_x as Electron-Blocking Transparent Electrodes for Flexible Organic Solar Cells. J Am Chem Soc 137:7982–7985

29. Cho D-Y, Eun K, Choa S-H, Kim H-K (2014) Highly flexible and stretchable carbon nanotube network electrodes prepared by simple brush painting for cost-effective flexible organic solar cells. Carbon N Y 66:530–538

30. Jeon I, Chiba T, Delacou C, Guo Y, Kaskela A, Reynaud O, Kauppinen EI, Maruyama S, Matsuo Y (2015) Single-Walled Carbon Nanotube Film as Electrode in

Indium-Free Planar Heterojunction Perovskite Solar Cells: Investigation of Electron-Blocking Layers and Dopants. Nano Lett 15:6665–6671

31. Yu L, Shearer C, Shapter J (2016) Recent Development of Carbon Nanotube Transparent Conductive Films. Chem Rev 116:13413–13453

32. Papageorgiou DG, Kinloch IA, Young RJ (2017) Mechanical properties of graphene and graphene-based nanocomposites. Prog Mater Sci 90:75–127

33. Yen M-Y, Hsiao M-C, Liao S-H, Liu P-I, Tsai H-M, Ma C-CM, Pu N-W, Ger M-D (2011) Preparation of graphene/multi-walled carbon nanotube hybrid and its use as photoanodes of dye-sensitized solar cells. Carbon N Y 49:3597–3606

34. Zhang C, Wang S, Zhang H, et al (2019) Efficient stable graphene-based perovskite solar cells with high flexibility in device assembling *via* modular architecture design. Energy Environ Sci 12:3585–3594

35. Rudrapati R (2020) Graphene: Fabrication Methods, Properties, and Applications in Modern Industries. In: Graphene Production and Application. IntechOpen, pp 9–22

36. Wang J, Fei F, Luo Q, Nie S, Wu N, Chen X, Su W, Li Y, Ma C-Q (2017) Modification of the Highly Conductive PEDOT:PSS Layer for Use in Silver Nanogrid Electrodes for Flexible Inverted Polymer Solar Cells. ACS Appl Mater Interfaces 9:7834–7842

37. Song M, Kim H-J, Kim CS, Jeong J-H, Cho C, Lee J-Y, Jin S-H, Choi D-G, Kim D-H (2015) ITO-free highly bendable and efficient organic solar cells with Ag nanomesh/ZnO hybrid electrodes. J Mater Chem A Mater 3:65–70

38. Li Y, Chen Y, Qiu M, Yu H, Zhang X, Sun XW, Chen R (2016) Preparation of Aluminum Nanomesh Thin Films from an Anodic Aluminum Oxide Template as Transparent Conductive Electrodes. Sci Rep 6:1–7

39. Sun K, Zhang S, Li P, Xia Y, Zhang X, Du D, Isikgor FH, Ouyang J (2015) Review on application of PEDOTs and PEDOT:PSS in energy conversion and storage devices. Journal of Materials Science: Materials in Electronics 26:4438–4462

40. Mochizuki T, Takigami Y, Kondo T, Okuzaki H (2018) Fabrication of flexible transparent electrodes using PEDOT:PSS and application to resistive touch screen panels. J Appl Polym Sci 135:1–6

41. la Notte L, Villari E, Palma AL, Sacchetti A, Michela Giangregorio M, Bruno G, di Carlo A, Bianco GV, Reale A (2017) Laser-patterned functionalized CVD-graphene as highly transparent conductive electrodes for polymer solar cells. Nanoscale 9:62–69

42. Chen X, Guo W, Xie L, Wei C, Zhuang J, Su W, Cui Z (2017) Embedded Ag/Ni Metal-Mesh with Low Surface Roughness As Transparent Conductive Electrode for Optoelectronic Applications. ACS Appl Mater Interfaces 9:37048–37054

43. Jiu J, Suganuma K (2016) Metallic Nanowires and Their Application. IEEE Trans Compon Packaging Manuf Technol 6:1733–1751

44. Fahad S, Yu H, Wang L, Zain-ul-Abdin, Haroon M, Ullah RS, Nazir A, Naveed K-R, Elshaarani T, Khan A (2019) Recent progress in the synthesis of silver nanowires and their role as conducting materials. J Mater Sci 54:997–1035

45. Pierson JF, Rolin E, Clément-Gendarme C, Petitjean C, Horwat D (2008) Effect of the oxygen flow rate on the structure and the properties of Ag–Cu–O sputtered films deposited using a Ag/Cu target with eutectic composition. Appl Surf Sci 254:6590–6594

46. Hwang B, An Y, Lee H, Lee E, Becker S, Kim Y-H, Kim H (2017) Highly Flexible and Transparent Ag Nanowire Electrode Encapsulated with Ultra-Thin Al2O3: Thermal, Ambient, and Mechanical Stabilities. Sci Rep 7:1–7

47. Yu S, Li X, Zhao L, Wu M, Ren Q, Gong B, Li L, Shi H (2020) Simultaneously improved conductivity and adhesion of flexible AgNW networks via a simple hot lamination process. Synth Met 267:1–8

48. Núñez CG, Navaraj WT, Polat EO, Dahiya R (2017) Energy-Autonomous, Flexible, and Transparent Tactile Skin. Adv Funct Mater 27:1–12

49. Polat EO, Balci O, Kakenov N, Uzlu HB, Kocabas C, Dahiya R (2015) Synthesis of Large Area Graphene for High Performance in Flexible Optoelectronic Devices. Sci Rep 5:1–10

50. Park J-S, Park T-G, Park J-S (2021) Characterization of Silver Nanowire Flexible Transparent Electrode with Grid Pattern Formed via Thermocompression. 17:260–267

51. Scardaci V (2021) Copper Nanowires for Transparent Electrodes: Properties, Challenges and Applications. Applied Sciences 11:1–16

52. Ohiienko O, Oh Y-J (2020) Preparation of narrow copper nanowires with less oxidized surface for flexible and transparent electrodes under octadecylamine. Mater Chem Phys 246:1–11

53. Carvill J (1993) Thermodynamics and heat transfer. In: Mechanical Engineer's Data Handbook, 1st ed. Elsevier, Oxford, pp 102–145

54. Mayousse C, Celle C, Carella A, Simonato J-P (2014) Synthesis and purification of long copper nanowires. Application to high performance flexible transparent electrodes with and without PEDOT:PSS. Nano Res 7:1–10

55. Huang W, Li J, Han F, Zhang G, Sun R, Wong C-P (2017) Controllable Synthesis and Study on Morphology of Copper Nanowires. Journal of the Chinese Chemical Society 64:1354–1359

56. Wang Y, Liu P, Zeng B, Liu L, Yang J (2018) Facile Synthesis of Ultralong and Thin Copper Nanowires and Its Application to High-Performance Flexible Transparent Conductive Electrodes. Nanoscale Res Lett 13:1–10

57. Won Y, Kim A, Yang W, Jeong S, Moon J (2014) A highly stretchable, helical copper nanowire conductor exhibiting a stretchability of 700%. NPG Asia Mater 6:e132–e132

58. Shi Y, Li H, Chen L, Huang X (2005) Obtaining ultra-long copper nanowires via a hydrothermal process. Sci Technol Adv Mater 6:761–765

59. Chang Y, Lye ML, Zeng HC (2005) Large-Scale Synthesis of High-Quality Ultralong Copper Nanowires. Langmuir 21:3746–3748

60. Zhang S, Xie Y, Yan L (2020) Ultra-fast and visual detection of hydrazine hydrate based on a simple coumarin derivative. Spectrochim Acta A Mol Biomol Spectrosc 230:1–6

61. Matsumoto M, Kano H, Suzuki M, Katagiri T, Umeda Y, Fukushima S (2016) Carcinogenicity and chronic toxicity of hydrazine monohydrate in rats and mice by two-year drinking water treatment. Regulatory Toxicology and Pharmacology 76:63–73

62. Wang Y, Liu P, Wang H, Zeng B, Wang J, Chi F (2019) Flexible organic light-emitting devices with copper nanowire composite transparent conductive electrode. J Mater Sci 54:2343–2350

63. Pradel KC, Sohn K, Huang J (2011) Cross-Flow Purification of Nanowires. Angewandte Chemie International Edition 50:3412–3416

64. Pradel KC, Sohn K, Huang J (2011) Cross-Flow Purification of Nanowires. Angewandte Chemie International Edition 50:3412–3416

65. Li B, Ye S, Stewart IE, Alvarez S, Wiley BJ (2015) Synthesis and Purification of Silver Nanowires To Make Conducting Films with a Transmittance of 99%. Nano Lett 15:6722–6726

66. Jarrett R, Crook R (2016) Silver nanowire purification and separation by size and shape using multi-pass filtration. Materials Research Innovations 20:86–91

67. Liu X, Kang J, Liu B, Yang J (2018) Separation of gold nanowires and nanoparticles through a facile process of centrifugation. Sep Purif Technol 192:1–4

68. Kang C, Yang S, Tan M, Wei C, Liu Q, Fang J, Liu G (2018) Purification of Copper Nanowires To Prepare Flexible Transparent Conductive Films with High Performance. ACS Appl Nano Mater 1:3155–3163

69. Lin Z, Liu Y, Wong C (2010) Facile Fabrication of Superhydrophobic Octadecylamine-Functionalized Graphite Oxide Film. Langmuir 26:16110–16114

70. Li W, Tang X-Z, Zhang H-B, Jiang Z-G, Yu Z-Z, Du X-S, Mai Y-W (2011) Simultaneous surface functionalization and reduction of graphene oxide with octadecylamine for electrically conductive polystyrene composites. Carbon N Y 49:4724–4730

71. Zhang H, Wang S, Tian Y, Wen J, Hang C, Zheng Z, Huang Y, Ding S, Wang C (2020) High-efficiency extraction synthesis for high-purity copper nanowires and their applications in flexible transparent electrodes. Nano Materials Science 2:164–171

72. Liu S-H, Fichthorn KA (2017) Interaction of Alkylamines with Cu Surfaces: A Metal–Organic Many-Body Force Field. The Journal of Physical Chemistry C 121:22531–22541

73. Li W, Tang X-Z, Zhang H-B, Jiang Z-G, Yu Z-Z, Du X-S, Mai Y-W (2011) Simultaneous surface functionalization and reduction of graphene oxide with octadecylamine for electrically conductive polystyrene composites. Carbon N Y 49:4724–4730

74. Rathmell AR, Nguyen M, Chi M, Wiley BJ (2012) Synthesis of Oxidation-Resistant Cupronickel Nanowires for Transparent Conducting Nanowire Networks. Nano Lett 12:3193–3199

75. Stewart IE, Rathmell AR, Yan L, Ye S, Flowers PF, You W, Wiley BJ (2014) Solution-processed copper–nickel nanowire anodes for organic solar cells. Nanoscale 6:5980–5988

76. Kim K, Kwon H-C, Ma S, Lee E, Yun S-C, Jang G, Yang H, Moon J (2018) All-Solution-Processed Thermally and Chemically Stable Copper–Nickel Core–Shell Nanowire-Based Composite Window Electrodes for Perovskite Solar Cells. ACS Appl Mater Interfaces 10:30337–30347

77. Gelves GA, Lin B, Sundararaj U, Haber JA (2006) Low Electrical Percolation Threshold of Silver and Copper Nanowires in Polystyrene Composites. Adv Funct Mater 16:2423–2430

78. Zhao J, Zhang D, Zhang X (2015) Preparation and characterization of copper/silver bimetallic nanowires with core-shell structure. Surface and Interface Analysis 47:529–534

79. Stewart IE, Ye S, Chen Z, Flowers PF, Wiley BJ (2015) Synthesis of Cu–Ag, Cu–Au, and Cu–Pt Core–Shell Nanowires and Their Use in Transparent Conducting Films. Chemistry of Materials 27:7788–7794

80. Shah A v., Schade H, Vanecek M, Meier J, Vallat-Sauvain E, Wyrsch N, Kroll U, Droz C, Bailat J (2004) Thin-film silicon solar cell technology. Progress in Photovoltaics: Research and Applications 12:113–142

81. Zhang B, Li W, Jiu J, Yang Y, Jing J, Suganuma K, Li C-F (2019) Large-Scale and Galvanic Replacement Free Synthesis of Cu@Ag Core–Shell Nanowires for Flexible Electronics. Inorg Chem. https://doi.org/10.1021/acs.inorgchem.8b03460

82. Niu Z, Cui F, Yu Y, et al (2017) Ultrathin Epitaxial Cu@Au Core–Shell Nanowires for Stable Transparent Conductors. J Am Chem Soc 139:7348–7354

83. Chen X, Mao SS (2007) Titanium Dioxide Nanomaterials: Synthesis, Properties, Modifications, and Applications. Chem Rev 107:2891–2959

84. Zhang Y, Zhou N, Zhang K, Yan F (2017) Plasmonic copper nanowire@TiO2 nanostructures for improving the performance of dye-sensitized solar cells. J Power Sources 342:292–300

85. Babu B, Mallikarjuna K, Reddy ChV, Park J (2016) Facile synthesis of Cu@TiO 2 core shell nanowires for efficient photocatalysis. Mater Lett 176:265–269

86. Shi L, Wang R, Liu Y, Sun J (2020) A facile strategy for the preparation of hybrid copper nanowire-TiO2 film. Thin Solid Films 693:1–6

87. Chen Z, Ye S, Stewart IE, Wiley BJ (2014) Copper Nanowire Networks with Transparent Oxide Shells That Prevent Oxidation without Reducing Transmittance. ACS Nano 8:9673–9679

88. Li H, Bredas J-L (2016) Comparison of the Impact of Zinc Vacancies on Charge Separation and Charge Transfer at ZnO/Sexithienyl and ZnO/Fullerene Interfaces. Advanced Materials 28:3928–3936

89. Zhu Q, Bao X, Yu J, Zhu D, Zhang Q, Gu C, Dong H, Yang R, Dong L (2016) Low-temperature, solution-processed aluminum-doped zinc oxide as electron transport layer for stable efficient polymer solar cells. Thin Solid Films 605:202–207

90. Won Y, Kim A, Lee D, Yang W, Woo K, Jeong S, Moon J (2014) Annealing-free fabrication of highly oxidation-resistive copper nanowire composite conductors for photovoltaics. NPG Asia Mater 6:1–9

91. Hwang H, Ahn J, Lee E, Kim K, Kwon H-C, Moon J (2017) Enhanced compatibility between a copper nanowire-based transparent electrode and a hybrid perovskite absorber by poly(ethylenimine). Nanoscale 9:17207–17211

92. Bhoomanee C, Ruankhama P, Choopun S, Prathan A, Wongratanaphisan D (2019) Effect of Al-doped ZnO for Electron Transporting Layer in Planar Perovskite solar cells. Mater Today Proc 17:1259–1267

93. Yang H, Kwon HC, Ma S, Kim K, Yun SC, Jang G, Park J, Lee H, Goh S, Moon J (2020) Energy Level-Graded Al-Doped ZnO Protection Layers for Copper Nanowire-Based Window Electrodes for Efficient Flexible Perovskite Solar Cells. ACS Appl Mater Interfaces 12:13824–13835

94. Allen MJ, Tung VC, Kaner RB (2010) Honeycomb Carbon: A Review of Graphene. Chem Rev 110:132–145

95. Kholmanov IN, Magnuson CW, Aliev AE, et al (2012) Improved Electrical Conductivity of Graphene Films Integrated with Metal Nanowires. Nano Lett 12:5679–5683

96. Zhang W, Yin Z, Chun A, Yoo J, Kim YS, Piao Y (2016) Bridging Oriented Copper Nanowire–Graphene Composites for Solution-Processable, Annealing-Free, and Air-Stable Flexible Electrodes. ACS Appl Mater Interfaces 8:1733–1741

97. Li C, Zhou J, Song J, et al (2021) Non-fullerene acceptors with branched side chains and improved molecular packing to exceed 18% efficiency in organic solar cells. Nat Energy 6:605–613

98. Riede M, Spoltore D, Leo K (2021) Organic Solar Cells—The Path to Commercial Success. Adv Energy Mater 11:1–10

99. Liu F, Zhou L, Liu W, et al (2021) Organic Solar Cells with 18% Efficiency Enabled by an Alloy Acceptor: A Two-in-One Strategy. Advanced Materials 33:1–8

100. Kaltenbrunner M, Adam G, Głowacki ED, et al (2015) Flexible high power-per-weight perovskite solar cells with chromium oxide–metal contacts for improved stability in air. Nat Mater 14:1032–1039

101. Kang S, Jeong J, Cho S, Yoon YJ, Park S, Lim S, Kim JY, Ko H (2019) Ultrathin, lightweight and flexible perovskite solar cells with an excellent power-per-weight performance. J Mater Chem A Mater 7:1107–1114

102. Tavakoli MM, Lin Q, Leung S-F, Lui GC, Lu H, Li L, Xiang B, Fan Z (2016) Efficient, flexible and mechanically robust perovskite solar cells on inverted nanocone plastic substrates. Nanoscale 8:4276–4283

103. Seong S, Liu Y, Gong X (2022) Mechanical study of perovskite solar cells: opportunities and challenges for wearable power source. Opt Mater Express 12:772–787

Chapter 3. Characterization Techniques and Synthesis Methods

3.1 Introduction

This chapter covers various characterization techniques that are used to analyse the synthesized electrodes as well as the synthesis methods used to prepare them. These techniques will allow exploration of the properties of the electrodes such as the structure, morphology, optical transmittance, optical absorbance, surface roughness, thickness and, the tensile strength of the electrodes. These are studied using X-ray diffractometer (XRD, Rigaku Smartlab), High Resolution Scanning Electron Microscopy coupled with an Energy-Dispersive X-ray Spectroscopy (HRSEM, JEOL JSM-7800F thermal field), Perkin Elmer Lambda 650 S UV/VIS Spectrophotometer, WITec alpha300 A AFM microscope and, a Deben Tensile 200N microtest.

3.2 Characterisation techniques

3.2.1 X-ray Diffractometer (XRD)

X-ray diffraction (XRD) is a non-destructive powerful analysis tool that is used to characterize the crystalline phases in thin films and thus identify the materials based on the diffraction pattern that emerges. It can also yield potential information with regards to internal stresses and potential defects within the structure [1]. It generally works by irradiating the sample with an incident X-rays (θ_i) and then measuring the deflected X-rays (θ_f) and finding an intensity maximum for a given lattice plane spacing d_{hkl} when the relationship between these two rays is an internal number of wavelengths as shown by equation 3.1:

$$n\lambda = 2d_{hkl}\sin\left(\frac{\theta_i + \theta_f}{2}\right) \quad (3.1)$$

which is the Bragg equation [2]. An illustration of this process can be found in Figure 3.1.

In order to analyse the results from the XRD, the diffraction pattern (which consists of the 2θ angles and relative intensities) is compared with standard line patterns available from previous research done and logged with the Rigaku PDXL XRD analysis software database [3]. If the sample is not in the database, by using the three most intense peaks from the given pattern, the crystalline phase can still be found and studied that way.

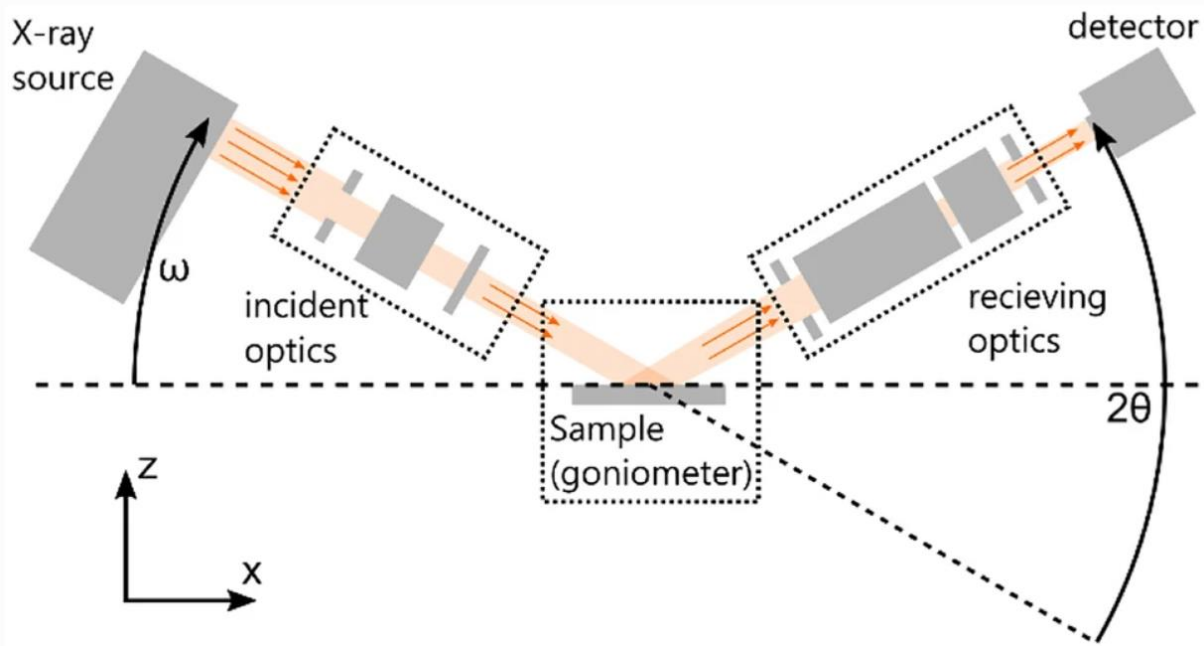

Figure 3. 1: X-ray diffraction illustration [4]

3.2.2 Scanning electron microscope (SEM)

SEM allows the insight of surface topography, and if attached with an energy-dispersive X-ray detector (EDS) it can also be used to analyse the local elemental compositions in the sample [5]. The principle behind the SEM is to focus a beam of electrons onto a spot on the sample which interacts with it. This interaction generates signals which reflect the local properties of the sample. Moving along the sample from point to point the signal intensity is picked up and used to map respective pixels of an image. This way an image of the sample is formed [6]. An advantage of this technique is that the samples surface is not impacted by the usage of the SEM and thus gives a true account of the surface of the obtained sample. The illustration in Figure 3.2 showcases the components of what SEM is made up of.

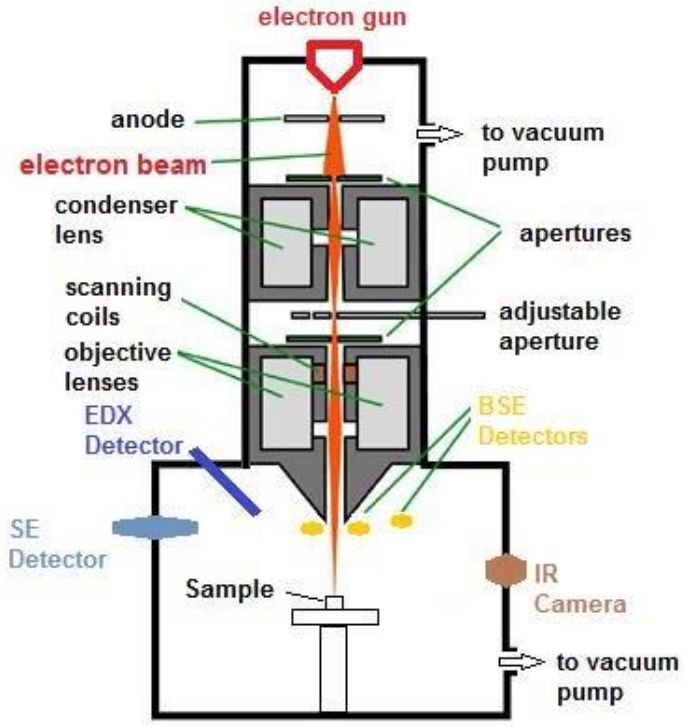

Figure 3. 2: Scanning Electron Microscope illustration [7]

3.2.3 Ultraviolet-visible spectroscopy (UV-Vis)

UV-Vis spectroscopy is a technique which is used to analyse and investigate the various optical properties of samples such as the transmittance, reflectance and, absorbance. UV-Vis spectrometers use a light source which is usually across the ultraviolet to the visible wavelength range (190-900 nm). The instrument then measures the amount of light that passes through the sample and can detect how much light has been transmitted, absorbed and reflected by the sample. Furthermore, by studying the absorbance of the sample the bandgap energy of the material can be found. The bandgap energy can be defined as the energy difference between the lowest unoccupied molecular orbital and the highest occupied molecular orbital. This occurs when a photon strikes a molecule and is absorbed, resulting in the molecule being promoted into a higher energetic state [8]. The illustration of how the process is completed is shown in Figure 3.3.

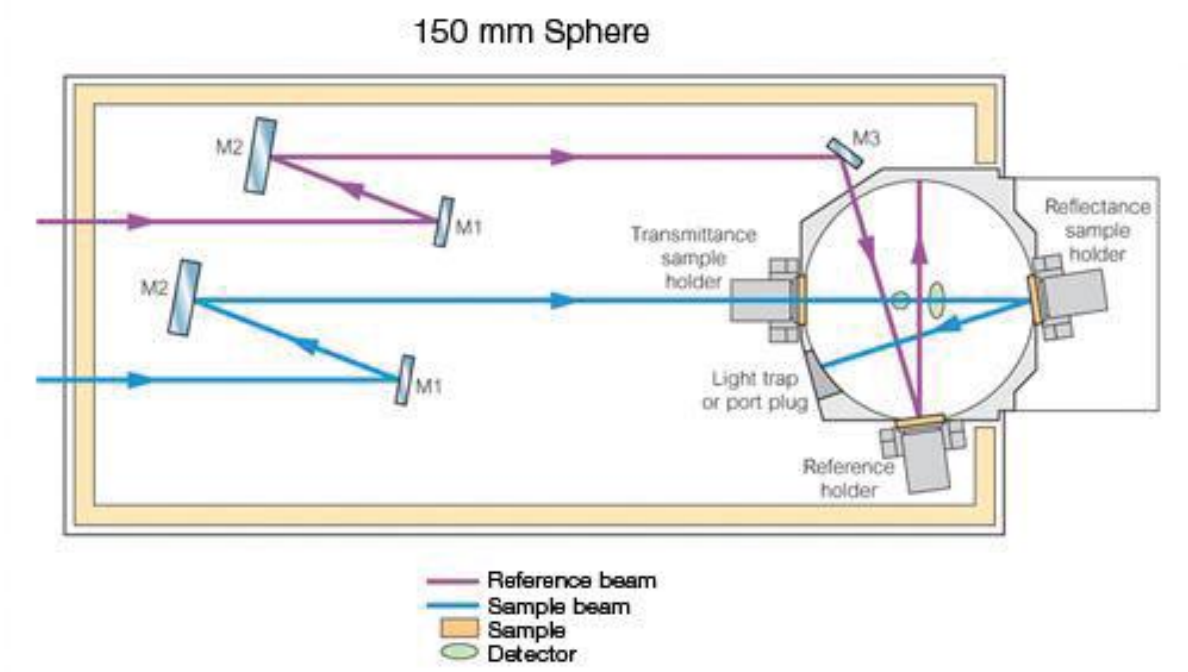

Figure 3. 3: UV-Vis-NIR measurements illustration [9]

3.2.4 Atomic Force Microscopy (AFM)

AFM measurements are typically used in order to study the thickness and surface roughness of a material which impacts the various properties of the proposed sample. These measurements are done by using the force between the tip and the surface to generate an image. Typically, a laser beam is reflected off the top of a cantilever (which carries the tip) and as the tip moves up and down along the surface of the sample this reflected laser beam allows for the analysis of the surface of the structure; observing the roughness of it [10]. AFM measurements are usually completed using either contact or non-contact modes. With contact modes the tip is in contact with the surface of the sample which puts both the tip and the sample at risk of being damaged while giving the more accurate reading of the surface. While non-contact modes generally do not impact the sample or pose too high a risk of damaging the tip. An illustration of the schematic of AFM is shown in Figure 3.4.

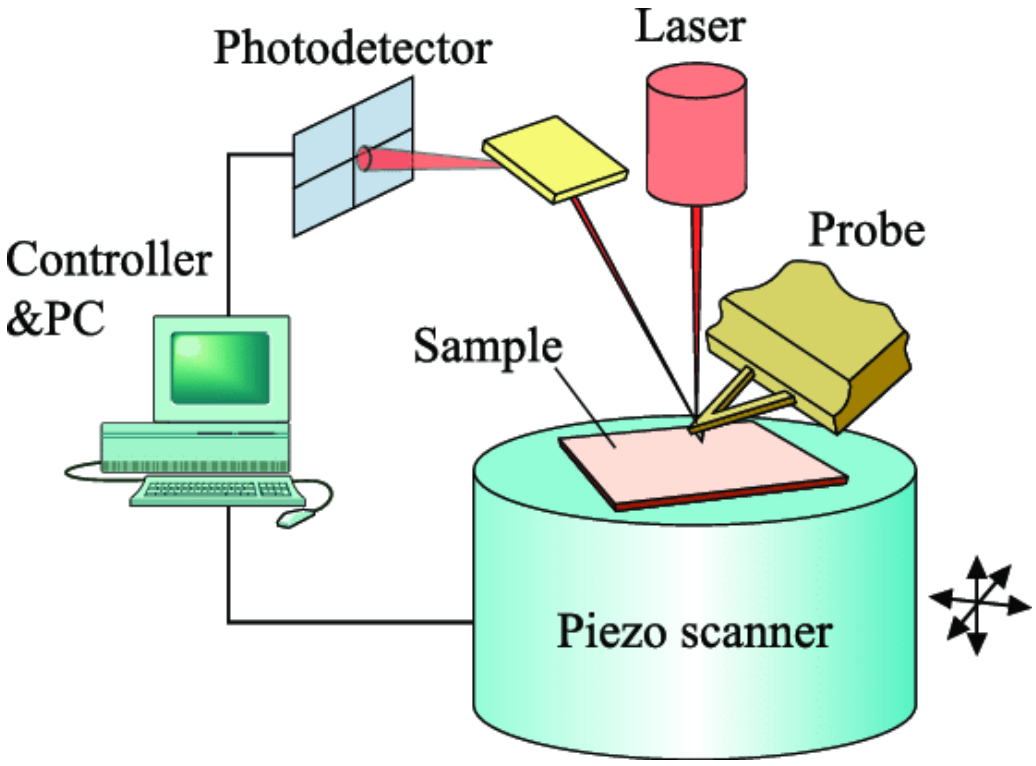

Figure 3. 4: AFM illustration [11]

3.2.5 Tensile strength test

Testing the tensile strength of any potential film is an important aspect to study in order to understand how viable a film will be in a practical setting. A tensile strength test involves placing a sample of film, with known length and thickness, between two jaws of a tensile tester. The jaws are then slowly pulled apart at a fixed rate [12] applying a force to the sample which is recorded. This is done either until the film fails and breaks or until the tensile tester reaches its maximum elongation length. From there the data obtained reflects the applied force at any given time as well as the amount the film that had been stretched, at that point. This can be used to determine the stress and strain of the sample and thus find other properties of the sample such as the yield strength, ultimate strength and, the Young's modulus to list a few [13]. Figure 3.5 illustrates the process used to obtain these parameters.

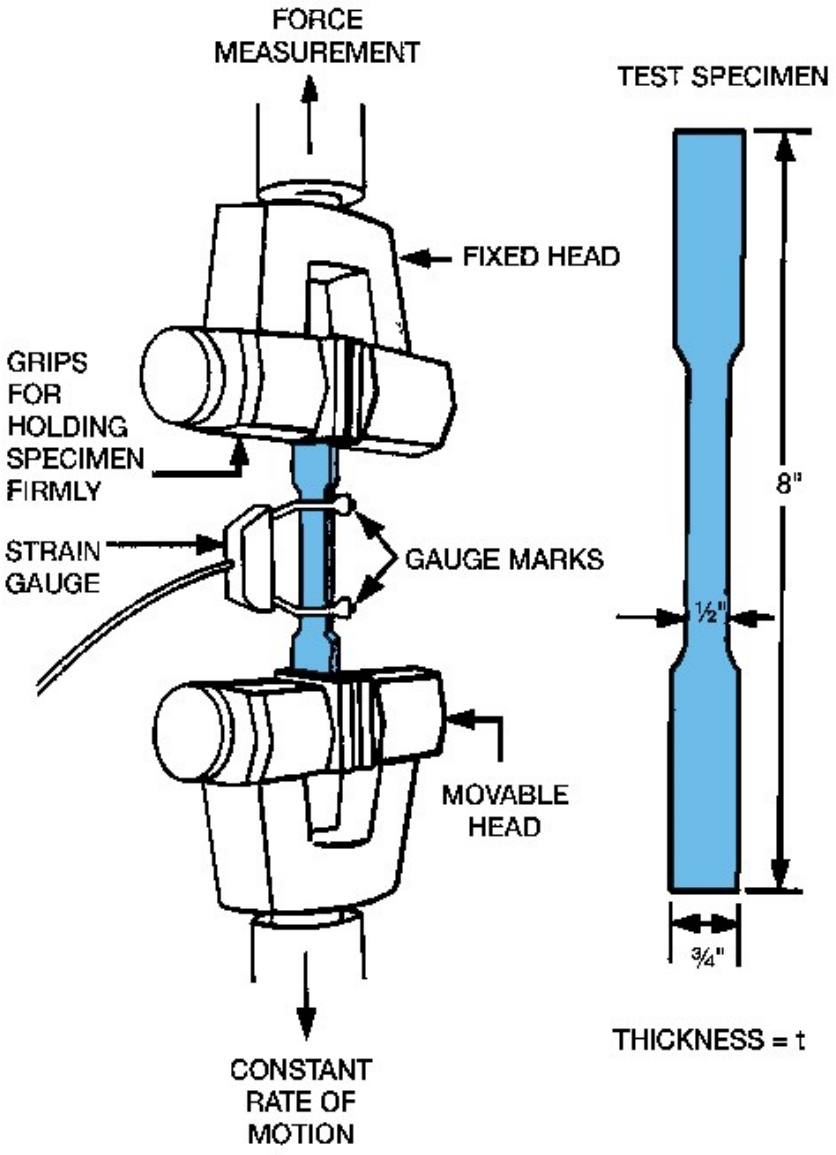

Figure 3. 5: Tensile tester with sample illustration [14]

3.3 Synthesis and depositing methods used in this study

3.3.1 Hydrothermal method

The hydrothermal method utilizes hydrolysis reactions at high temperatures within a sealed autoclave. Through this method the nanostructures of the synthesized products are more easily controlled by properly choosing the required reaction time, temperature, or the solvent used for the reaction without much other synthesis deviations or additional steps [15]. Thus, by controlling the precursors as well as the time the autoclave remained in the oven for the reaction, the length and thickness of the synthesized nanowires can be easily controlled for their fabrication purpose. After the synthesis process the final products have to be washed to remove any unwanted by-products (such as Cl^-) and excess chemicals that might not have completely reacted within the autoclave [16]. The flowchart in Figure 3.6 illustrates the procedure used for the hydrothermal method, and Figure 3.7 shows how the CuNWs are formed with the capping agent within the autoclave.

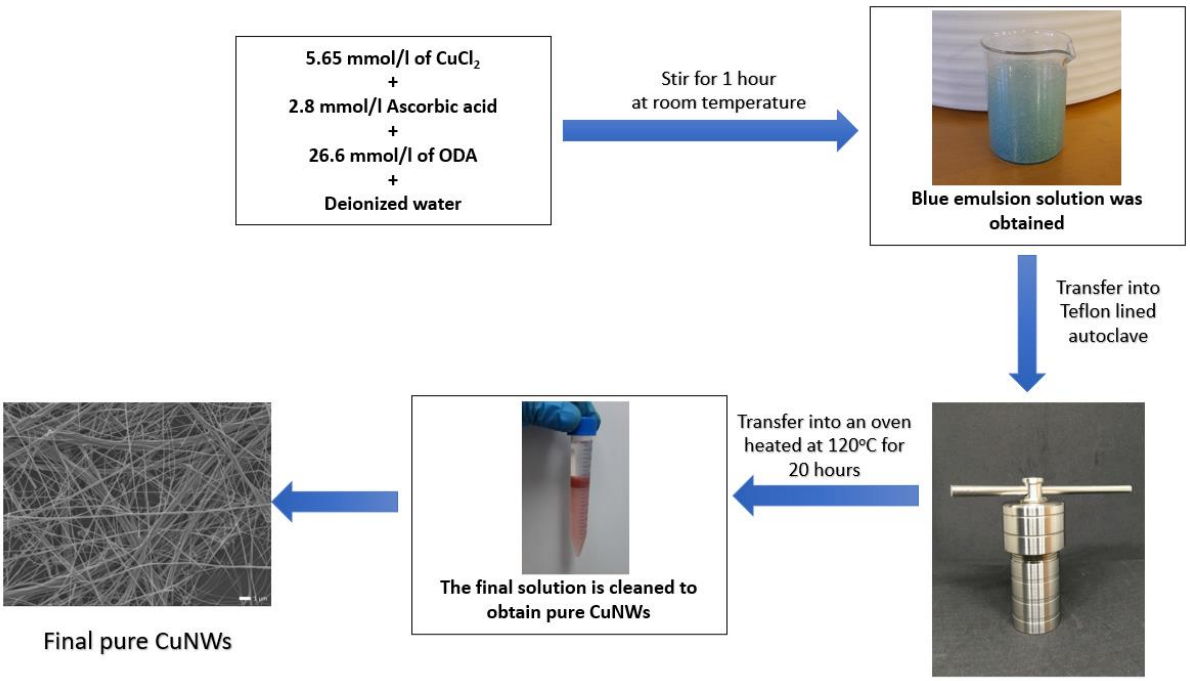

Figure 3. 6: Illustration of hydrothermal method steps.

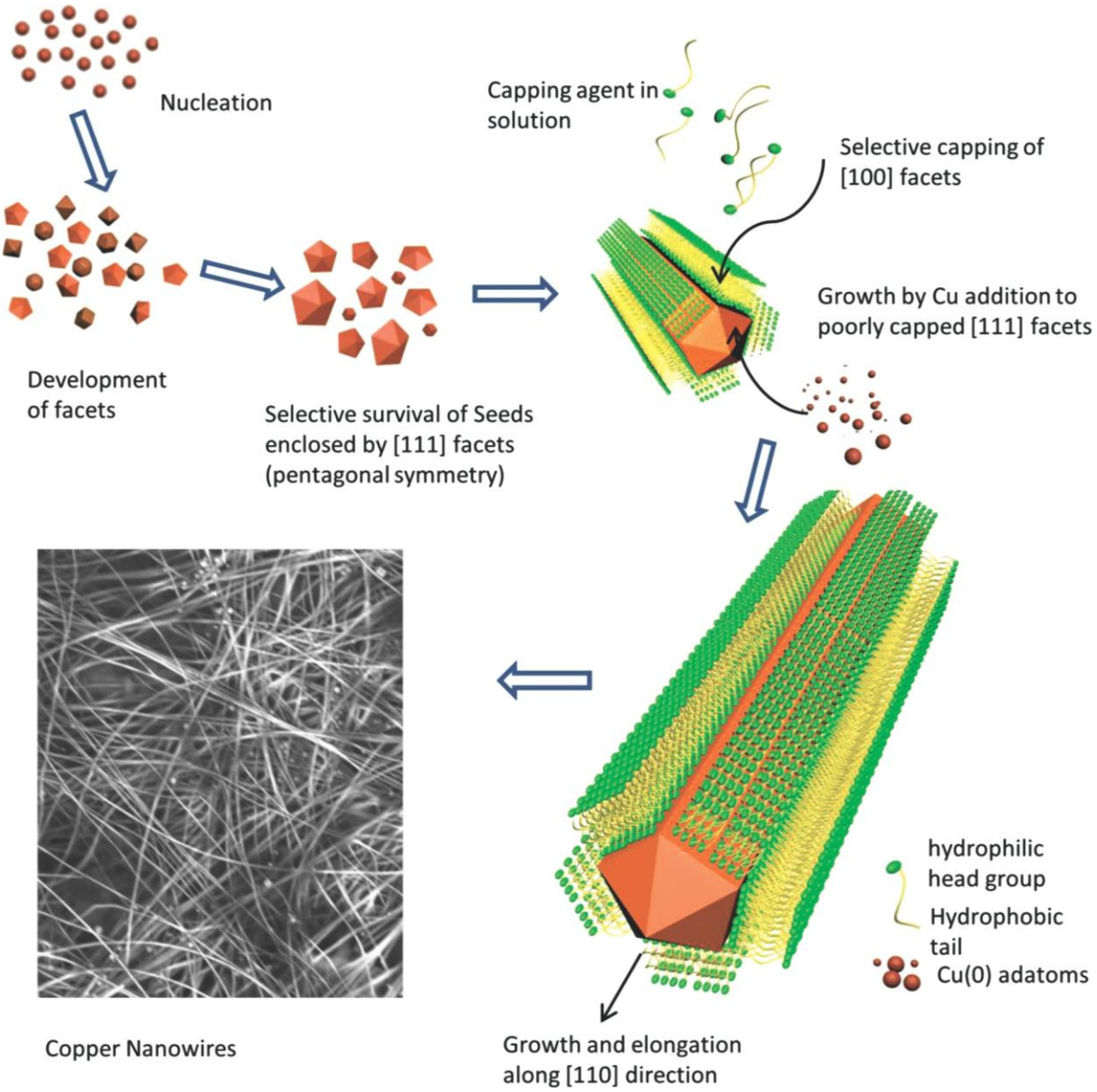

Figure 3. 7: Illustration of CuNW synthesis [17]

3.3.2 Solution method

Of the various fabrication methods (including atomic layer deposition, chemical vapour deposition, and magneton sputtering) the solution-processing method is the simplest to carry out. Additionally, it also has some advantages for thin film fabrication including its minimal power and material consumption resulting in the methods being much cheaper to synthesize [18], and being able to mix compositions at a molecular level [19]. Generally, the process involves the preparation of metal precursors that are dissolved in solvents with heat to encourage the growth before washing the solution to remove any impurities.

3.3.3 Materials used

For the purposes of the experiments performed in this study, the following materials were used for AZO/GZO-NFs: zinc acetate (99.99% trace metals basis), sodium hydroxide (≥98% reagent grade pellets), aluminium nitrate nonahydrate (ACS reagent ≥ 98%), gallium(III) nitrate hydrate (crystalline 99.9% trace metal basis). The following materials were also used for CuNWs: copper(II) chloride (99.999% trace metal basis), L-Ascorbic acid (ACS reagent ≥ 99%), octadecylamine (≥ 99.0% GC), n-hexane (≥ 98% GC) and, isopropanol (anhydrous 99.5%).

3.3.4 Spin-coating method

The spin-coating is the method which is used to apply a uniformly spread thin film onto a flat substrate. Usually, the process involves depositing a small amount of liquid solution onto the centre of a spinning film at high speeds[20]. The centrifugal force will result in the solution spreading off the edge of the substrate while leaving a thin film of the solution behind on the surface. The final thickness of the thin film will depend on various factors of the procedure including the viscosity of the solution, percent solids, as well as the final spinning speed [21]. One ideal aspect of the spin-coating method is repeatability. By using the same conditions and the same thickness of sample reliability can be obtained from the process. Figure 3.8 illustrates the spin-coating method.

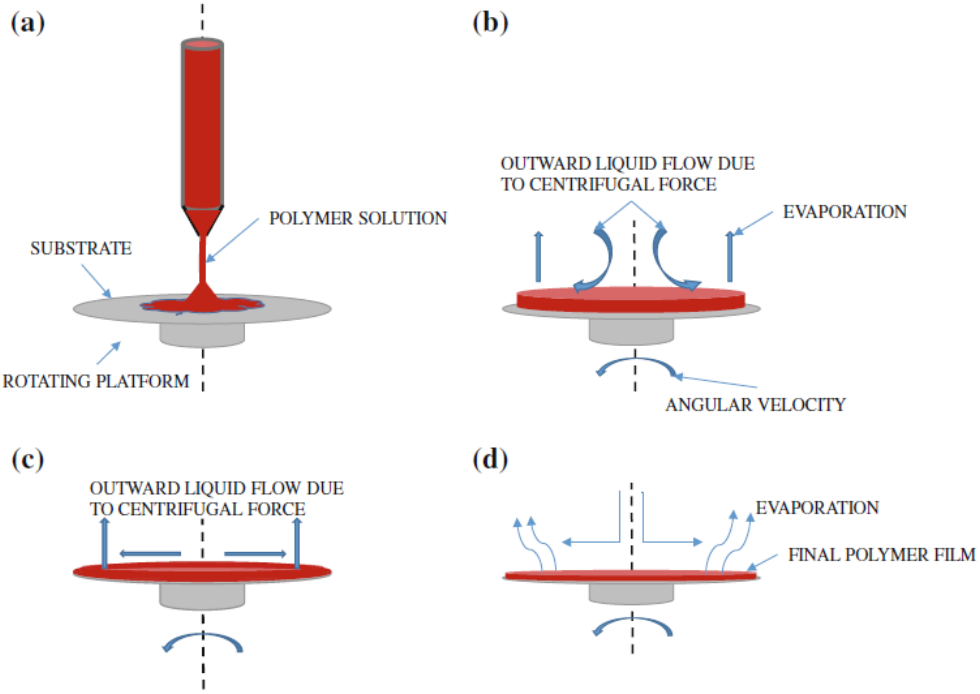

Figure 3. 8: Illustration of spin-coating method [22]

References

1. Amano H, Iwaya M, Kashima T, Katsuragawa M, Akasaki I, Han J, Hearne S, Floro JA, Chason E, Figiel J (1998) Stress and Defect Control in GaN Using Low Temperature Interlayers. Jpn J Appl Phys 37:L1540–L1542
2. Durose K, Asher SE, Jaegermann W, et al (2004) Physical characterization of thin-film solar cells. Progress in Photovoltaics: Research and Applications 12:177–217
3. Rajeshkumar S, Bharath LV, Geetha R (2019) Broad spectrum antibacterial silver nanoparticle green synthesis: Characterization, and mechanism of action, Micro and Nano Technologies. In: Shukla AK, Iravani S (eds) Green Synthesis, Characterization and Applications of Nanoparticles, 1st ed. Elsevier, pp 429–444
4. Harrington GF, Santiso J (2021) Back-to-Basics tutorial: X-ray diffraction of thin films. J Electroceram 47:141–163
5. Abou-Ras D, Nichterwitz M, Romero MJ, Schmidt SS (2016) Electron Microscopy on Thin Films for Solar Cells. In: Advanced characterization techniques for thin film solar cells, Second. Wiley-VCH, pp 299–345
6. Schmitt R (2014) Scanning Electron Microscope. In: CIRP Encyclopedia of Production Engineering. Springer Berlin Heidelberg, Berlin, Heidelberg, pp 1085–1089
7. (2022) http://www4.nau.edu/microanalysis/Microprobe-SEM/Instrumentation.html.
8. Abbas Q (2019) Understanding the UV-Vis Spectroscopy for Nanoparticles. Journal of Nanomaterials & Molecular Nanotechnology 8:239–250
9. Dharma J, Pisal A (2009) Simple Method of Measuring the Band Gap Energy Value of TiO2 in the Powder Form using a UV/Vis/NIR Spectrometer. PerkinElmer 1–4
10. Binnig G, Quate CF, Gerber Ch (1986) Atomic Force Microscope. Phys Rev Lett 56:930–933
11. Ishida N, Craig VSJ (2019) Direct Measurement of Interaction Forces between Surfaces in Liquids Using Atomic Force Microscopy. KONA Powder and Particle Journal 36:187–200
12. Campo EA (2008) Mechanical Properties of Polymeric Materials. In: Selection of Polymeric Materials: How to Select Design Properties from Different Standards, revised. William Andrew, pp 41–103
13. Joun M, Choi I, Eom J, Lee M (2007) Finite element analysis of tensile testing with emphasis on necking. Comput Mater Sci 41:63–69
14. (2022) Mechanical Testing. In: https://medium.com/@sakshibose1/mechanical-testing-a7b2adb416d1.
15. Tenne R, Margulis L, Genut M, Hodes G (1992) Polyhedral and cylindrical structures of tungsten disulphide. Nature 360:444–446

16. MODAN EM, PLĂIAȘU AG (2020) Advantages and Disadvantages of Chemical Methods in the Elaboration of Nanomaterials. The Annals of “Dunarea de Jos” University of Galati Fascicle IX, Metallurgy and Materials Science 43:53–60

17. Bhanushali S, Ghosh P, Ganesh A, Cheng W (2015) 1D Copper Nanostructures: Progress, Challenges and Opportunities. Small 11:1232–1252

18. Ahn B du, Jeon H-J, Sheng J, Park J, Park J-S (2015) A review on the recent developments of solution processes for oxide thin film transistors. Semicond Sci Technol 30:1–15

19. Trinh BNQ, Chien TD, Hoa NQ, Minh DH (2020) Solution-processable zinc oxide based thin films with different aluminum doping concentrations. Journal of Science: Advanced Materials and Devices 5:497–501

20. Ohara T, Matsumoto Y, Ohashi H (1989) The film formation dynamics in spin coating. Physics of Fluids A: Fluid Dynamics 1:1949–1959

21. Mitzi DB, Kosbar LL, Murray CE, Copel M, Afzali A (2004) High-mobility ultrathin semiconducting films prepared by spin coating. Nature 428:299–303

22. Das R, Chanda A (2016) Fabrication and Properties of Spin-Coated Polymer Films. In: Nano-size Polymers. Springer International Publishing, Cham, pp 283–306

Chapter 4. Hydrothermal synthesis of CuNWs, AZO, and GZO-NFs: Evaluation of potential properties for usage as the bottom electrode organic solar cells

4.1 Introduction

In this chapter the production of bottom electrodes for solar cells utilising metal nanowires as the main focus of the device is explored. CuNWs are a viable option to be utilized as a bottom transparent electrode due to its properties which include its excellent metal conductivity [1], low production cost, and flexibility [2]. Beside these ideal properties the nanowires might have, there are still undesirable properties that hinder its usage in many electronic systems. These issues include how easily copper can be oxidized [3] and its poor adhesion to most substrates [4]. These issues have to be addressed in order to increase the viability of CuNWs being used more widely.

Over the years various methods have been attempted to better protect the CuNWs and address the other issues around them (such as the poor adhesion). Some of these methods have included metal coatings (such as nickel [5, 6], silver [7–9]), metal oxides (such as TiO_2 [10, 11], ZnO [12, 13], AZO [14, 15]), and graphene [16–18]. Not all of these methods are ideal though as some methods require expensive techniques to synthesize the films or the materials required are expensive and make the films an unattractive concept to attempt to mass produce as the costs of the materials outweigh the potential returns. From these techniques metal oxides (with focus on ZnO and AZO) have demonstrated favourable results in solar cell devices obtaining higher PCEs compared to the other options and will be further examined here.

The synthesis method of the CuNWs also needs to be carefully chosen as the method influences the size and shape of the products. There are three main different types of synthesis methods which include vapor-phase synthesis [19, 20], templated synthesis [21, 22], and solution-phase synthesis [23, 24]. For various past studies solution-phase synthesis, namely using the hydrothermal method, has been the favoured synthesis method of CuNWs. This is due to the solution-phase synthesis having many advantages over the other types of synthesis such as low cost, easy scalability, and

relatively low synthesis temperature methods [25]. This method also allows for various substrates (organic or inorganic) as well as solutions (aqueous or organic) to be used in the depositing and growth processes [26, 27]. It is for these reasons that the hydrothermal method is an ideal method to follow.

This chapter reports on the synthesis of the CuNWs using the hydrothermal method as well as the protective layers of AZO-NFs and GZO-NFs. The properties and characteristics of the various synthesized samples will be examined in order to confirm the successful synthesis as well as their properties to be used in a solar cell device.

4.2. Experimental section

4.2.1 Synthesis of copper nanowires

The hydrothermal method was used in the synthesis of CuNWs. Initially 0.0607g copper chloride (5.65 mmol/l) and 0.0394g ascorbic acid (2.8 mmol/l) were stirred together with 40 ml of deionized water until the solution was completely dissolved. $CuCl_2$ was used over other metal salts due to the ease at which the Cl^- controls the growth of the CuNWs [28]. Then 0.5713g of ODA (26.5 mmol/l) was also stirred in 40 ml of deionized water until it was completely dissolved. The two mixtures were then added into a larger beaker which was followed by the solution being magnetically stirred together for 1 hour until the final mixture was a blue emulsion (Figure 4.1(a)) which was then placed into an autoclave and then in an oven heated at 120℃ for 20 hours.

During the synthesis process unwanted by-products also formed (copper nanoparticles and nanocubes) which may pose the risk of reducing the transmittance and potential efficiency of the solar cell and need to be removed along with any reactants that might not have been completely used up. For the cleaning of CuNWs solution it was first mixed with 80 ml deionized water and centrifuged at 2500 rpm for five minutes to remove any excess ODA, Cl^-, and other chemicals in the solution. Thereafter, the solution was mixed with an equal amount of n-hexane and deionized water to separate the CuNWs from the CuNPs that also would have formed in this reaction which was done before by Pradel *et al*. [29] which can be seen in Figure 4.1(b). This step was repeated five times before the final product was placed in isopropanol to prevent any oxidation of the CuNWs during the storage period.

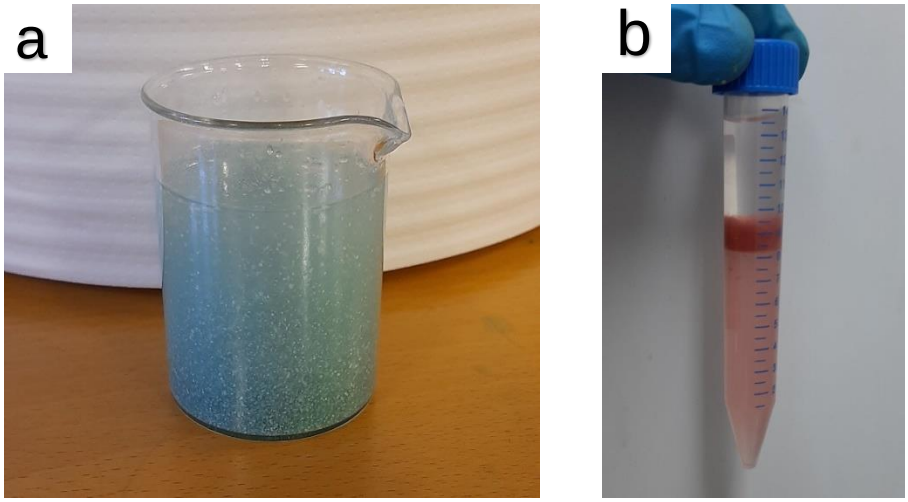

Figure 4. 1: (a) Final Blue emulsion mixture for CuNWs synthesis and (b) hydrophobic separation process of CuNWs

4.2.2 Synthesis of aluminium- and gallium-doped zinc oxide nanoflakes

For the synthesis of AZO, 2g of zinc acetate was added into 10.9 ml of deionized water until it was completely dissolved. While the initial solution mixed, 0.436g of NaOH pellets were first crushed with a mortar and pestle to make them dissolve quicker before being mixed with 10.9 ml of deionized water and stirred until they were completely dissolved. This solution was then added dropwise into the zinc acetate solution very slowly to prevent a white precipitate from rapidly forming. Thereafter, 0.08345 g (2 mol%) of $Al(NO_3)_3{\cdot}9H2O$ was stirred with 5 ml of deionized water and then added to the solution dropwise once more. The solution was then left to stir at 850 rpm for 4 hours. For the entire procedure the solutions were kept at 65 ^{o}C on a hot plate to encourage the growth of the nanoflakes. Once the process was complete the final solution was cleaned via centrifugation at 5000 rpm for 2 minutes which resulted in the AZO-NFs to gather at the bottom of the holder. The water along with unwanted chemicals were removed with a pipette, thereafter ethanol was added and the centrifugation process was repeated three more times to ensure the AZO NFs were cleaned.

Similar steps were followed for the synthesis of GZO, however instead of $Al(NO_3)_3{\cdot}9H_2O$, 0.0609 g (2 mol%) of $Ga(NO_3)_3{\cdot}H_2O$ was used.

4.2.3 Deposition of CuNWs films

The CuNWs were deposited onto the films via drop casting-method onto the polymer substrates (PET, PC, PES and PEN), which yielded a fairly equal distribution of the nanowires. For the nanowires, coating with AZO and GZO the spin-coating technique was used, and the solutions were spin-coated over the nanowires at 2000 rpm once. Figure 4.2 shows the deposited layers on a polycarbonate film to illustrate how they appear after coating.

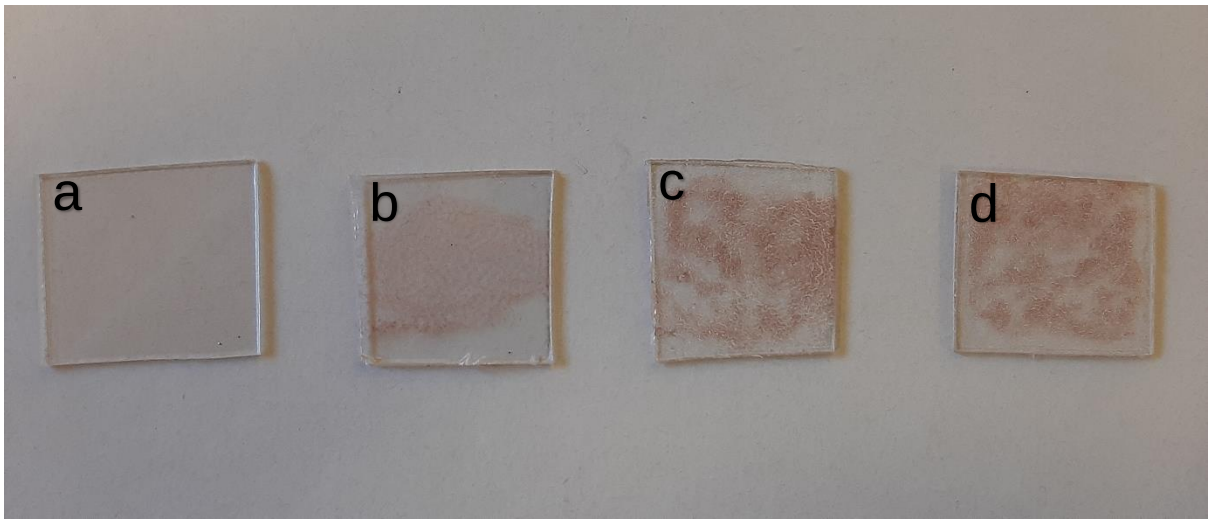

Figure 4. 2: a) Bare PC, b) PC/CuNW, c) PC/CuNW/AZO-NFs and d) PC/CuNW/GZO-NFs

4.2.4 Characterisation of films

Using a JEOL JSM-7800F field emission scanning electron microscopy (SEM) which is coupled with an Oxford Aztec 350 X-Max80 electron dispersive spectroscopy (EDS), the morphology and chemical composition were observed while being kept under vacuum pressure of 9 x 10^{-5} Pa for the measurements. This was followed by using a Rigaku smartLab X-ray diffractometer (Cu Kα, 45kV and 200 mA) to determine the crystallite size and phase of the prepared films. Perkin Elmer Lambda 650 S UV/VIS Spectrophotometer was used to obtain the optical transmittance as well as the optical absorbance of the films. Atomic force microscopy (AFM) using WITec alpha300 A AFM microscope measurements were taken to determine the roughness and height of the various layers of the films.

4.3. Results and discussion

4.3.1 XRD analysis

Figures 4.3– 4.6 presents the XRD pattern of the synthesized CuNW, AZO-NFs and, GZO-NFs deposited onto the various substrates (PC, PEN, PES and PET). The broad and intense diffraction peaks in the films 18º-25º (for PC Figure 4.3), 24º-28º (for PEN Figure 4.4), 13º-24º (for PES Figure 4.5) and, 22º-28º (for PET figure 4.6) are linked to their respective polymer substrates. These polymer substrates were confirmed using PDXL software containing standard database corresponding to the following card numbers: for PC 00-060-1506, PEN 00-061-1411, PES 00-066-1658 and, PET 00-061-1413. For the CuNWs pattern, diffraction peaks at 2θ = 43.36º and 50.64º which corresponds to the (111) and (200) lattice planes of copper face-centered cubic structures with a preferred orientation of (111) which was confirmed with the reference card number: 03-065-9026 from PDXL. This is an important aspect to note as it signifies that pure CuNWs had been formed since no peaks for either copper oxide or copper nanocubes had been detected. This confirmed the successful synthesis as any of these impurities would impact the electrode negatively, reducing the conductivity and making them unusable as electrodes [12]. These are most noticeable from the NWs deposited on the PC and PES substrates. Although the peaks can still be found in the PEN and PET substrates when zoomed in due to their low intensity compared to the substrate used, this is a result of the layer of CuNW being far thinner than the substrate layer thus the intensity from the CuNWs is reduced. For both AZO-NFs and GZO-NFs, the XRD patterns did not yield the expected results compared to previous XRD studies on AZO- and GZO-NFs from the literature. However, this could be due to interference from the substrates broad and intense peaks that were observed in the patterns. Regardless of this, cubic structures with a preferred orientation of (202) plane were observed.

Using the Debye-Scherrer's formula (equation 4.1) [30] the crystallite size of the prepared CuNWs, AZO and GZO-NFs were determined:

$$D = \frac{k\lambda}{\beta \cos\theta} \quad (4.1)$$

where *D* is the crystallite size, *k* is a dimensionless constant which has been taken to be 0.94, *λ* is the wavelength of X-ray radiation (1.5406 Å) for CuKα, *β* is the full width

at half maximum for the main peak (converting the degrees to radians), and θ is the angle of diffraction. Using equation 4.1, the crystallite size for the CuNWs of the most prominent peak (111) at 43.36^{o} was found to be ~24.51 nm. This is an important aspect to note as it is linked to the strength of the copper nanowires, as a decrease in the crystallite size can result in a decrease in the strength of the nanowires [31]. It has also been observed that an increase in the crystallite size results in a decrease in the strain value which impacts the strength of the nanowires [32]. For the AZO-NFs and GZO-NFs the crystallite size was found to be ~11.08 nm and ~10.19 nm, respectively. The smaller crystallite size of the GZO-NFs indicates that it might have a lower structural strength than the AZO-NFs which will be discussed further, later in chapter 5, with the tensile test. Table 4.1 summarizes the results of the crystallite size results and used values to obtain it.

Table 4. 1: XRD sample details with regards to FWHM, plane orientation and, crystalline size

Sample	FWHM (deg)	Lattice Plane	D (nm)
CuNW	0.3487	(111)	24.51
AZO-NFs	0.7603	(202)	11.08
GZO-NFs	0.7921	(202)	10.19

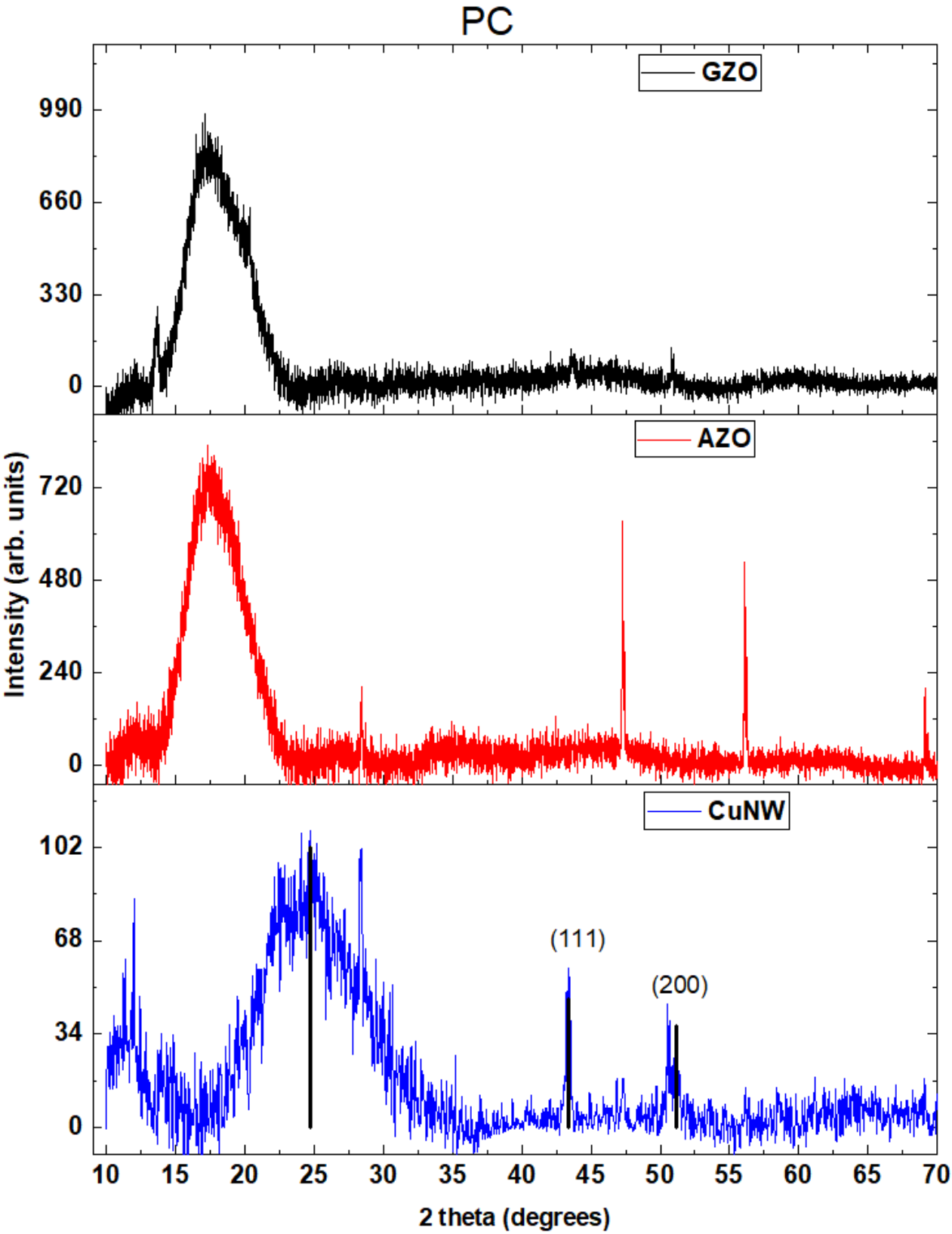

Figure 4. 3: XRD pattern of the CuNW, AZO-NFs and, GZO-NFs on PC substrate

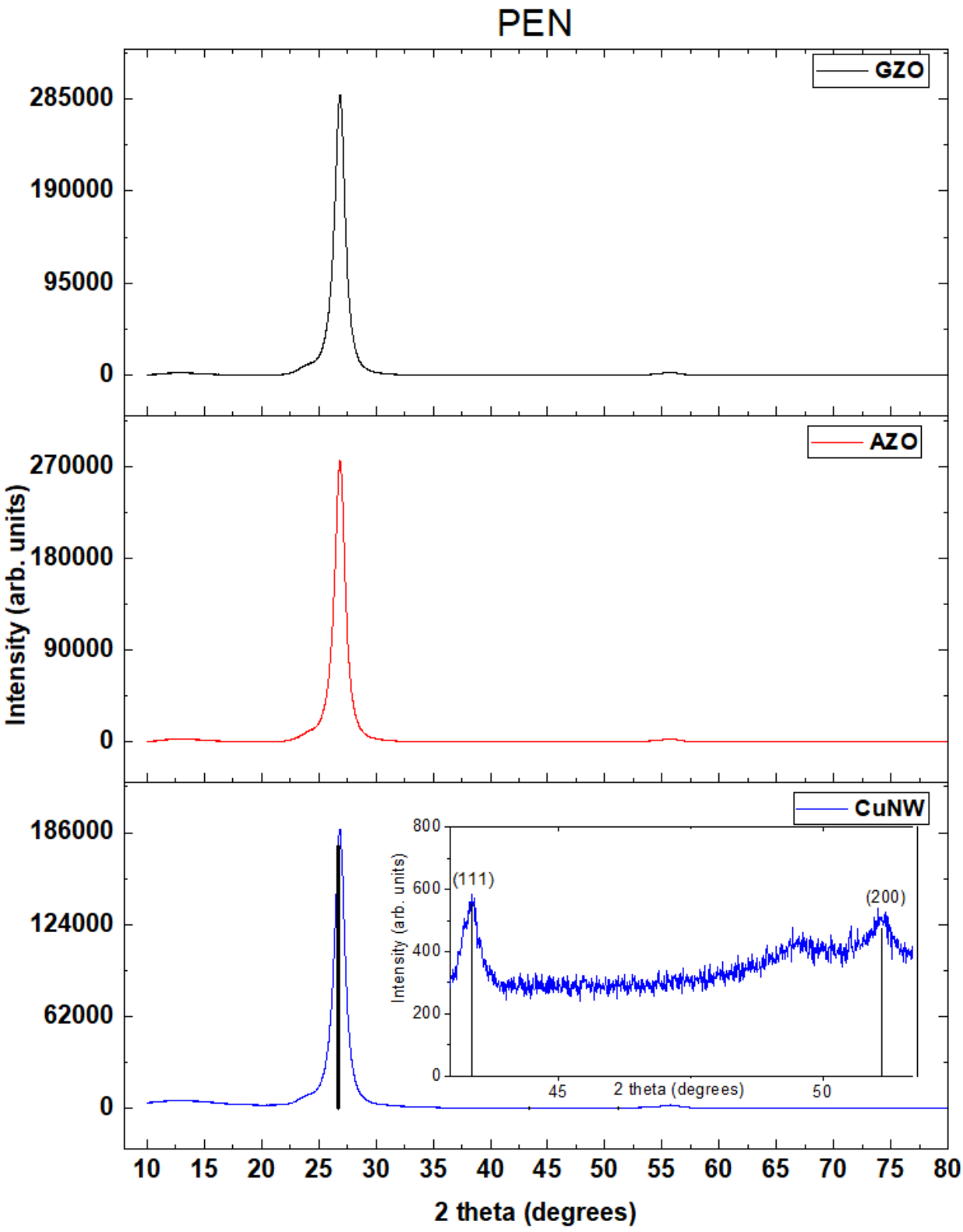

Figure 4. 4: XRD pattern of the CuNWs, AZO-NFs and, GZO-NFs on PEN substrate

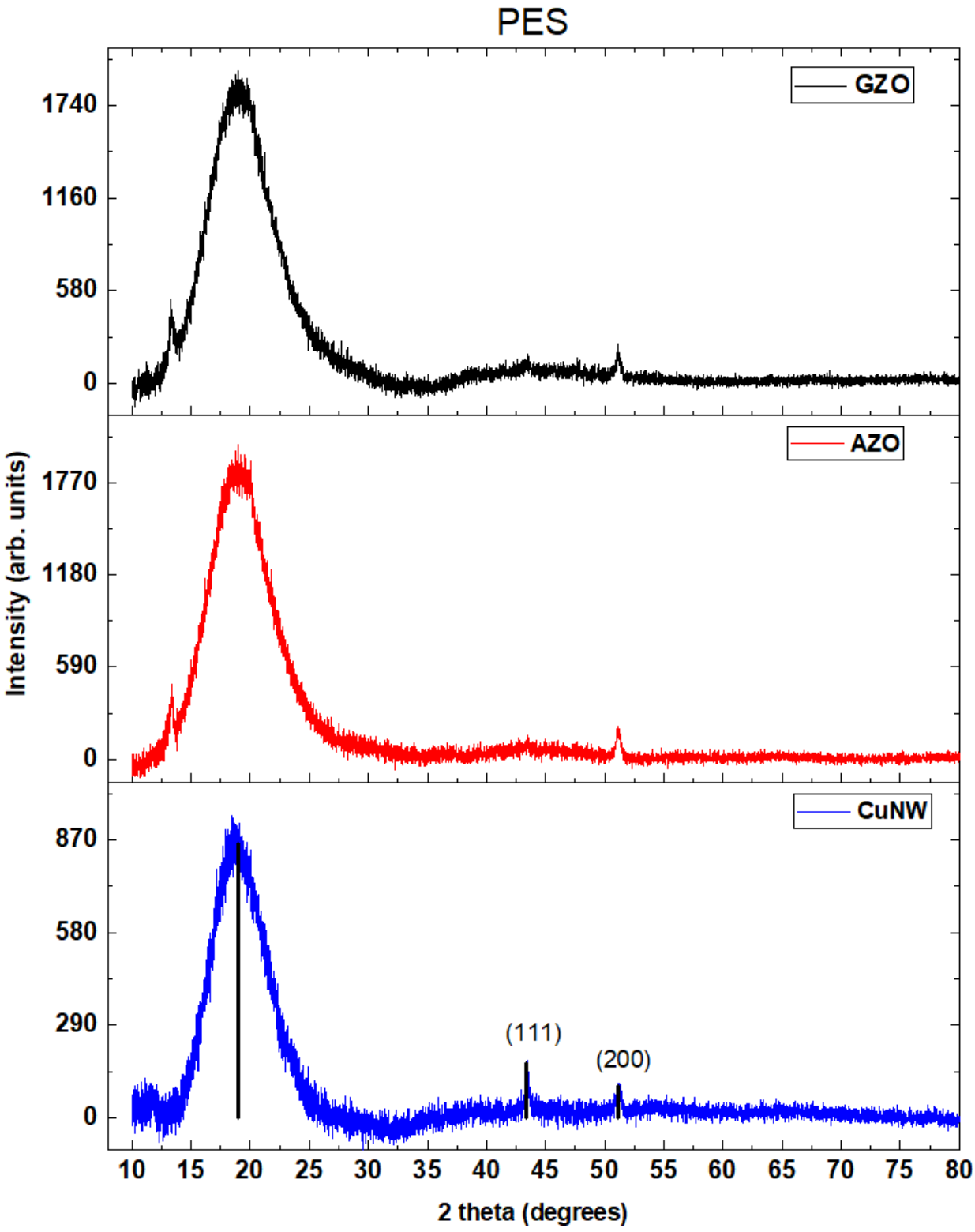

Figure 4. 5: XRD pattern of the CuNWs, AZO-NFs and, GZO-NFs on PES substrate

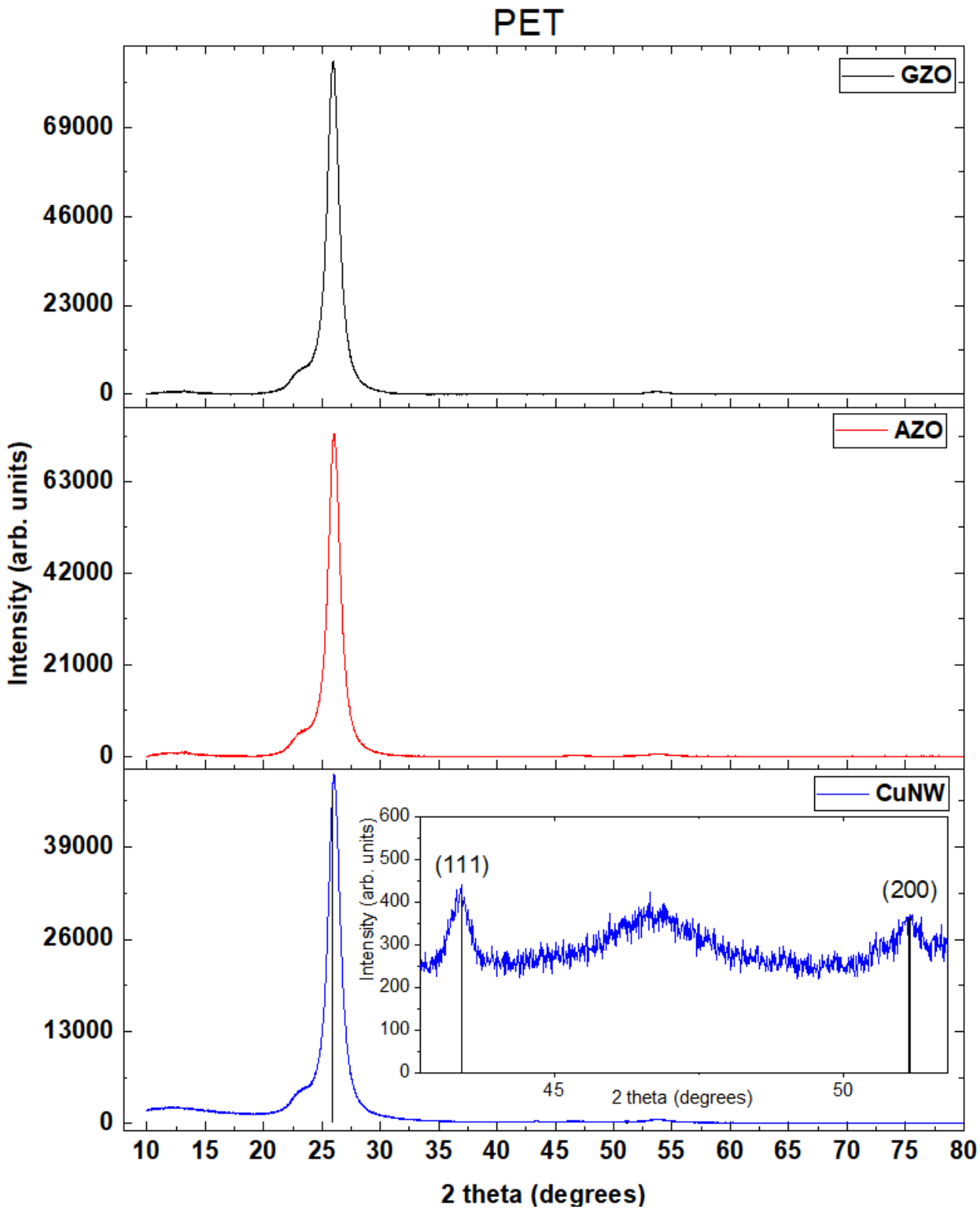

Figure 4. 6: XRD pattern of the CuNWs, AZO-NFs and, GZO-NFs on PET substrate

4.3.2 SEM and EDS analysis

Figures 4.7 – 4.10 present the SEM images for the CuNWs, AZO-NFs, and GZO-NFs respectively. As can be observed from Figures 4.7 to 4.10, multiple, long, and smooth CuNWs were successfully synthesized and that the final cleaning steps were able to remove the majority of the unwanted copper nanoparticles. This is a necessary requirement in order to achieve both a high electrical conductivity and suitable transmittance for the bottom electrodes. The average diameter of the CuNWs was found from images to be 112.82 ± 1.2 nm which was found from the Gaussian distribution in Figure 4.11 with an ultra-long length of over 50 μm. This is an excellent result as other studies have found that larger aspect ratios result in lower sheet resistance in electrodes [33]. Smooth CuNWs are also important for the electrode as smoother CuNWs have a reduced light scattering effect which is an important parameter to have for thin films designed to be used in solar cells as that directly impacts the transmittance of the films[34].

The SEM images for AZO and GZO-NFs were also recorded. The NFs can be observed to be well layered on top of one another and this uniform spread of the NFs will be beneficial for the protection of CuNWs against potential oxidation. This spread of nanoflakes can also be observed to be layered on top of one another. This layering effect has been observed in other nanoflake materials to improve the tensile strength of the films. The increased surface areas in contact with one another of the flakes compared to particles results in more friction between the layers thus improving the tensile strength of the film [35, 36].

The SEM images for the GZO-NFs appeared similar to that of the AZO NFs and would potentially share similar properties with regards to protection of the CuNWs as well as the tensile strength.

Despite the promising potential properties, the NFs layers possess, it can be observed in the images that neither the AZO-NFs or the GZO-NFs completely covered the deposited CuNWs. This can be remedied by either additional spin-coating steps, which will result in a thicker layer of the NFs thereby posing a risk of reducing transmittance and impacting the conductivity of the film, or by optimizing the spin-coating step to result in a more even distributed layer of NFs.

It can also be observed that in the PEN and PES samples the AZO-NFs and GZO-NFs were less uniformly spread out compared to the samples using PET and PC. This is most likely due to the different surfaces that the substrates have, indicating that for the particular sample PET and PC are better suited to be deposited on. This, however, can be remedied by changing the depositing parameters on the PES and PEN substrates to allow for a more uniform spread and can be done either by optimizing the spin coating method by altering the speeds and amount of solution dropped onto the substrate.

The EDS spectrum (Figures 4.12 a-e) of each of the samples were also recorded, confirming the elemental composition of the samples. The elemental mapping (Figure 4.12(a)) of the CuNWs indicates that the copper nanowires had been formed with no other trace metals detected. The unexpected chlorine from the mapping was linked to the precursor used in the synthesis of the nanowires ($CuCl_2$) and had potentially not been entirely washed away during the cleaning process. While having no immediate impact on the electrode the Cl^- could potentially impact any additional layers placed the electrode. The oxygen on the wires is also potentially linked to the oxidation of the CuNWs, which as previously mentioned, the CuNWs are especially susceptible to which has a negative impact on the conductivity of the electrode.

The elemental mapping (Figure 4.12(b)) of the AZO-NFs clearly shows that the AZO-NFs were composed of the aluminium (Al), zinc (Zn) and oxygen (O) elements. This is an indication that the synthesis process was a success, and that the aluminium was successfully doped into zinc oxide. However, for the GZO-NFs (Figure 4.12(c)), only zinc and oxygen were detected. This however, could be explained by the broad peak of the zinc with an energy position of 1.012 keV which is very close to the expected gallium peak of 1.098 keV. Also due to there being only a small amount of gallium in the sample (2 mol%) it could potentially not be completely detected during the elemental mapping. Inoperable

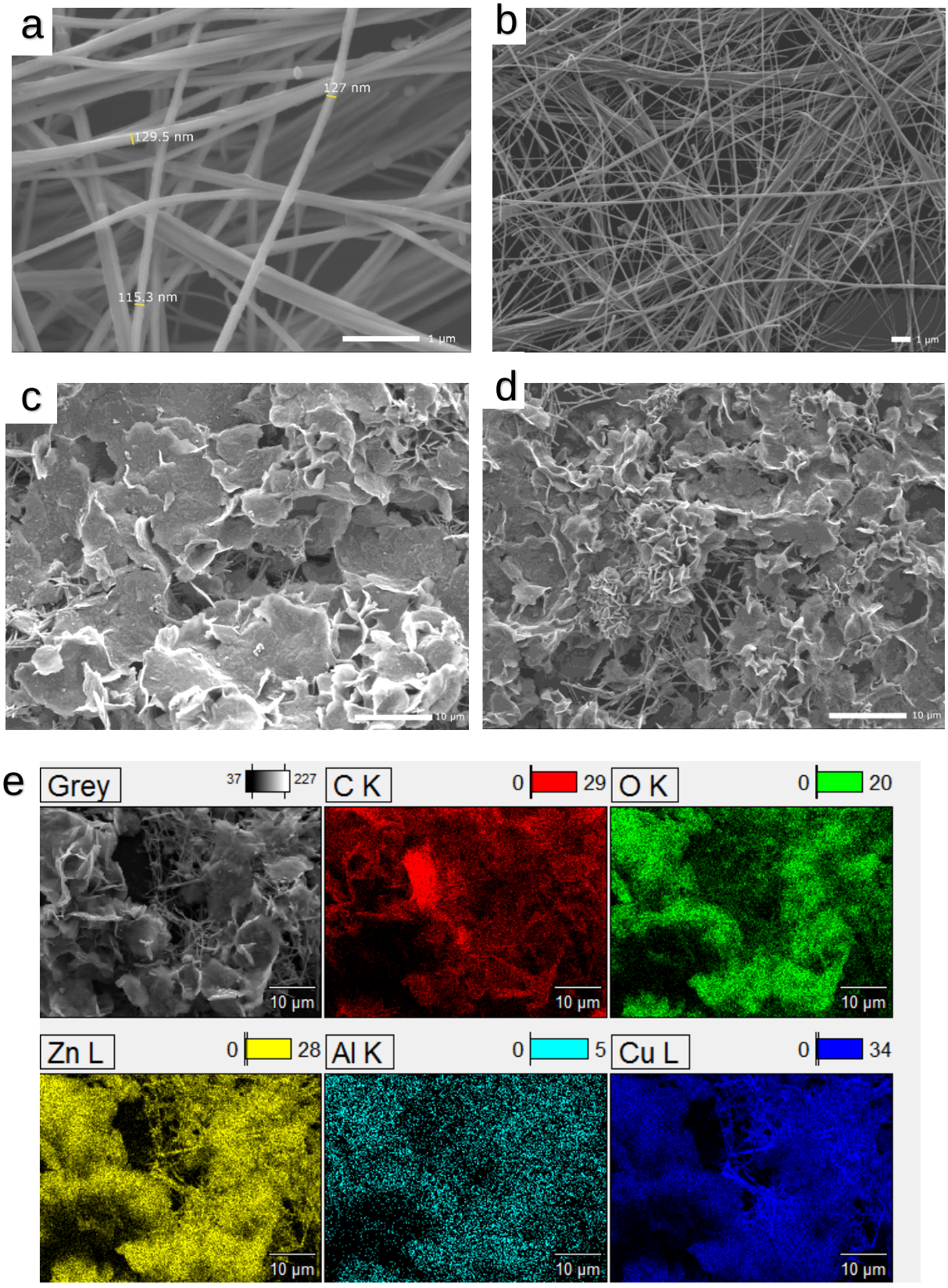

Figure 4. 7: SEM images of (a-b) CuNWs, (c) AZO-NFs/CuNWs, (d) GZO-NFs/CuNWs and, (e) elemental mapping of the AZO-NFs/CuNWs deposited on PC substrate.

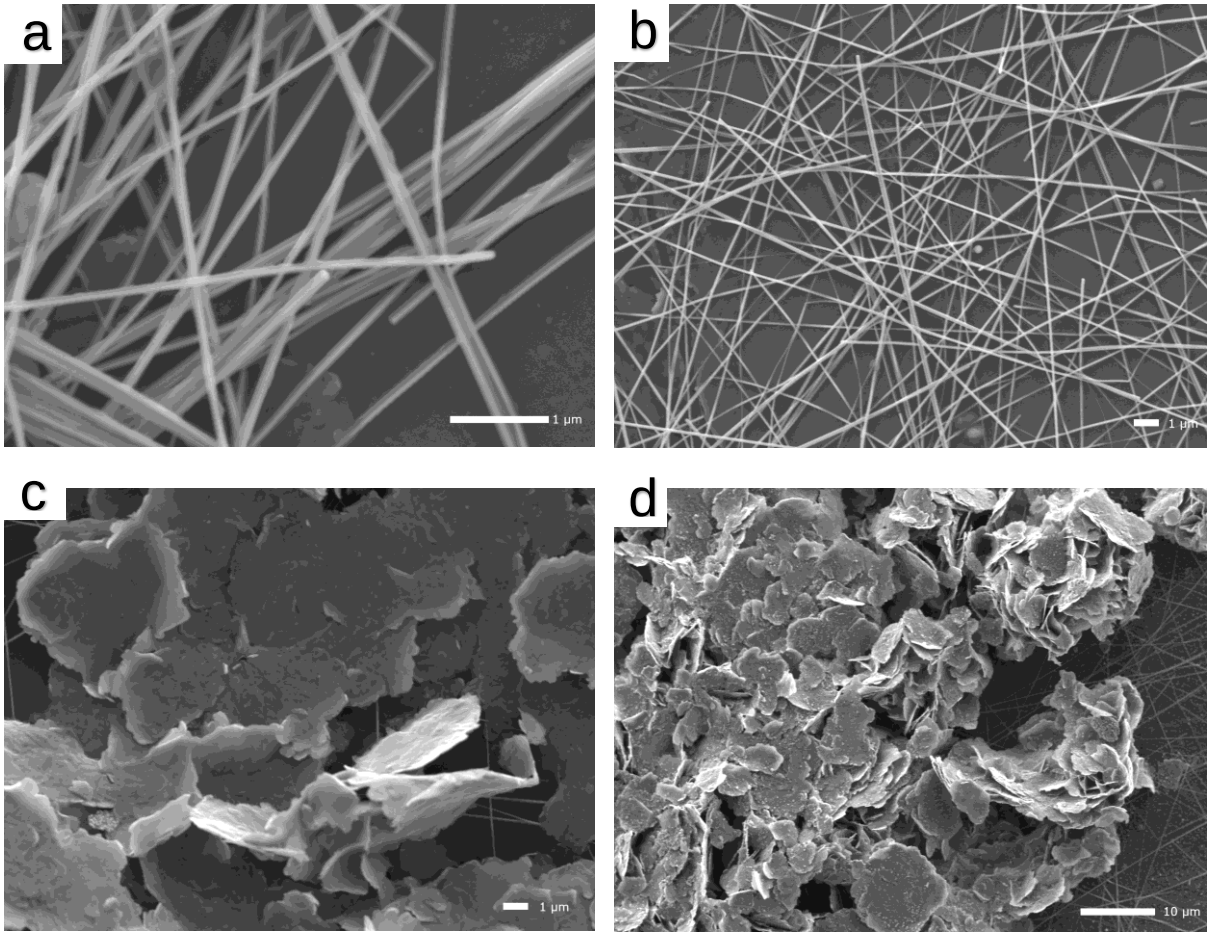

Figure 4. 8: SEM images of (a-b) CuNWs, (c) AZO-NFs/CuNWs and (d) GZO-NFs/CuNWs deposited on PEN substrate.

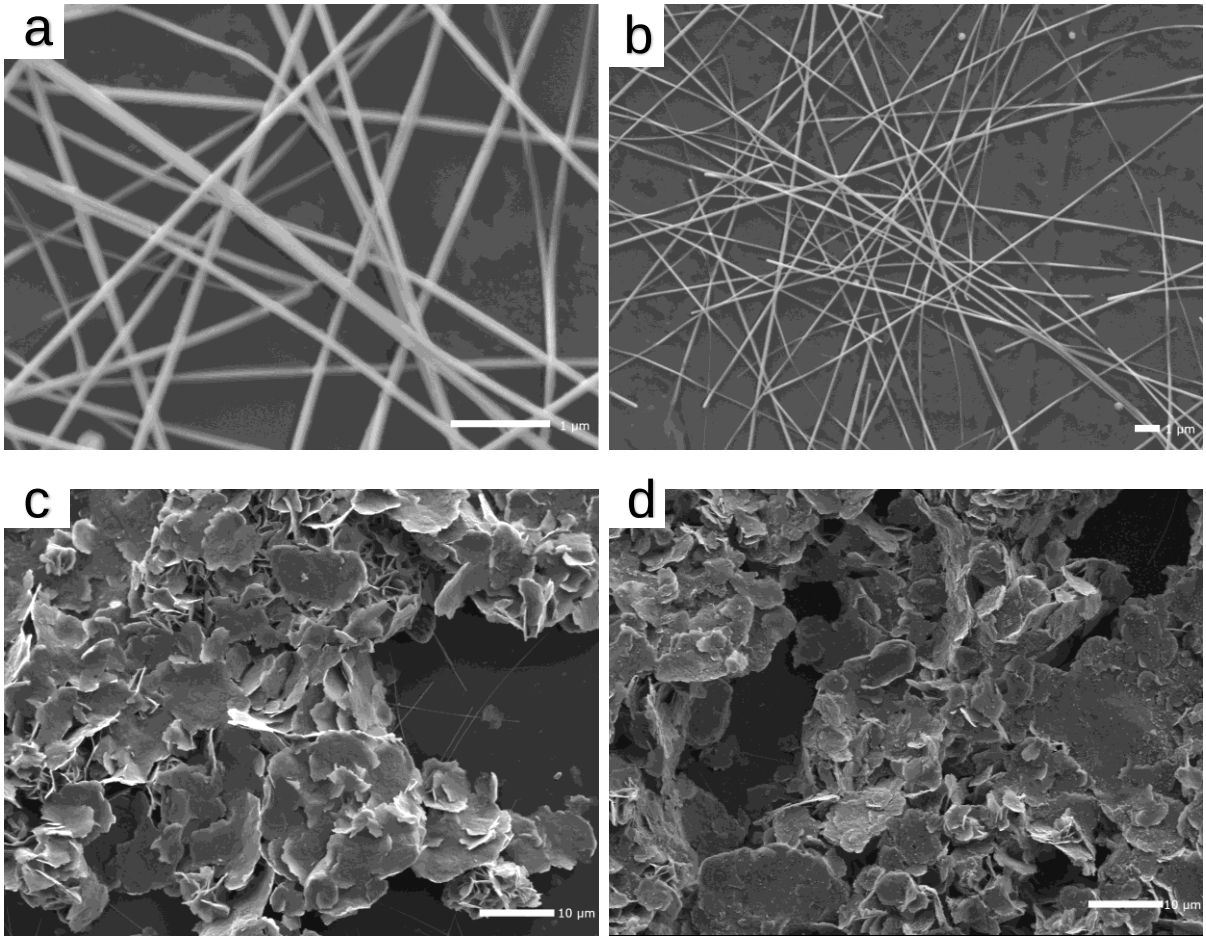

Figure 4. 9: SEM images of (a-b) CuNWs, (c) AZO-NFs/CuNWs and (d) GZO-NFs/CuNWs deposited on PES substrate.

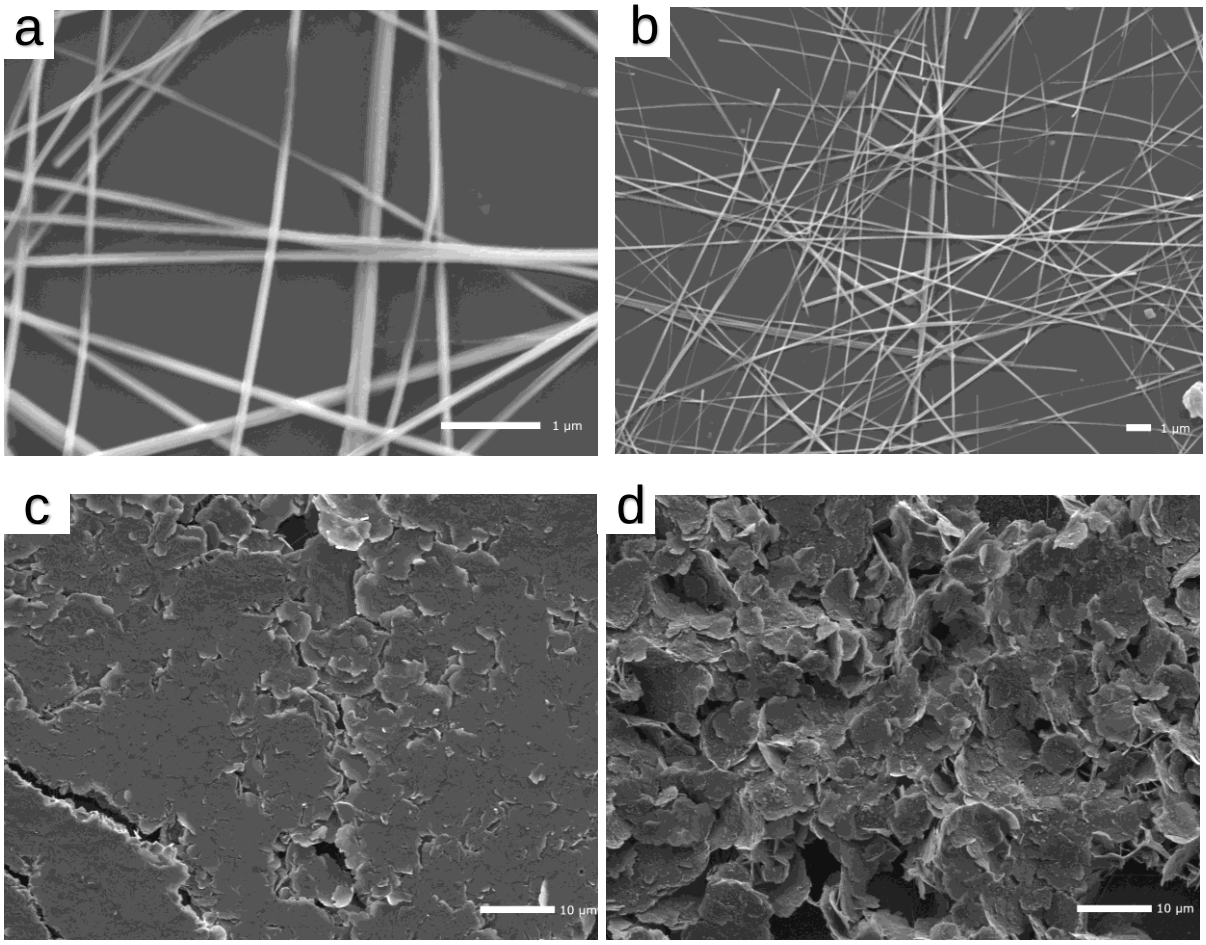

Figure 4. 10: SEM images of (a-b) CuNWs, (c) AZO-NFs/CuNWs and (d) GZO-NFs/CuNWs deposited on PET substrate.

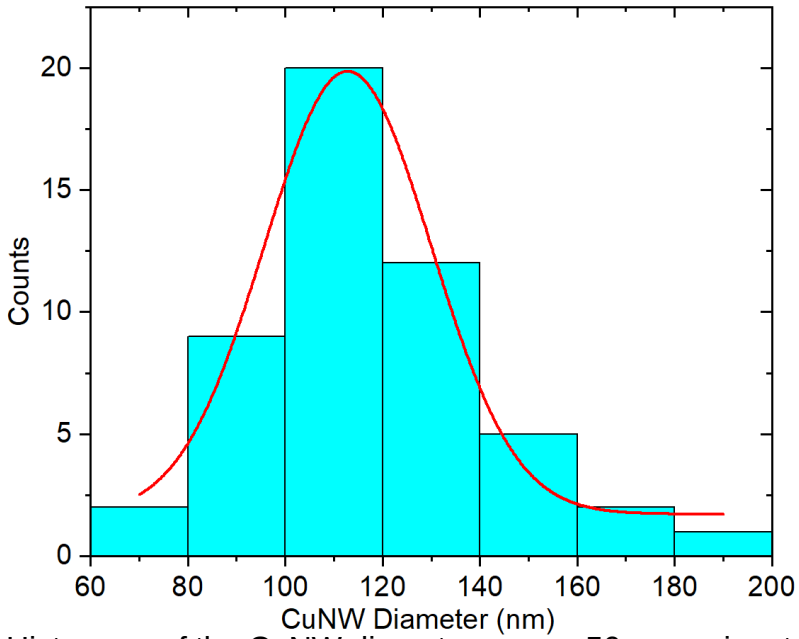

Figure 4. 11: Histogram of the CuNW diameter across 50 nanowires to determine the Gaussian distribution

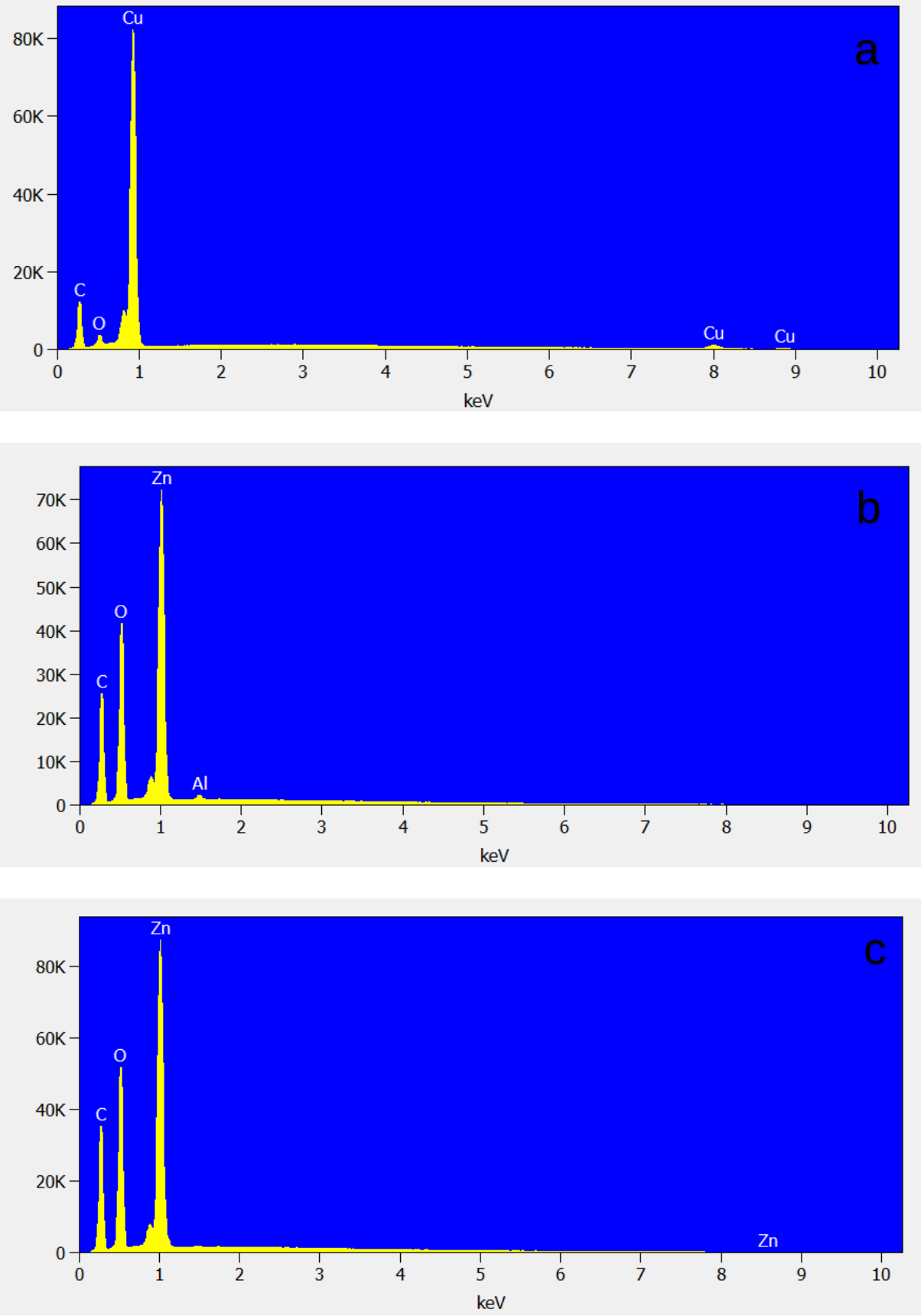

Figure 4. 12: EDS spectrum of (a) CuNWs, (b) AZO-NFs and (c) GZO-NFs

4.3.3 UV-VIS analysis

The optical transmittance and absorbance spectra of the prepared electrodes and the various coatings were prepared at room temperature and are shown in Figures 4.13-4.15. In Figure 4.13(a) the transmittance spectrum of the various bare polymer substrates was recorded and compared to one another. It can be seen, that while PC has the higher transmittance at λ = 550 nm, which is the standard method of comparing transmission results between samples. PET showed a slightly lower transmittance after PC, with the average transmittance of 88.64% across the entire visible range. By analysing the spectrum, the PET substrate tends to blue shift with the shorter wavelengths, while with PC, PES and, PEN are more inclined towards red shifted. This red shift is an indication of the decrease in optical bandgap that these polymer substrates will have in comparison to the PET substrate. Furthermore, the dropping in transmittance percentage closer to the λ = 400 nm range for the PC, PES and, PEN while the PET only dropped around λ = 300 nm, is an indication that the PET would be able to transmit more light into the solar cell and thus be more efficient in the harvesting of light which is ideal for solar cell applications.

When evaluating the transmittance for the deposited films (Figures 4.13 - 4.15 and Table 4.2) it is clear that as the layers of CuNWs, AZO-NFs and, GZO-NFs are deposited onto the substrates, the transmittance of the films reduces the transmittance efficiency. This is most noticeable in the films deposited on PC and PEN substrates with the largest deteriorations between them while with PET the deterioration was smaller than 5%. The reduction in the transmittance for AZO-NFs and GZO-NFs is attributed to the difference in crystallite size the two layers had, as well as the possible increase in film thickness. However, it should be noted that a layer of CuNWs alone, without coating with AZO and GZO-NFs, does not deteriorate the transmittance with a large margin. This is a good indication that CuNWs still retain light transmission efficiency.

The bandgap values of the films were also examined and reported on. The reason why the bandgap is an important factor for solar cells is that it indicates what energy the electrons have to have in order to be transferred to the next layer. In most single-junction cell a small bandgap value of around 1.5 eV is required for the greatest efficiency making smaller bandgaps more desirable. However, there are several drawbacks to using small bandgaps materials such as the photo-generated charge

carriers in them lose most of their energy which is a result of the thermalization down to bandgap energy [37], and that they do not permit visible light transmission [38]. Wide bandgap absorber materials can thus offer a new technological advancement in transparent solar cells and be potentially used in building integrated photovoltaic concepts [39]. Wide bandgap can also achieve higher voltages which is necessary to reduce the energy loss due to series resistance in solar cells [40].

To calculate the optical bandgap of the films Tauc's relation was used to estimate it using the equation 4.2 below [41]:

$$(\alpha hv)^n = K\left(hv - E_g\right) \quad (4.2)$$

Where α is the absorption coefficient, *hv* is the incident photon energy, *K* is a constant, E_g is the films optical bandgap and, *n* is the transition mode which depends on the nature of the material. *'n'* usually has two values that are used, $n = 2$ for direct transistions and $n = \frac{1}{2}$ for indirect transitions. For the purposes of this study the direct bandgap was looked at so $n = 2$. The bandgap was determined by evaluating the plot of a graph for $(\alpha hv)^2$ vs hv and extrapolating the linear portion of it. The unknown values of the formula can be found using the following equations:

$$\alpha = 2.302\frac{A}{t} \quad (4.3)$$

$$hv = \frac{1240}{\lambda} \quad (4.4)$$

where *A* is the absorbance of the film, *t* the thickness, and λ the wavelength of the light. The thickness of the film was determined from the AFM results. Using equation 4.3 and 4.4, Figure 4.15(b) was produced and the bandgap values of the films were found and summarized in Table 4.2.

As was anticipated, the PET substrate showed the higher overall bandgap of ~3.918 eV with the other substrates on the lower end of the spectrum. It should also be noted that the addition of the CuNW, AZO-NFs and, GZO-NFs layers reduced the bandgap values further which could be attributed to the lowered transmittance that was observed and the slight redshift.

Table 4. 2: Transmittance and bandgap characteristics of bare and coated polymer substrates

Substrate	Transmittance λ=550nm (%)	Average transmittance λ=380-800nm	Bandgap (eV)
Bare PC	90.23%	87.93%	3.271
PC CuNW	78.64%	78.44%	3.248
PC AZO	72.52%	72.79%	3.237
PC GZO	68.39%	69.27%	3.234
Bare PEN	87.11%	85.78%	3.205
PEN CuNW	81.55%	81.52%	3.204
PEN AZO	80.63%	80.07%	3.200
PEN GZO	74.54%	74.45%	3.198
Bare PES	74.80%	70.43%	3.127
PES CuNW	71.00%	67.48%	3.126
PES AZO	68.84%	65.21%	3.122
PES GZO	63.90%	60.97%	3.121
Bare PET	88.79%	88.64%	3.918
PET CuNW	86.70%	87.26%	3.916
PET AZO	85.83%	86.01%	3.917
PET GZO	82.97%	83.56%	3.915

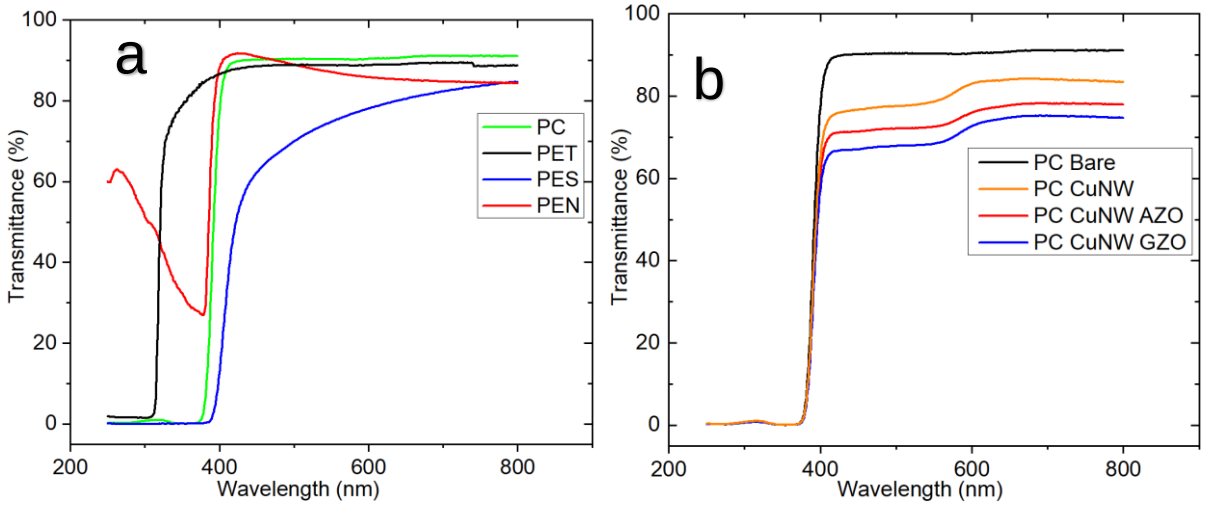

Figure 4. 93: Comparison transmittance spectra of (a) Bare and (b) Coated PC substrates.

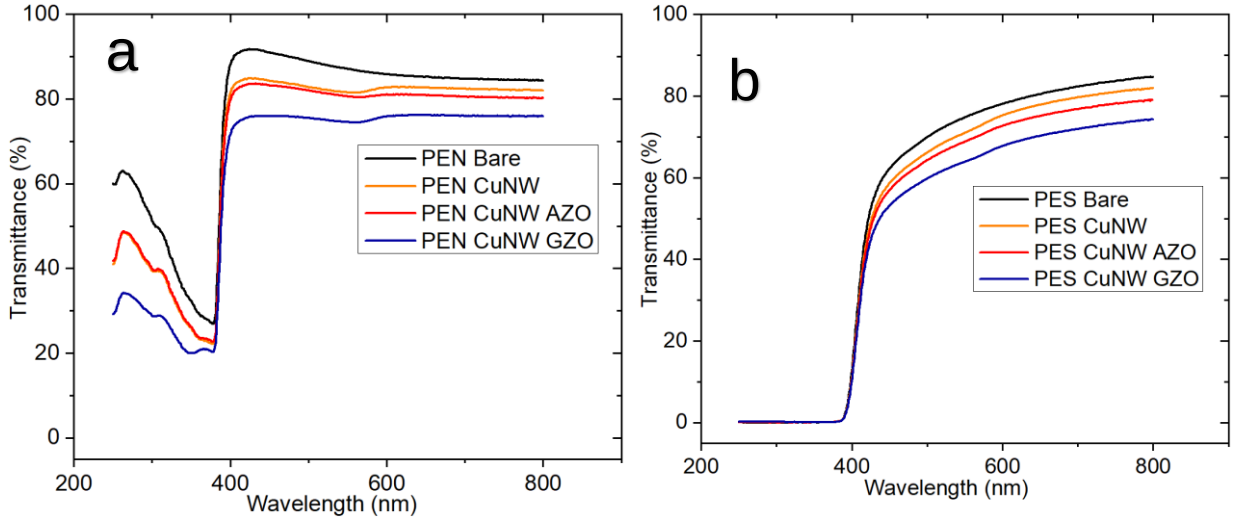

Figure 4. 104: Comparison transmittance spectra of (a) coated PEN and (b) coated PES substrates

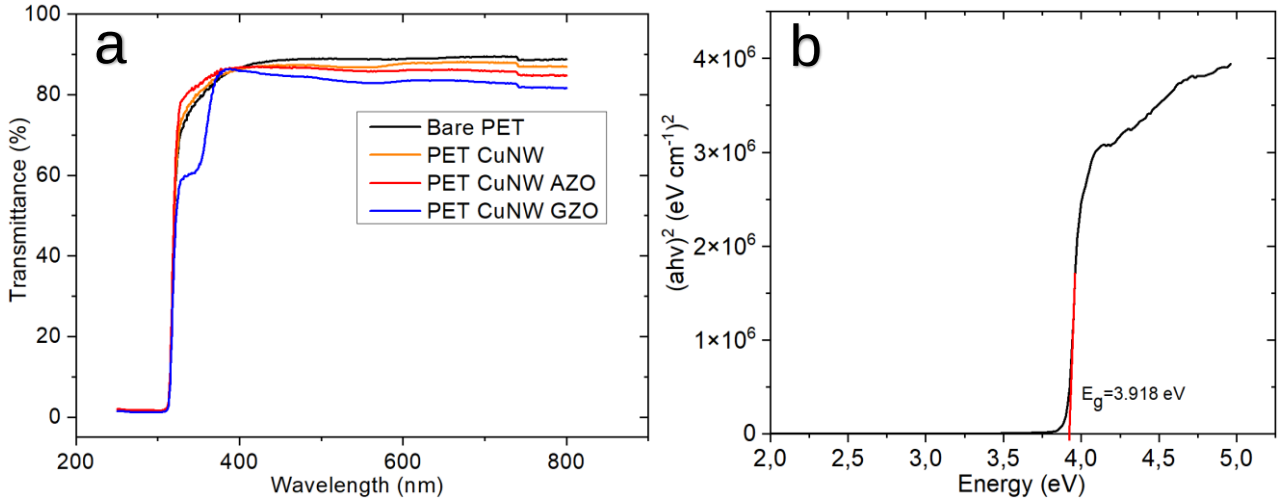

Figure 4. 115: Comparison transmittance spectrum of (a) coated PET films and (b) Bandgap estimation using Tauc's relation.

4.3.4 AFM analysis

Figures 4.16- 4.27 show the AFM images of the substrates and the layers that make up the bottom electrode. From the scans the roughness and height of the films were obtained using the Project 4 software and the obtained parameters are summarized in Tables 4.3 and Table 4.4. The roughness of the films increased with the addition of the various layers which was anticipated. The roughness of the GZO-NFs was more noticeable (excluding the PES sample) than the AZO-NFs which can be corroborated with the SEM images of the layers taken where the GZO-NFs were not all horizontally spread out and the larger gaps between the flakes observed would also contribute to this increase in the roughness. The roughness of the films has been associated with an increase in the light trapping for solar cell devices which results in the reflection losses being reduced and with gains in the optical length of the incident light inside the absorber layer [42, 43].

By using the height distribution of the various films, the average heights of each layer were found and recorded in Table 4.4. From this data it can be seen that the GZO-NFs had the thickest layer which could potentially have an impact on the observed roughness of the film.

Table 4. 3: Roughness values (nm) of the various substrates and the layers deposited onto them

	PC	**PET**	**PES**	**PEN**
	Roughness (nm)			
CuNWs	109.01	73.24	77.51	46.35
CuNW/AZO-NFs	154.28	318.09	455.59	347.00
CuNW/GZO-NFs	534.02	1054.39	330.90	797.30

Table 4. 4: Heights of the corresponding layers

	Height (nm)
Individual CuNWs	87.24
AZO-NFs	1022.43
GZO-NFs	2630.33

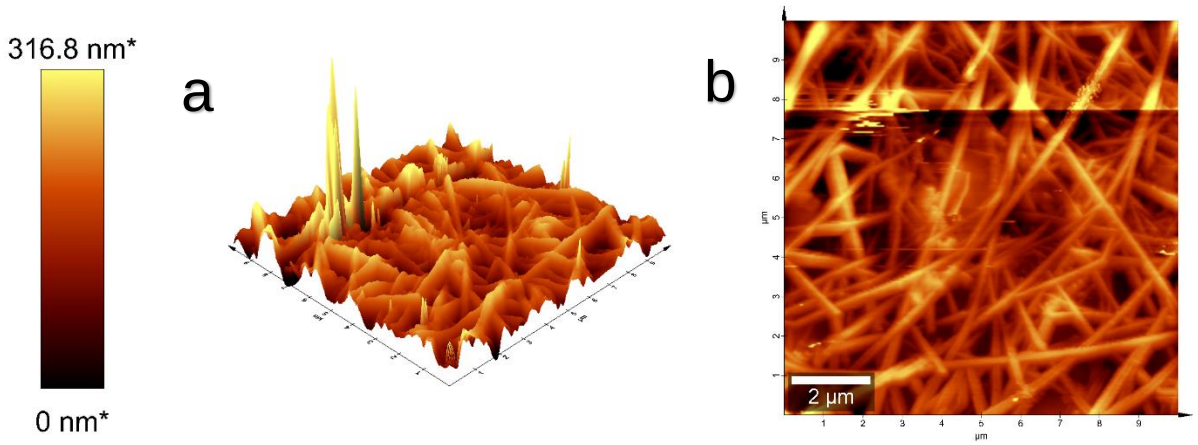

Figure 4. 126: AFM images of PC/CuNWs (a) 3D (b) 2D

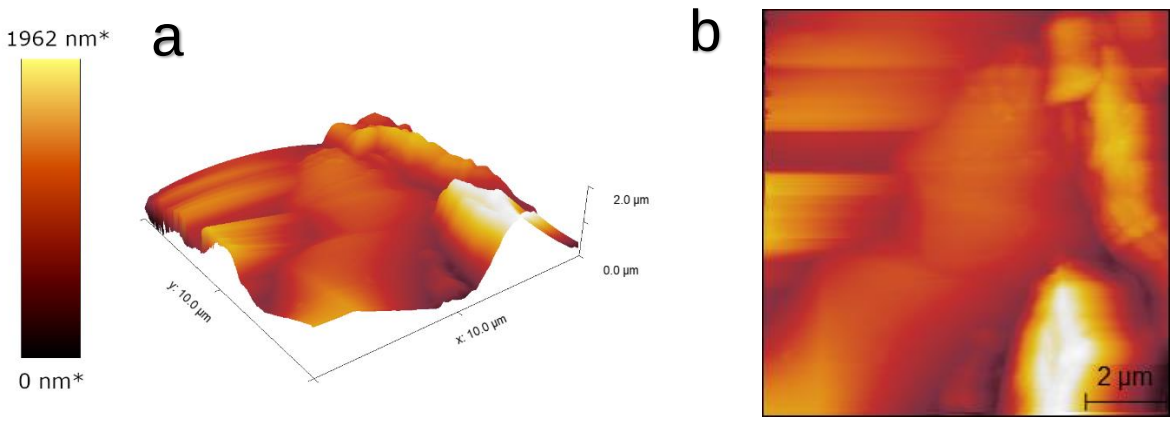

Figure 4. 137: AFM images of PC/CuNWs/AZO (a) 3D (b) 2D

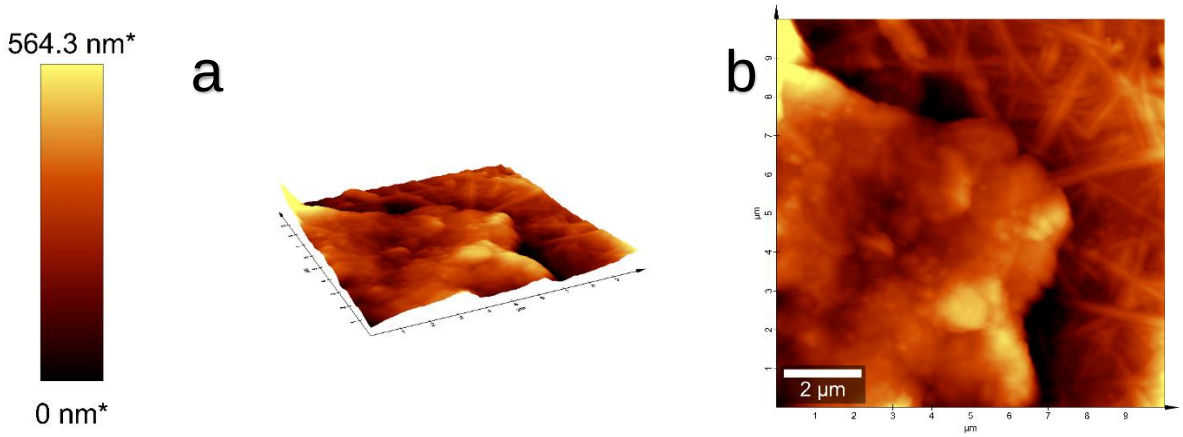

Figure 4. 148: AFM images of PC/CuNWs/GZO(a) 3D (b) 2D

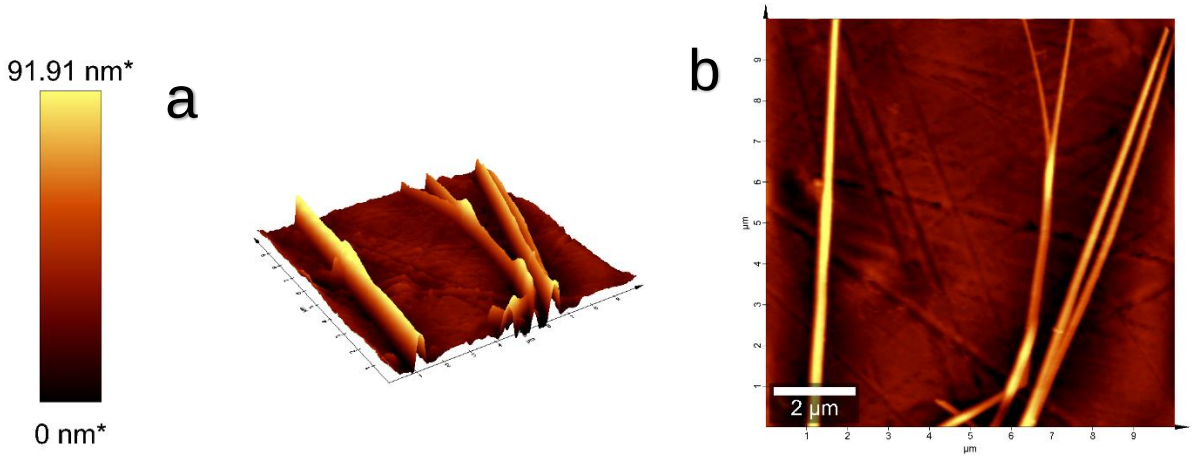

Figure 4. 159: AFM images of PEN/CuNW (a) 3D (b) 2D

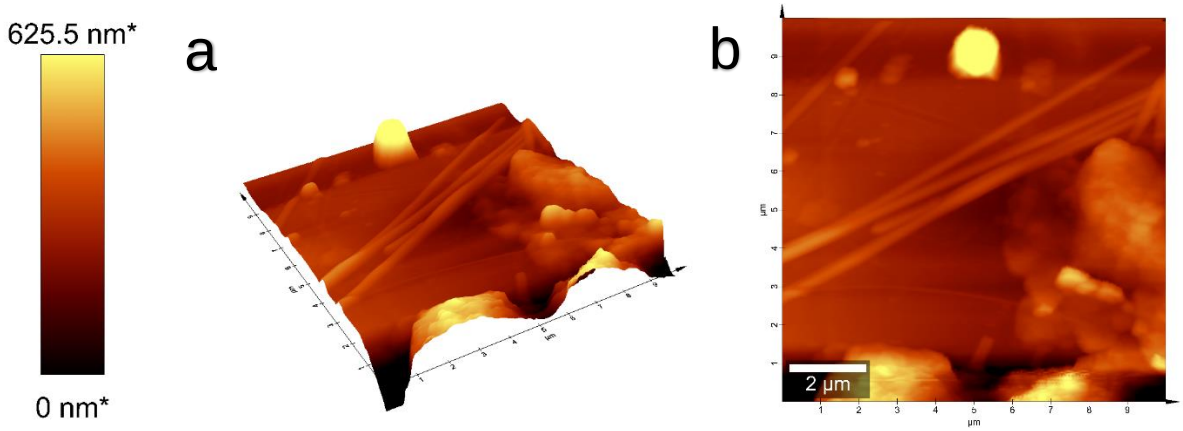

Figure 4. 20: AFM images of PEN/CuNWs/AZO (a) 3D (b) 2D

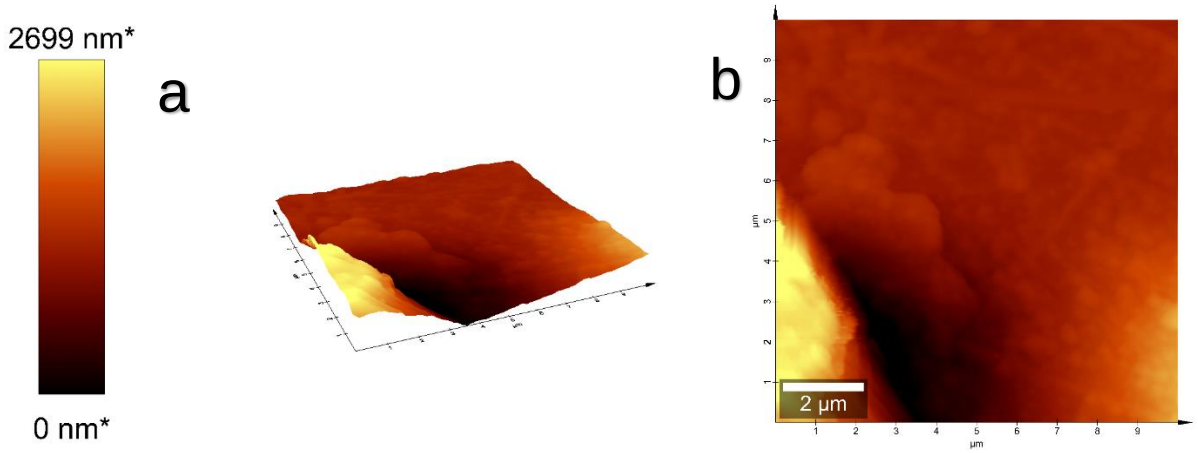

Figure 4. 161: AFM images of PEN/CuNWs/GZO (a) 3D (b) 2D

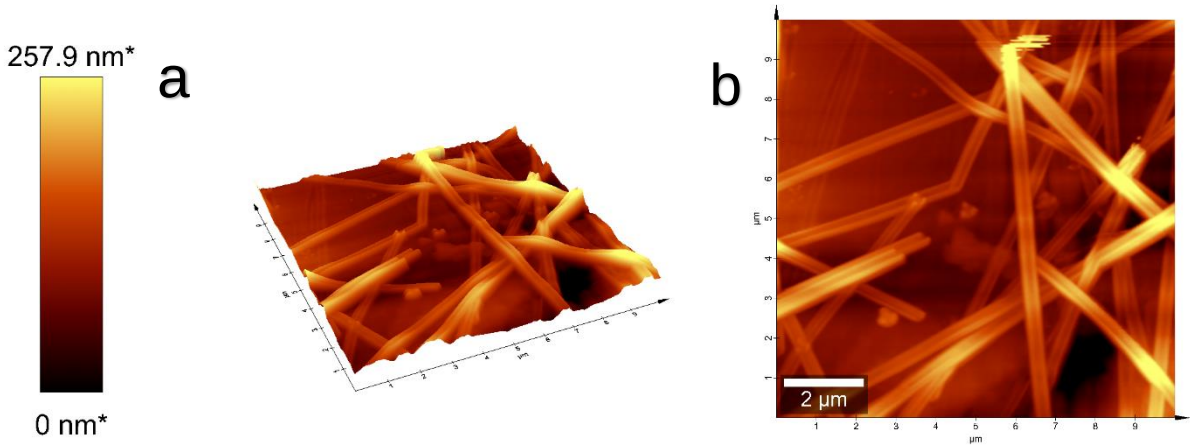

Figure 4. 172: AFM images of PES/CuNWs (a) 3D (b) 2D

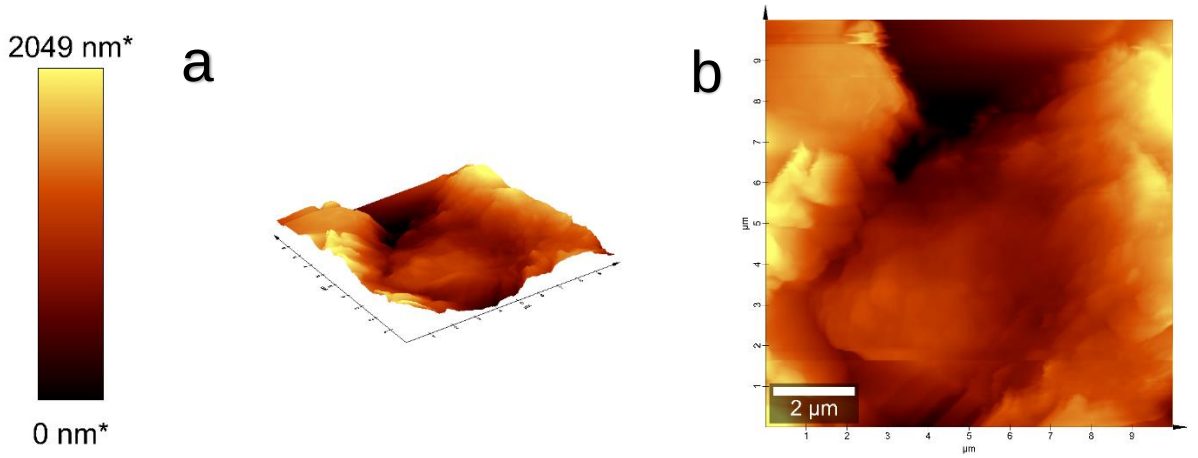

Figure 4. 183: AFM images of PES/CuNWs/AZO (a) 3D (b) 2D

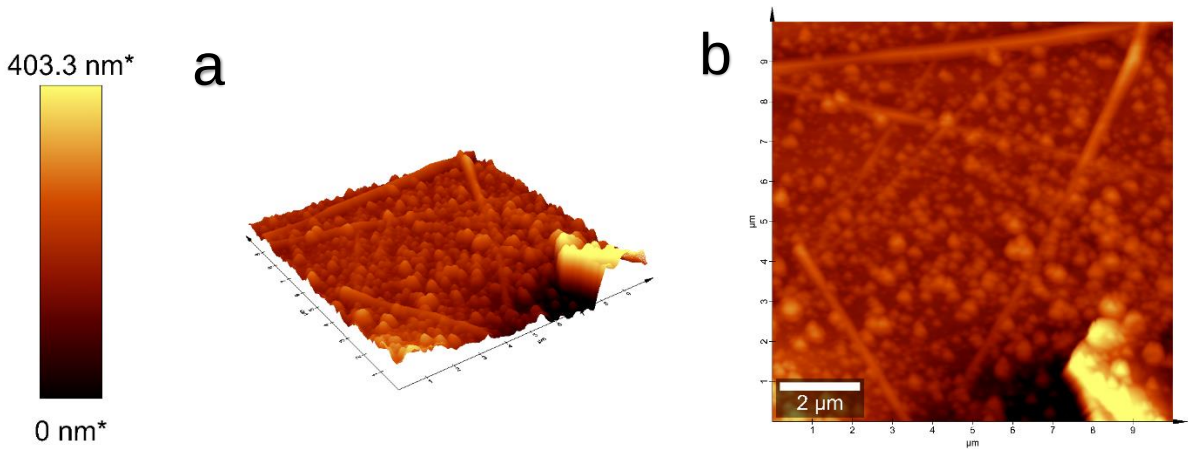

Figure 4. 194: AFM images of PES/CuNWs/GZO (a) 3D (b) 2D

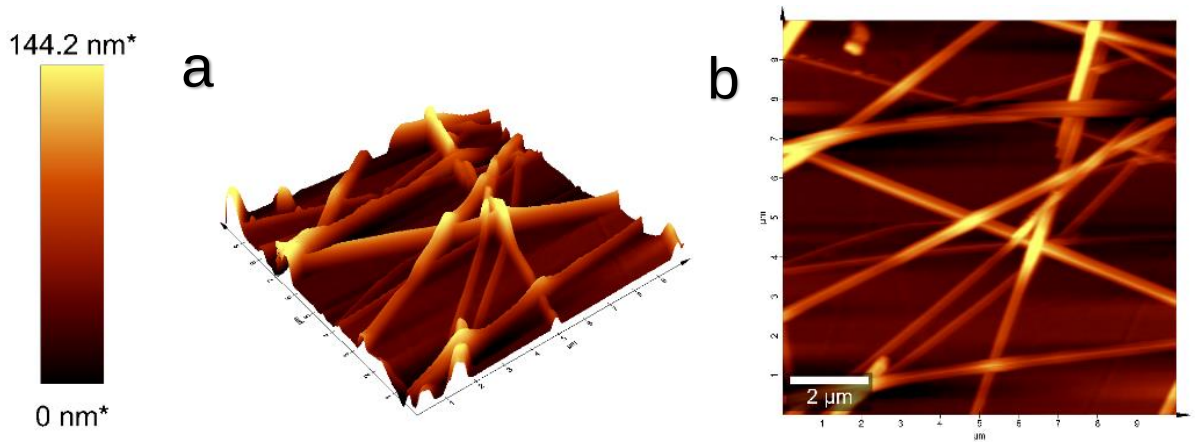

Figure 4. 205: AFM images of PET/CuNWs (a) 3D (b) 2D

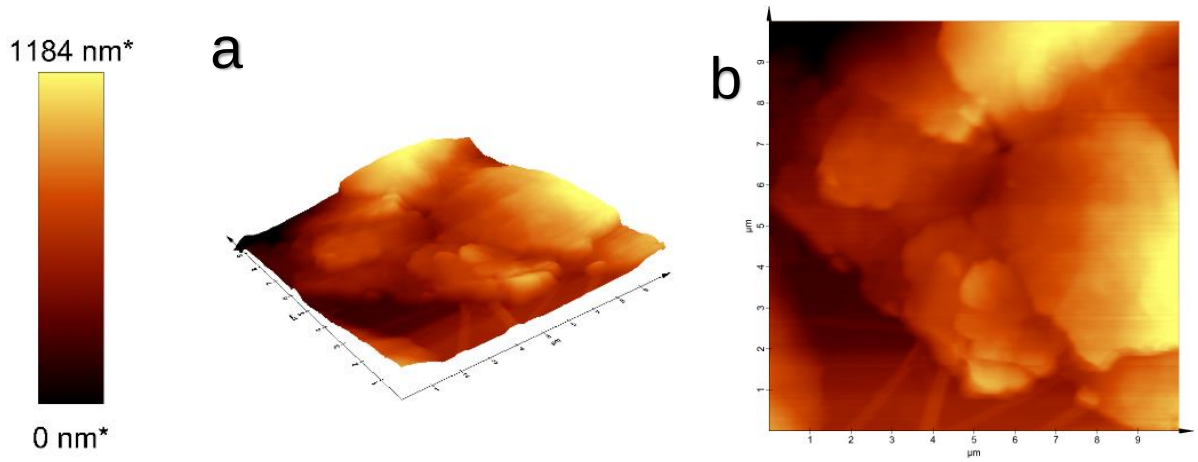

Figure 4. 216: AFM images of PET/CuNWs/AZO (a) 3D (b) 2D

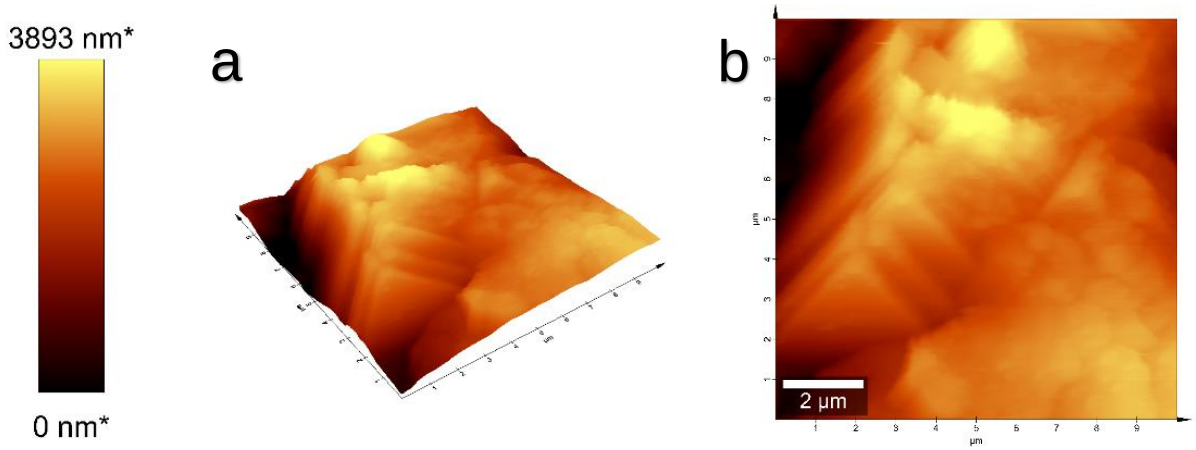

Figure 4. 227: AFM images of PET/CuNWs/GZO (a) 3D (b) 2D

4.4 Conclusion

CuNWs were succesfully synthesized using hydrothermal method and coated onto various polymer substrates. AZO- and GZO-NFs were used as protective layers which were then analysed. The XRD showed the cubic structure of the CuNWs, which confirmed the succesful synthesis of CuNWs. From the SEM images, ultra-long and thin CuNWs and a well distributed layer of NFs were observed. This will be ideal for protecting the CuNWs both from oxidation and potentially improve the tensile strength of the films. The UV-VIS spectra demonstrated that the PET substrate has the best transmittance over the others as well as the wide bandgap which is optimal for transparent flexible solar cells. It was also observed that AZO-NFs had a better transmittance on all films than GZO-NFs which is attributed to the dopants used as well as the smaller crystalite sizes. The AFM results indicated that while both the AZO-NFs and GZO-NFs increased the roughness of the film, the GZO-NFs increased it by the greatest amount which could be benificial for light trapping properties in photovoltaic devices if utilized correctly. From this it can be concluded that PET is the best substrate for the films in terms of transmittance, while both the AZO-NFs and GZO-NFs have their advantages.

References

1. Lin B, Gelves GA, Haber JA, Sundararaj U (2007) Electrical, Rheological, and Mechanical Properties of Polystyrene/Copper Nanowire Nanocomposites. Ind Eng Chem Res 46:2481–2487
2. Duong T-H, Tran N-H, Kim H-C (2017) Low cost fabrication of flexible transparent electrodes using copper nanowires. Thin Solid Films 622:17–22
3. Yu S, Li J, Zhao L, Wu M, Dong H, Li L (2021) Simultaneously enhanced performances of flexible CuNW networks by covering ATO layer for polymer solar cells. Solar Energy Materials and Solar Cells 221:99–113
4. Sun Y, Du C, Wu M, Zhao L, Yu S, Gong B, Ding Q (2020) Synchronously improved reliability, figure of merit and adhesion of flexible copper nanowire networks by chitosan transition. Nanotechnology 31:1–10
5. Stewart IE, Rathmell AR, Yan L, Ye S, Flowers PF, You W, Wiley BJ (2014) Solution-processed copper–nickel nanowire anodes for organic solar cells. Nanoscale 6:5980–5988
6. Zhang H, Wang S, Tian Y, Liu Y, Wen J, Huang Y, Hang C, Zheng Z, Wang C (2020) Electrodeposition fabrication of Cu@Ni core shell nanowire network for highly stable transparent conductive films. Chemical Engineering Journal 390:1–7
7. Luo X, Gelves GA, Sundararaj U, Luo J-L (2013) Silver-coated copper nanowires with improved anti-oxidation property as conductive fillers in low-density polyethylene. Can J Chem Eng 91:630–637
8. Zhao J, Zhang D, Zhang X (2015) Preparation and characterization of copper/silver bimetallic nanowires with core-shell structure. Surface and Interface Analysis 47:529–534
9. Navik R, Ding X, Huijun T, Zhao Y (2021) Facile Synthesis of Highly Oxidation Stable Nanosilver-Coated Copper Nanowires for Transparent Flexible Electrodes. Ind Eng Chem Res 60:263–272
10. Zhang Y, Zhou N, Zhang K, Yan F (2017) Plasmonic copper nanowire@TiO2 nanostructures for improving the performance of dye-sensitized solar cells. J Power Sources 342:292–300
11. Shi L, Wang R, Liu Y, Sun J (2020) A facile strategy for the preparation of hybrid copper nanowire-TiO2 film. Thin Solid Films 693:1–6
12. Chen Z, Ye S, Stewart IE, Wiley BJ (2014) Copper Nanowire Networks with Transparent Oxide Shells That Prevent Oxidation without Reducing Transmittance. ACS Nano 8:9673–9679
13. Duong TH, Hoang HM, Kim H-C (2019) A zinc-based shell for copper nanowires network to prevent oxidation. pp 1–5

14. Won Y, Kim A, Lee D, Yang W, Woo K, Jeong S, Moon J (2014) Annealing-free fabrication of highly oxidation-resistive copper nanowire composite conductors for photovoltaics. NPG Asia Mater 6:1–9

15. Yang H, Kwon HC, Ma S, Kim K, Yun SC, Jang G, Park J, Lee H, Goh S, Moon J (2020) Energy Level-Graded Al-Doped ZnO Protection Layers for Copper Nanowire-Based Window Electrodes for Efficient Flexible Perovskite Solar Cells. ACS Appl Mater Interfaces 12:13824–13835

16. Kholmanov IN, Domingues SH, Chou H, Wang X, Tan C, Kim J-Y, Li H, Piner R, Zarbin AJG, Ruoff RS (2013) Reduced Graphene Oxide/Copper Nanowire Hybrid Films as High-Performance Transparent Electrodes. ACS Nano 7:1811–1816

17. Zhang W, Yin Z, Chun A, Yoo J, Kim YS, Piao Y (2016) Bridging Oriented Copper Nanowire–Graphene Composites for Solution-Processable, Annealing-Free, and Air-Stable Flexible Electrodes. ACS Appl Mater Interfaces 8:1733–1741

18. Navik R, Xiao D, Gai Y, Tan H, Zhao Y (2020) One-pot synthesis of copper nanowire-graphene composite with excellent stability and electrical performance for flexible electrodes. Appl Surf Sci 527:1–8

19. Hwang S, Choi H, Shim I (1996) Copper CVD Precursors Containing Alkyl 3-Oxobutanoate Ligands. Chemistry of Materials 8:981–983

20. Choi H, Park S-H (2004) Seedless Growth of Free-Standing Copper Nanowires by Chemical Vapor Deposition. J Am Chem Soc 126:6248–6249

21. Pileni M-P (2003) The role of soft colloidal templates in controlling the size and shape of inorganic nanocrystals. Nat Mater 2:145–150

22. Hurst SJ, Payne EK, Qin L, Mirkin CA (2006) Multisegmented One-Dimensional Nanorods Prepared by Hard-Template Synthetic Methods. Angewandte Chemie International Edition 45:2672–2692

23. Jia B, Qin M, Zhang Z, Chu A, Zhang L, Liu Y, Qu X (2013) The influence of reagents on the preparation of Cu nanowires by tetradecylamine-assisted hydrothermal method. J Mater Sci 48:4073–4080

24. Li S, Chen Y, Huang L, Pan D (2014) Large-Scale Synthesis of Well-Dispersed Copper Nanowires in an Electric Pressure Cooker and Their Application in Transparent and Conductive Networks. Inorg Chem 53:4440–4444

25. Allami S (2021) ZnO nanowires growth direction and parameters affecting their surface morphology. Nanowires - Synthesis, Properties and Applications [Working Title]. https://doi.org/10.5772/intechopen.80538

26. Liu B, Zeng HC (2003) Hydrothermal Synthesis of ZnO Nanorods in the Diameter Regime of 50 nm. J Am Chem Soc 125:4430–4431

27. An G, Sun Z, Zhang Y, Ding K, Xie Y, Tao R, Zhang H, Liu Z (2011) CO_2 -Mediated Synthesis of ZnO Nanorods and Their Application in Sensing Ethanol Vapor. J Nanosci Nanotechnol 11:1252–1258

28. Saw MJ, Nguyen MT, Kunisada Y, Tokunaga T, Yonezawa T (2022) Anisotropic Growth of Copper Nanorods Mediated by Cl^- Ions. ACS Omega 7:7414–7420

29. Kang C, Yang S, Tan M, Wei C, Liu Q, Fang J, Liu G (2018) Purification of Copper Nanowires To Prepare Flexible Transparent Conductive Films with High Performance. ACS Appl Nano Mater 1:3155–3163

30. Kumar N, Kumar R, Kumar S, Chakarvarti SK (2014) Structural and electrical studies of template synthesized copper nanowires. Current Applied Physics 14:1547–1552

31. Gupta R, Kumar R (2019) Influence of low energy ion beam implantation on Cu nanowires synthesized using scaffold-based electrodeposition. Nano-Structures & Nano-Objects 18:1–11

32. Rana P, Narula C, Rani A, Chauhan RP, Gupta R, Kumar R (2017) Ion implantation effects of negative oxygen on copper nanowires. Journal of Materials Science: Materials in Electronics 28:9998–10006

33. Jiu J, Araki T, Wang J, et al (2014) Facile synthesis of very-long silver nanowires for transparent electrodes. J Mater Chem A 2:6326–6330

34. Preston C, Xu Y, Han X, Munday JN, Hu L (2013) Optical haze of transparent and conductive silver nanowire films. Nano Res 6:461–468

35. Karakassides A, Ganguly A, Kelly J, Sharma PK, Papakonstantinou P (2021) Radially Grown Graphene Nanoflakes for Tough and Strong Carbon Fiber Epoxy Composites. ACS Appl Nano Mater 4:9167–9180

36. Rasul MG, Kiziltas A, Arfaei B, Shahbazian-Yassar R (2021) 2D boron nitride nanosheets for polymer composite materials. NPJ 2D Mater Appl 5:1–18

37. Demeo D, MacNaughton S, Sonkusale S, Vandervelde T (2011) Electrodeposited Copper Oxide and Zinc Oxide Core-Shell Nanowire Photovoltaic Cells. In: Dr. Hashim A (ed) Nanowires - Implementations and Applications. InTECH, pp 141–156

38. Moon SH, Park SJ, Hwang YJ, Lee D-K, Cho Y, Kim D-W, Min BK (2015) Printable, wide band-gap chalcopyrite thin films for power generating window applications. Sci Rep 4:4408

39. Ruiz-Perona A, Guc M, Sánchez Y, Kodalle T, Merino JM, León M, Caballero R (2021) Wide band gap Cu2ZnGe(S,Se)4 thin films and solar cells: Influence of Na content and incorporation method. Solar Energy 226:251–259

40. Siebentritt S (2002) Wide gap chalcopyrites: material properties and solar cells. Thin Solid Films 403–404:1–8

41. Tauc J (1974) Optical Properties of Amorphous Semiconductors. In: Amorphous and Liquid Semiconductors, 1st ed. Plenum Press, London and New York, pp 159–220

42. Shah A v., Schade H, Vanecek M, Meier J, Vallat-Sauvain E, Wyrsch N, Kroll U, Droz C, Bailat J (2004) Thin-film silicon solar cell technology. Progress in Photovoltaics: Research and Applications 12:113–142

43. Konagai M (2011) Present Status and Future Prospects of Silicon Thin-Film Solar Cells. Jpn J Appl Phys 50:1–12

Chapter 5. Mechanical properties of CuNW/AZO-NFs and CuNW/GZO-NFs on various polymer substrates

5.1 Introduction

In this chapter the mechanical properties of the prepared bottom electrodes will be examined and compared to observe the impact of using the different components will have on the final electrode. It is an important parameter to study for many potential devices would require a transparent flexible electrode in order to use them in day-to-day life. A potential example of this could be a small transparent solar panel on a smart phone or watch device, where in the normal course of the day will come under strain and impact, be it from accidentally dropping the device or pressing down on it at the bottom of a bag. If the electrode and substrate are not robust enough the solar cell might become damaged and deformed which would result in it not working at its optimal efficiency. This would require the device to be replaced and the potential waste of valuable resources if it is not recycled efficiently negating any positive environmental impact of using the device.

In this regard, flexible solar cell devices offer the best as the cell is thinner and thus more prone to getting damaged, a flexible substrate will allow the device to take more strain and damage compared to a rigid substrate which will not withstand the applied energy as readily. Besides the mechanical robustness of the potential device other advantages of having a thin flexible device include a smaller weight (allowing for it be utilised in small portable devices), formability (allowing the device to be a shaped into whatever form it is needed to be), and potential lower cost due to the total amount of resources required to build one, being fewer [1]. Of the flexible substrates that have been studied over the years (which include metal [2] and ceramic substrates [3]) polymer substrates have shown the greatest potential. Whilst plastic polymers have poorer thermal [4] and environmental stability [5] when compared to other substrates, its excellent flexibility and optical properties are more appealing as the poor thermal stability can be worked around by only using synthesis techniques that have low

temperature methods while the layering of the device will be able to impact the environmental stability of the device.

This chapter reports on the findings of tensile strength tests for PC (1mm), PES (0.25mm), PEN (0.125mm) and PET (0.1mm) polymer substrates which have been coated with CuNWs, AZO-NFs, and GZO-NFs as potential bottom electrodes to observe what strengths they have and to compare them to find which will have the best practical usage as a protective bottom electrode. The synthesis and depositing of the various layers of the electrode have already been discussed in Chapter 4 section 4.2, experimental section.

5.2 Experimental Section

To study the tensile strength of the polymer substrates, a Deben 200N Microtester was used to gather the required data. The samples were firmly secured between two jaws of the device with the distance between them carefully measured and monitored throughout the experiment. Thereafter, a force would be applied to the film as the jaws were slowly pulled apart with a sample time of 200ms and a constant speed of 0.1mm/min to ensure consistent results as the speed the jaws are pulled apart have been recorded to impact the results [6]. The data obtained from the test is given as force and elongation as shown in Figure 5.1 below.

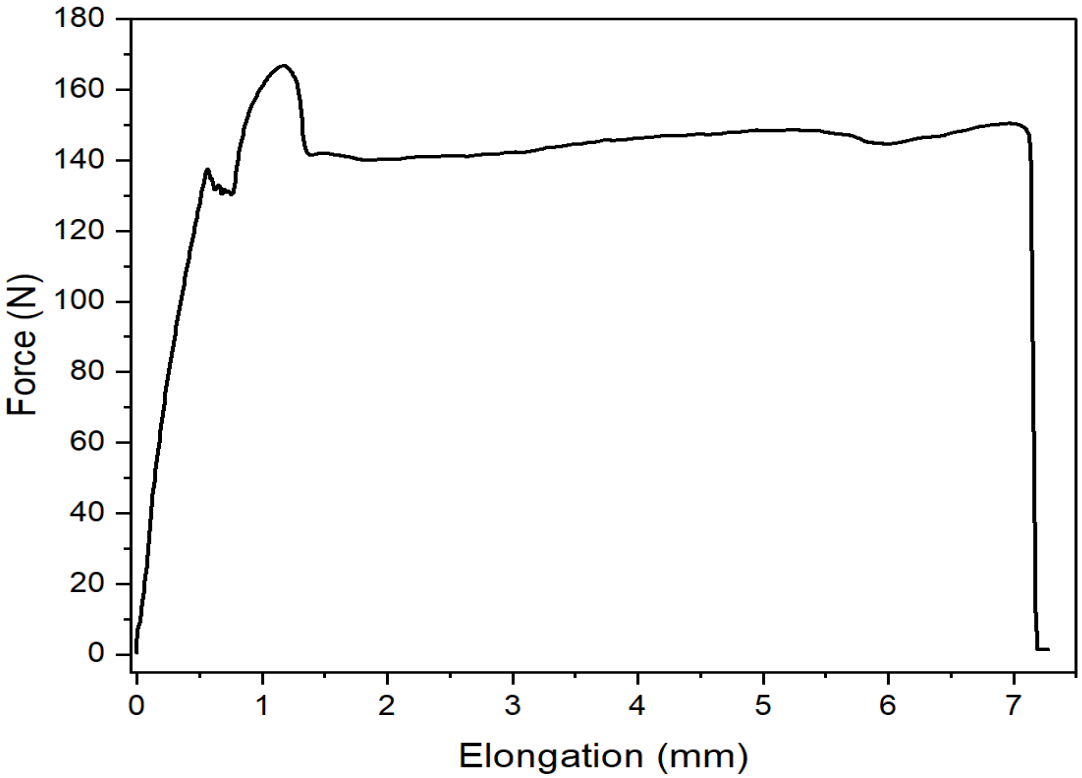

Figure 5. 1: Illustration of the Force vs Elongation graph from the polymer substrate.

In order to use this data, the points would have to be converted to stress and strain respectively. The following equations are used for these conversions [7]:

$$\sigma = \frac{F}{A} \qquad (5.1)$$

$$\varepsilon = \frac{\Delta L}{L_i} \qquad (5.2)$$

In equation 5.1, σ denotes the stress of the sample (MPa), *F* is the measured force (N), and *A* is the cross-sectional area of the sample (mm^2) and in equation 5.2, ε denotes the strain of the sample, ΔL is the elongation of the sample (mm), and L_i is the initial length of the sample (mm). Using these equations, Figure 5.2 can be produced which has been labelled with some of the corresponding parameters that can be found and studied from this gathered data. From this graph the yield strength, ultimate strength, and fracture strength can all be found and studied [8]. The yield strength is an important aspect to study as it is an indication of how much energy the substrate can withstand before it becomes deformed permanently. The substrate behaves elastically to any stress smaller than the yield strength applied to it and does not change the substrate in anyway as the substrate can revert to its original form. However, after the yield strength is reached the substrate behaves as a plastic and

does not revert to its original state though it is not completely damaged [9]. From this it can be reasoned that a substrate with a larger yield strength is more ideal as it can experience a larger amount of force before its structure changes and the device is partially damaged. If the yield strength could not be determined by studying the graph, it could also be found using the 0.2% offset yield strength where the offset would be plotted with the original graph, and where the two intercept, would be the yield strength [10].

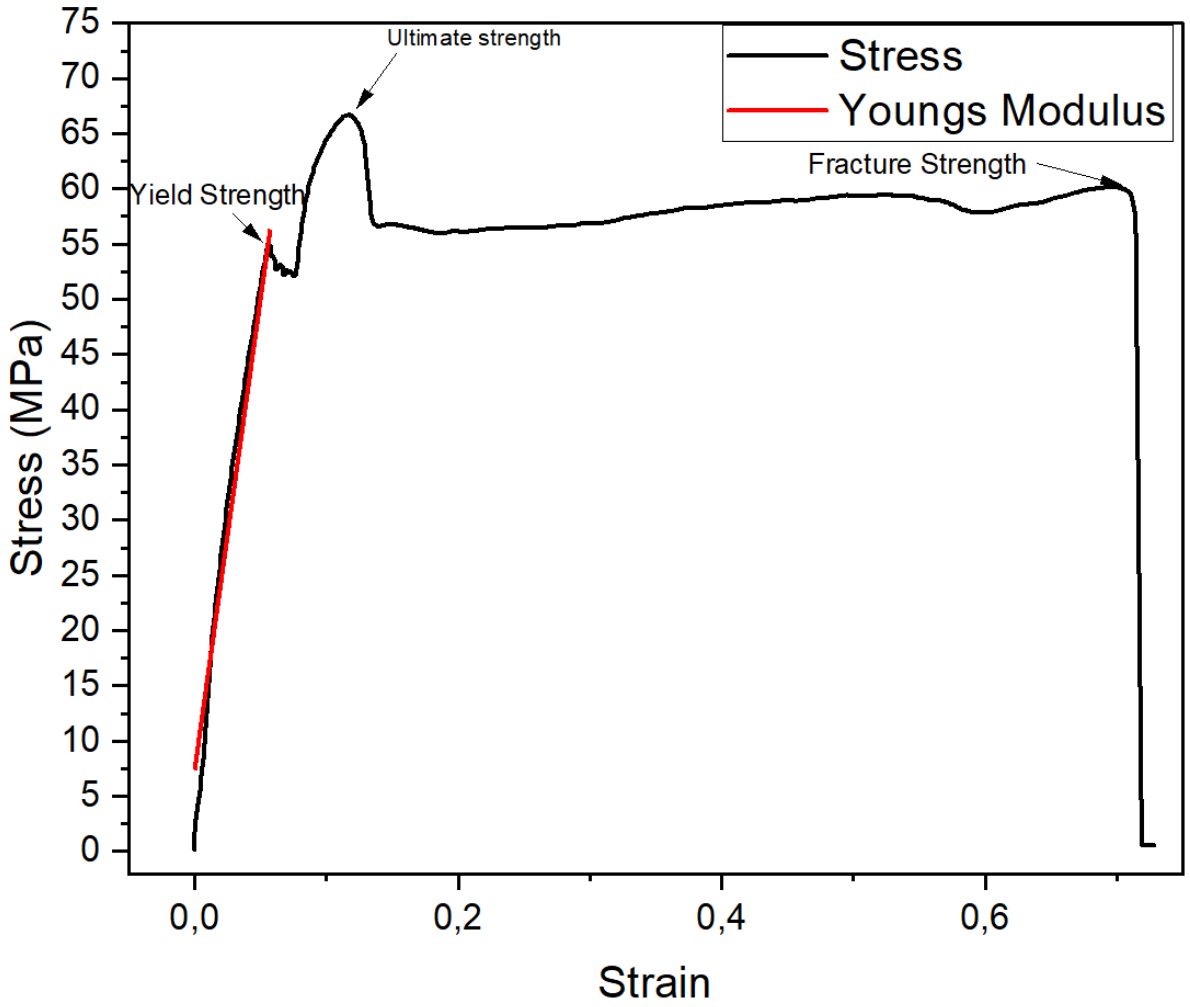

Figure 5. 2: Illustration of the Stress-Strain graph from the polymer substrate

The offset can be found using the following equations:

$$Offset\ Stress = \sigma \times Youngs\ Modulus \quad (5.3)$$

$$Offset\ Strain = \varepsilon \times Youngs\ Modulus \quad (5.4)$$

The ultimate strength is the maximum stress the substrate can withstand before it goes through a process called necking or potentially immediately breaks. During this necking phase the substrate becomes weaker and can withstand less stress before it

breaks. Thus, it is important to know the ultimate strength, as after this point the substrate will no longer be viable. The fracture strength is the final strength the substrate can withstand in the necking phase. Another important property that can also be identified from the graph is the Young's Modulus of the sample. The Young's Modulus is an indication of how stiff a material is, with larger values tending to be less elastic and observed to be stiffer [11]. This can be found by fitting a linear line on the graph before the yield strength. This can be determined also with equation 5.5 as follows:

$$Youngs\ Modulus = \frac{\Delta\sigma}{\Delta\varepsilon} \qquad (5.5)$$

Other potential measurements of interest include the modulus of resilience and the strain hardening ratio. The modulus of resilience is the total energy a material can absorb and still return to its original shape and form [12]. For the application in a solar cell device, it would be the maximum energy the protective substrate will be able to withstand before it starts to become damaged and deteriorates. It can be found as the total area under the stress-strain graph up until the yield strength. The strain hardening exponent *(n)* is an indication how the material will behave when it is being formed and deformed [13]. Materials with high values of *n* can undergo plastic hardening and are less brittle, with values closer to zero can experience microcracks when under high plastic deformation. Materials with large *n* values also possess better formability compared to materials with lower values. The formability of a material is an important aspect to know as it is the degree that a material can be deformed without resulting in any undesirable conditions (such as necking and cracking). This can be found by using the logarithmic graphs of the true stress-strain graph and finding the slope between the yield and ultimate strength. The true stress and strain equations are given by the following equations [14]:

$$\sigma_T = \sigma(1 + \varepsilon) \qquad (5.6)$$

$$\varepsilon_T = \ln(1 + \varepsilon) \qquad (5.7)$$

After the material undergoes strain hardening, it will then begin to start necking. Necking is the last phase a ductile material undergoing tensile testing will go through, as brittle materials will break before reaching this point (Figure 5.3(a) and (c) had limited necking). Up until this point the material will have deformed more uniformly along the gage length. After reaching the ultimate tensile strength however the

deformation of the material will be concentrated to one region which results in the width of the sample to decrease more than other regions on the sample and results in an hourglass shape [15], which can be clearly observed in Figure 5.3 (b) for PES substrate.

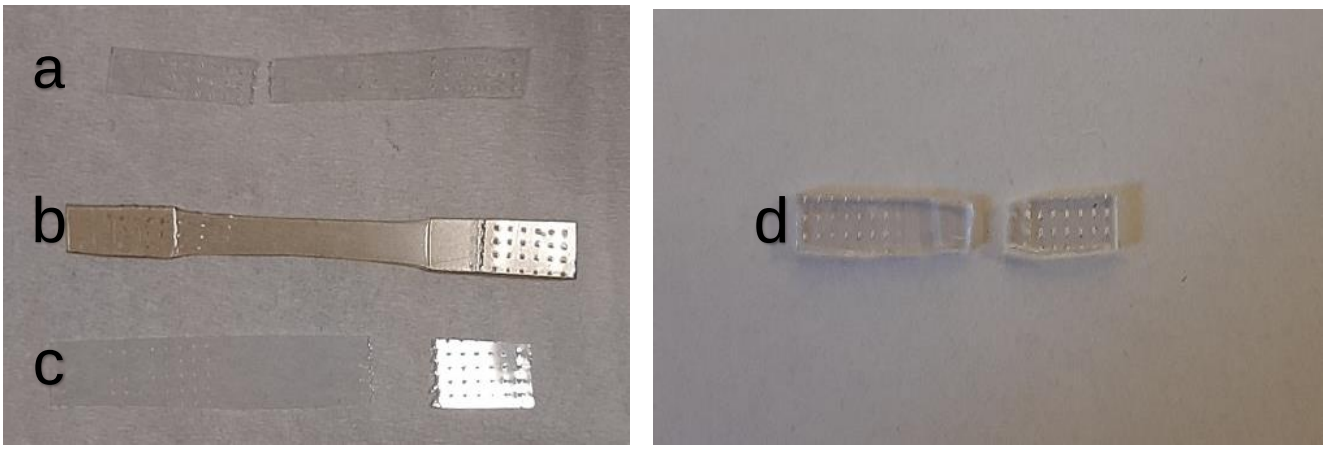

Figure 5. 3: Polymer substrates after stretched in the tensile tester (a) PET, (b) PES, (c) PEN and, (d) PC

5.3 Results and discussion.

5.3.1 Yield strength analysis

From studying Figures 5.4 to 5.7, it can be seen that for most of the samples using PET, PEN and, PES the initial peak that indicates the yield strength in the example Figure of 5.3 is absent. This behaviour is an indication that these substrates are not as ductile as the PC substrate, and are instead stronger materials which are more brittle in comparison. This means to find the yield strength for these substrates, equation 5.3 and 5.4 would be needed and an additional plot made.

Table 5.1 summarizes the measured yield strength values from various films deposited on polymer substrates. As can be observed from the first row of the data in the table, the bare PET substrate seems to offer the best yield strength which is an indication that potentially PET will be the ideal substrate to choose from. As can be seen from the data, the inclusion of the CuNWs improves the strength of the material which is linked to the CuNW network that covers the entire substrate and thus adding to its

strength and improving the elasticity of the substrate. This allows the substrate to be able to absorb more energy before it starts to deform. This however, needs to be properly monitored because if the CuNWs network of the film starts to break before the substrate does, the conductivity of the film would be severely impacted, with the solar cell becoming non-functional in this case.

The coating of the AZO- and GZO-NFs substantially improves all of the films potential yield strength they are able to maintain and thus the films are better able to protect the CuNWs as it would be the polymer and NFs layers that are taking the brunt of the applied stress. The improvement with the NFs layers could be attributed to their structure and distribution. As was observed in the SEM images discussed in chapter 4, the NFs were evenly distributed over the films and clearly observed to be layered on top of one another. This layer has been observed in other NFs materials and also been observed to improve the tensile strength of those materials [16, 17]. Due to the flakes large surface areas that can lay against one another. When compared to the CuNWs, these layers of flakes cause the overall deposited layer to be more adhesive to the film and more evenly share and distribute any stress applied to it. This makes the films stronger and offering the CuNWs layer more protection. With the CuNWs layered between the substrate and the NFs layers the previous adhesion problem that has been observed in other bottom electrodes has potentially been resolved here as they are firmly secured to the substrate.

Another key observation is that the AZO-NFs performed better than the GZO-NFs in regard to the yield strength. This could be linked to the difference in crystallite sizes between the NFs which has been linked to impact the strain hardening properties of a film which in turn impacts the yield strength [18]. This indicates that the AZO-NFs will offer the CuNWs better protection against any force applied to the device.

Table 5. 1: Yield Strength (MPa) of the polymer substrates and the coated electrodes.

	PC	PET	PES	PEN
Bare	25.710	68.866	38.848	46.182
CuNW	25.204	71.715	41.016	54.032
CuNW/AZO-NFs	55.0468	75.253	54.006	78.814
CuNW/GZO-NFs	51.5336	71.958	46.163	74.041

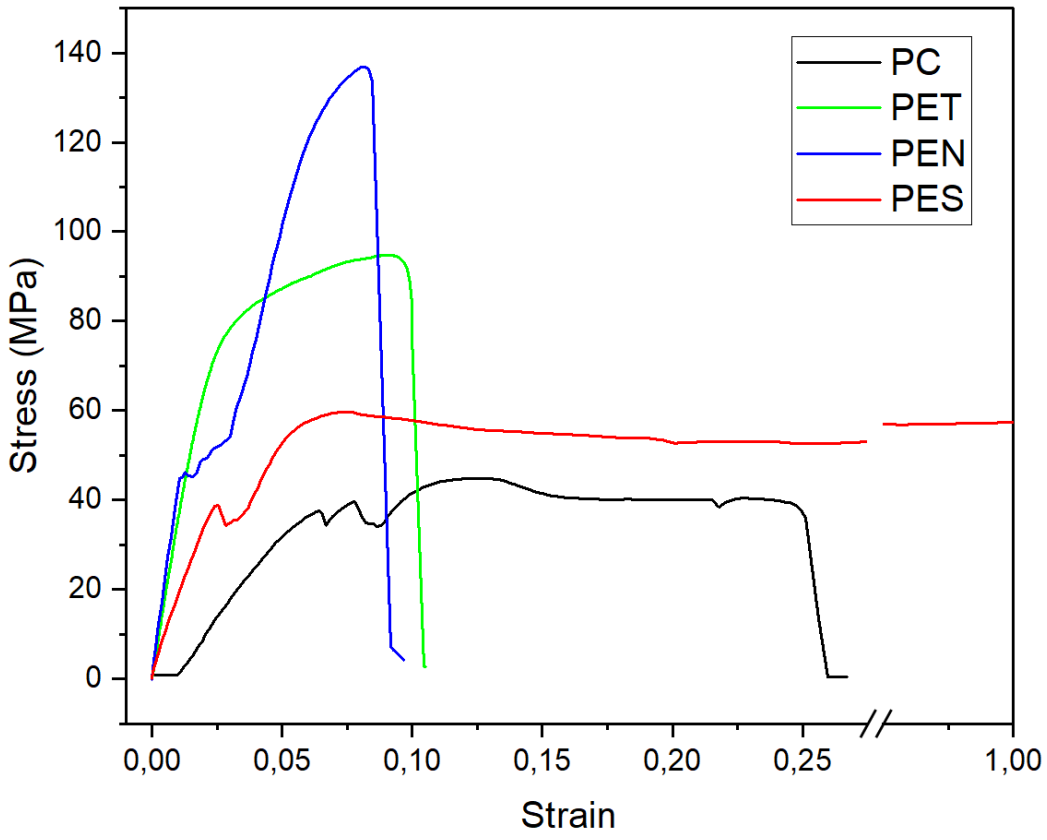

Figure 5. 4: Stress-Strain graph comparing the bare polymer substrates.

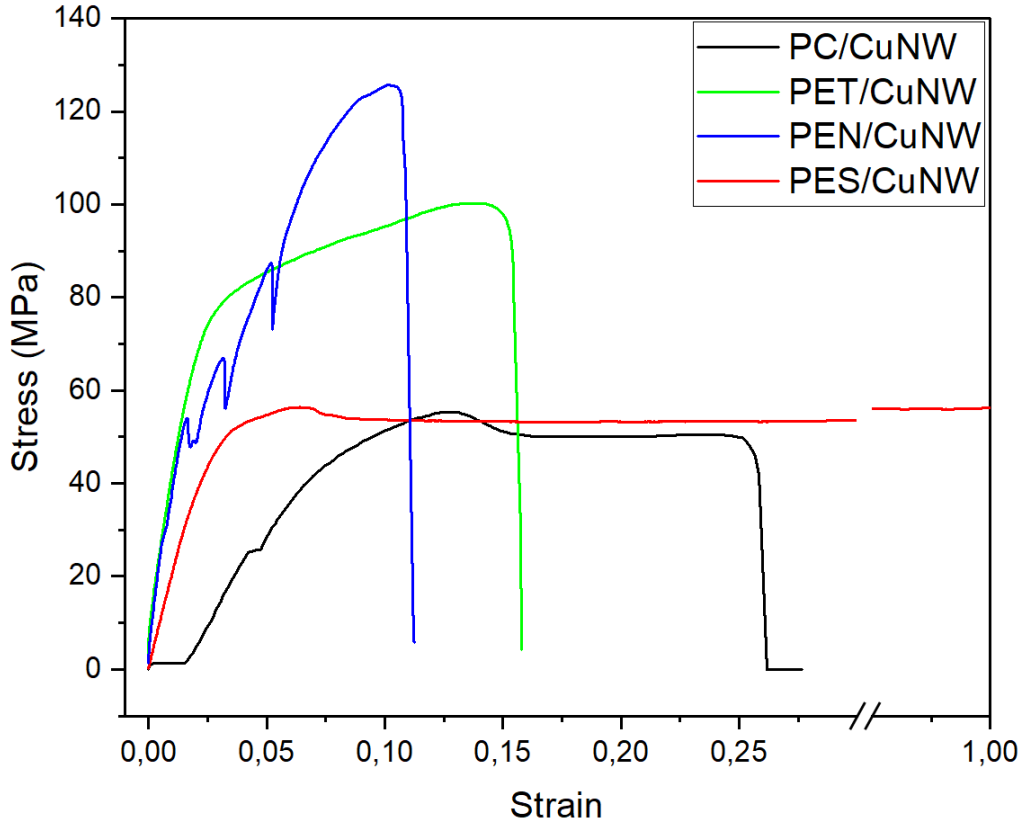

Figure 5. 5: Stress-Strain graph comparing the films of CuNWs on polymer substrates.

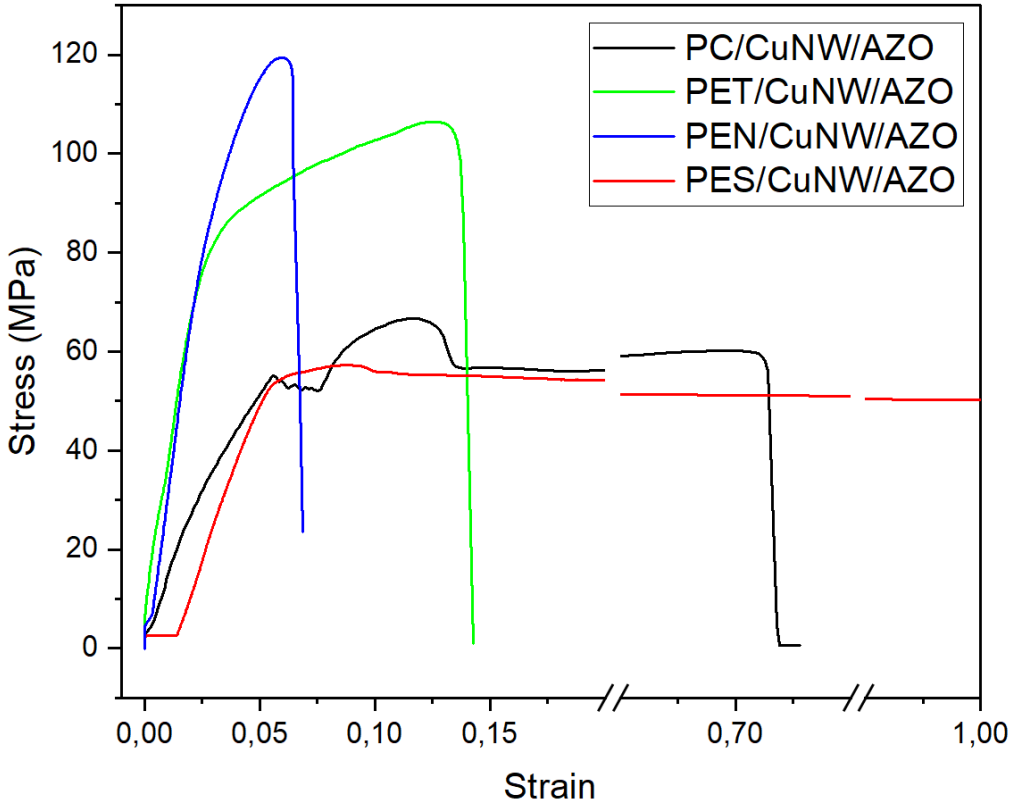

Figure 5. 6: Stress-Strain graph comparing the films of CuNW and AZO-NFs on polymer substrates.

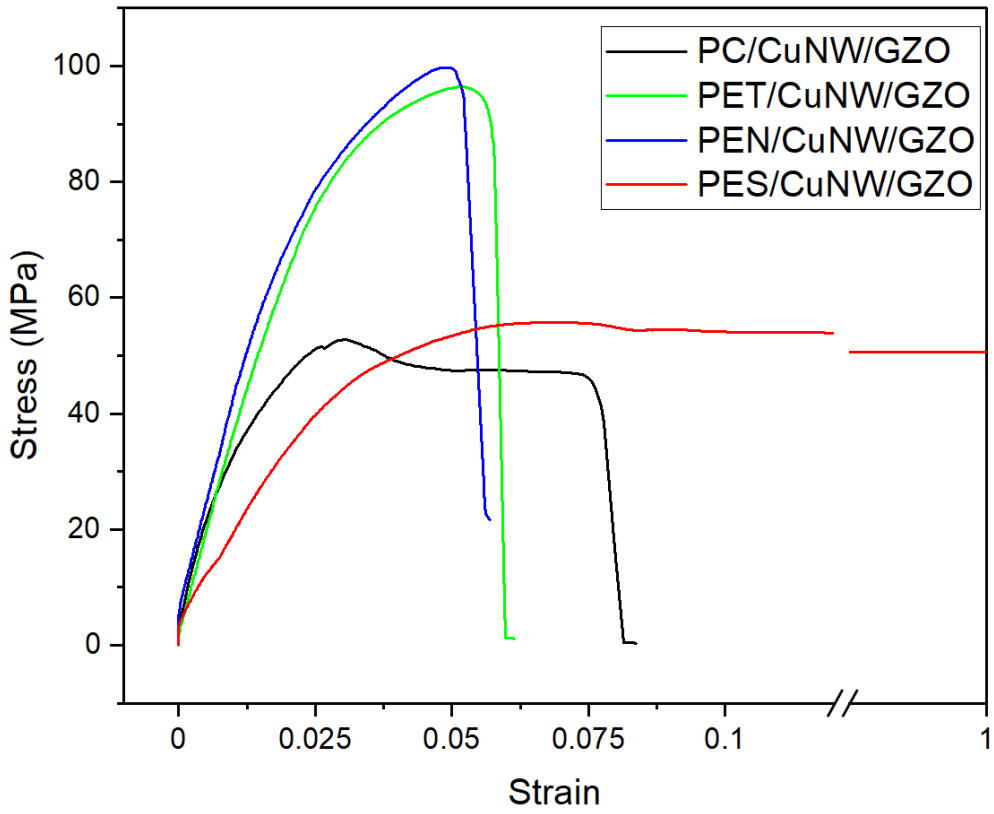

Figure 5. 7: Stress-Strain graph comparing the films of CuNW and GZO-NFs on polymer substrates.

5.3.2 Ultimate strength analysis

The values of the ultimate strength for the various polymer substrates and the coatings used with them are noted (Table 5.2). As the yield strength and ultimate strength are different for all of these values it is an indication that none of the materials were brittle and all managed to yield which is necessary characteristic for flexible solar cells.

As previously stated, the ultimate strength is the maximum stress the film is able to withstand before it undergoes necking which deteriorates the quality of the film and no longer strengthens it (as the strain hardening process does). Ideally, the solar cell would never reach the ultimate strength of the substrate or be required to withstand the applied stress within the strain hardening region. However, as not all situations can be avoided or safeguarded against, for the purpose of this study the ultimate strength will behave as a safety net for the potential device preventing it from breaking in such a manner that the other parts of it would leak out. This is especially important as certain layers of solar cell devices contain toxic components (such as the lead in

perovskite) that if it comes into contact with water and leaks out, it could do damage to both the environment and to any person that come into contact with it.

As can be observed in Table 5.2, the PET and PEN polymer substrates have the higher ultimate strength values with PEN having the better value between them. While both PES and PC also have larger ultimate strength values compared to their yield strength, their values are not substantially improved and thus the 'safety net' they provide for the electrode and potential solar cell device is diminished and not of much value. Once more, the addition of the CuNWs improves most of the ultimate strength values, the only one that isn't completely improved being the PES film. The ultimate strength value of the PES reduces as additional layers are added as it was already very ductile and plastic. The additional layering of materials diminishes the high ductility making the film behave more as a plastic. A similar phenomenon can be observed with the PEN films which are also more ductile than the PC and PET (though less so than the PES film). With the addition of the AZO- and GZO-NFs the ultimate strength is reduced as it behaves more plastically. This can be potentially linked to the thickness of the NFs layer, which is substantially thicker than the CuNWs layer, which would then impair the overall ductility of the film.

Once more, the AZO-NFs performed better than the GZO-NFs which can be corroborated to the different crystallite sizes of the two NFs layers and potentially the aluminium doping provides a stronger bond resulting in a greater ultimate strength before the film begins to undergo necking.

Table 5. 2: Ultimate Strength (MPa) of the polymer substrates and the coated electrodes.

	PC	**PET**	**PES**	**PEN**
Bare	44.839	94.772	59.869	136.887
CuNW	55.421	100.258	56.636	146.764
CuNW/AZO-NFs	66.696	106.460	57.276	119.411
CuNW/GZO-NFs	52.728	96.375	55.737	99.730

5.3.3 Strain hardening and necking analysis

The strain hardening of a material can be observed to be how much stress is required to continue to deform the material, while the material itself becomes more difficult to deform. As previously stated, strain hardening occurs between the yield strength and the ultimate strength. During this phase the material can no longer revert to its original shape and form and is instead permanently deformed. However, while continuing to undergo stress in this phase the material will instead be strengthened and have an increase of resistance. This means that the material will be able to withstand a greater force applied to it, however, it will be less ductile and thus less flexible potentially to the detriment of whatever application it was currently being used for. The strain hardening value can be studied in turn, using the strain hardening exponent.

As it was previously stated the strain hardening exponent determines how formable a material is and whether it will be brittle or not when placed under strain. Both PET and PEN behaved the least ductile of the materials, as they reached their ultimate strength and then proceeded to fracture which can be observed in the figures 5.4 to 5.7. This is supported by the strain hardening exponent values which have these two polymer substrates on the lower end of the values, which indicates that they will be brittle. From these values it can also then be noted that the PC and the PES substrates will have the best formability. This means that PC and PES can be deformed into a desirable shape for a specific product without becoming completely damaged.

Table 5. 3: Strain hardening exponent of the polymer substrates and the coated electrodes.

	PC	**PET**	**PES**	**PEN**
Bare	0.784	0.224	0.587	0.450
CuNW	0.798	0.239	0.780	0.597
CuNW/AZO-NFs	0.624	0.249	1.270	0.631
CuNW/GZO-NFs	0.389	0.244	0.754	0.406

After the material has undergone strain hardening, it will further undergo a process called necking. Both the PET and PEN failed to reach this point as they both fractured soon after reaching the ultimate tensile strength indicating that while the materials were strong, they were considerably more brittle. While the PC substrate did eventually fracture after a time the PES substrate was unable to reach its fracture point with the equipment on hand as the tensile tester could only extend the films from 10 mm to 20 mm. Should the tensile tester that was used for the measurements been able to extend further the fracture point would have been found at some point though for the purposes of this study it is sufficient to know that the necking phase of the PES was the greatest among the polymer substrates.

5.3.3 Young's modulus and resilience analysis

The Young's Modulus is an important parameter to know for materials as it is an indication of its strength and how the material will behave in potentially different loads. As can be seen from the data in Table 5.4, the addition of the CuNWs and the NFs generally increases the value which indicates an increase of the overall strength of the film which further supports the previous analysis with the yield and ultimate strength which came to a similar conclusion. Furthermore, the Young's Modulus is also an indication of how ductile a material will be with a lower value behaving more ductile while a larger one is more brittle. From this both the PC and PES would be expected to be more ductile which was observed to be the case and also corroborated with the strain hardening exponent values.

Table 5. 4: Young's modulus (MPa) of the polymer substrates and the coated electrodes

	PC	**PET**	**PES**	**PEN**
Bare	706.020	3392.414	1534.150	4170.637
CuNW	915.451	3335.548	1979.307	4147.937
CuNW/AZO-NFs	956.337	3586.366	1427.851	4148.278
CuNW/GZO-NFs	713.892	3392.525	1500.029	3612.465

Another parameter that can be looked at within the initial range is the resilience of the films. As stated previously the resilience of a material is the total energy a material can absorb and still return to its original shape without any deformations. The greater this value is the more resilient it is and thus the more energy it can safely absorb and be able to return to its original shape and form. This is important for application in small flexible devices as while the deformation of the film has limited impact on the structure and stability of the film, it could still result in other components of the device becoming irreversibly damaged. Thus, the ability for the outer film to be able to absorb and withstand taking a direct impact to it is an important feature for future developments.

From Table 5.5, the data of the resilience of the polymer substrates is observed and the addition of the CuNWs and AZO-NFs result in an improved resilience for the films. This indicates that the CuNWs network that is evenly distributed across the films strengthens the properties of the films. As was observed in the SEM images, the CuNWs were ultralong which better linked and interconnected the network which gives it improved strength. With the AZO-NFs the improvements come from the previously mentioned layering that is observed with the nanoflakes which are distributed across the film which further demonstrates the potential protective properties the AZO-NFs layer provides. It is only the GZO-NFs layer that does not improve, or in some cases not as substantially as the AZO-NFs were seen to. These results show that the GZO-NFs are not as well suited to protect the CuNWs, as they absorb less energy than the AZO-NFs.

Table 5. 5: Resilience (J/mm^3) of the polymer substrates and the coated electrodes

	PC	**PET**	**PES**	**PEN**
Bare	0.478	0.849	0.569	0.365
CuNW	0.498	1.050	0.530	0.556
CuNW/AZO-NFs	1.800	1.059	1.399	0.762
CuNW/GZO-NFs	0.891	0.825	0.909	0.995

5.4 Conclusion

The tensile strength properties of different polymer-based substrates bottom electrodes were investigated and compared to one another. Furthermore, the addition of CuNWs, AZO and GZO-NFs layers onto the substrate were investigated to analyse what impact they would have on the mechanical properties. From this data it can be observed that a PET based substrate would be the optimal choice for a flexible transparent substrate as it has the better values for the yield strength, Young's Modulus and, resilience for the prepared electrodes. Additionally, for the substrate that requires better formability (i.e., for the transparent electrode to be in a specific shape that isn't flat or slightly curved) the PES substrate offered the better formability while still having some protection for the CuNWs. Of the two nanoflake protective layers that were examined, AZO-NFs showed a clear advantage to GZO-NFs with the best results in all of the various aspects of the film ranging from the protective capabilities of the layer to the formability of the substrate.

References

1. Hu X, Li F, Song Y (2019) Wearable Power Source: A Newfangled Feasibility for Perovskite Photovoltaics. ACS Energy Lett 4:1065–1072
2. Wang X, Li Z, Xu W, Kulkarni SA, Batabyal SK, Zhang S, Cao A, Wong LH (2015) TiO2 nanotube arrays based flexible perovskite solar cells with transparent carbon nanotube electrode. Nano Energy 11:728–735
3. Dou B, Miller EM, Christians JA, et al (2017) High-Performance Flexible Perovskite Solar Cells on Ultrathin Glass: Implications of the TCO. J Phys Chem Lett 8:4960–4966
4. Huang J-M, Chu PP, Chang F-C (2000) Conformational changes and molecular motion of poly(ethylene terephthalate) annealed above glass transition temperature. Polymer (Guildf) 41:1741–1748
5. Venkatachalam S, G. S, V. J, R. P, Rao K, K. A (2012) Degradation and Recyclability of Poly (Ethylene Terephthalate). In: Polyester. InTech, pp 75–98
6. Singer R, Ollick AM, Elhadary M (2021) Effect of cross-head speed and temperature on the mechanical properties of polypropylene and glass fiber reinforced polypropylene pipes. Alexandria Engineering Journal 60:4947–4960
7. Kumar P, Mahanty M, Chattopadhyay A (2019) An Overview of Stress-Strain Analysis for Elasticity Equations. In: Elasticity of Materials - Basic Principles and Design of Structures. IntechOpen, pp 11–30
8. Dupen B (2016) Stress and Strain. In: Applied Strength of Materials for Engineering Technology, 10th ed. Purdue University, pp 17–22
9. Balani K, Verma V, Agarwal A, Narayan R (2015) Physical, Thermal, and Mechanical Properties of Polymers. In: Biosurfaces: A Materials Science and Engineering Perspective. Wiley: Hoboken, New Jersey, pp 329–344
10. Cahoon JR, Broughton WH, Kutzak AR (1971) The determination of yield strength from hardness measurements. Metallurgical Transactions 2:1979–1983
11. Alasfar RH, Ahzi S, Barth N, Kochkodan V, Khraisheh M, Koç M (2022) A Review on the Modeling of the Elastic Modulus and Yield Stress of Polymers and Polymer Nanocomposites: Effect of Temperature, Loading Rate and Porosity. Polymers (Basel) 14:1–31
12. Lin C-Y, Kang J-H (2021) Mechanical Properties of Compact Bone Defined by the Stress-Strain Curve Measured Using Uniaxial Tensile Test: A Concise Review and Practical Guide. Materials 14:1–16
13. Pintaude G (2022) Hardness as an indicator of material strength: a critical review. Critical Reviews in Solid State and Materials Sciences 1–19
14. Joun M, Choi I, Eom J, Lee M (2007) Finite element analysis of tensile testing with emphasis on necking. Comput Mater Sci 41:63–69

15. Muhammad S, Jar P-YB (2013) Determining stress–strain relationship for necking in polymers based on macro deformation behavior. Finite Elements in Analysis and Design 70–71:36–43

16. Rasul MG, Kiziltas A, Arfaei B, Shahbazian-Yassar R (2021) 2D boron nitride nanosheets for polymer composite materials. NPJ 2D Mater Appl 5:1–18

17. Karakassides A, Ganguly A, Kelly J, Sharma PK, Papakonstantinou P (2021) Radially Grown Graphene Nanoflakes for Tough and Strong Carbon Fiber Epoxy Composites. ACS Appl Nano Mater 4:9167–9180

18. Yasnikov IS, Kaneko Y, Uchida M, Vinogradov A (2022) The grain size effect on strain hardening and necking instability revisited from the dislocation density evolution approach. Materials Science and Engineering: A 831:1–12

Chapter 6. Summary and Conclusion of the study

This chapter summarizes and concludes the results of this study. In this study, the synthesis of smooth long CuNWs by hydrothermal method for deposition on polymer substrates was successful. The CuNWs were then deposited on PC, PET, PES and PEN polymer substrates for possible application in thin transparent flexible electrodes for the potential use and fabrication of solar cells. Additionally, AZO and GZO-NFs were also synthesized to be used as a protection layer for the CuNWs against oxidation, as well as to improve other properties of the films. The study was completed with these main objectives in mind: (i) compare the transmittance and tensile strength of the polymer substrates, (ii) compare the protective capabilities of the NFs layer, (iii) study the effects of the various layers and their potential impact on future solar cells device performance. Ultimately the structural, morphological, optical, and mechanical properties of the films were analysed and discussed in the structured chapters.

6.1 Summary

6.1.1 Hydrothermal synthesis of CuNWs, AZO-, and GZO-NFs: Potential properties for usage as the bottom electrode for solar cells

Smooth ultra-long CuNWs were successfully synthesized using the hydrothermal method and using ODA as the capping agent. Both AZO and GZO-NFs were also synthesized in order to be used as a protective layer against oxidation over the CuNWs. These were then deposited onto various polymer substrates and then analysed using different techniques. The XRD results were able to both confirm and identify the used polymer substrates, as well as confirming that pure CuNWs were produced and that they were made out of (111) cubic structures. Both the AZO and GZO-NFs structures were unable to be identified using XRD which was linked to the broad and very intense polymer peaks that were observed. The synthesized materials had various crystallite sizes with CuNWs being 24.51 nm, AZO-NFs being 11.08 nm and, GZO-NFs being 10.19 nm which were found to have an impact on the tensile strength of the films. From the SEM images, ultra-long and thin CuNWs were observed and a well distributed layer of nanoflakes were found for both the AZO and GZO NFs films. This

layering will be ideal for protecting the CuNWs both from oxidation and potentially improve the tensile strength of the film. The UV-VIS scans demonstrated that the PET substrate had the best transmittance (88.64%) over the widest range (380-800 nm) as well as the widest bandgap which is optimal for transparent flexible solar cells. It was also observed that AZO-NFs had a better transmittance on all films than GZO-NFs which is attributed to the different dopants that were used as well as the crystallite sizes. Finally, the AFM results showed that the additional layering of the nanoflakes increases the roughness of the films which could be beneficial for light trapping should the electrodes be used in solar cell devices.

6.1.2 Mechanical properties of CuNW/AZO-NFs and CuNW/GZO-NFs on various polymer substrates

The tensile properties of the different polymer-based substrates for bottom electrodes in solar cells were investigated and compared to one another with the different layered electrodes. The additional layering of the CuNWs as well as the protective nanoflakes layer was found to improve the yield strength, ultimate strength, as well as the Young's modulus which all play vital roles in the mechanical integrity of the films though with AZO-NFs showing the best improvement across all substrates compared to the GZO-NF layer. This indicates that AZO-NFs have the best potential to be able to protect the CuNW layer.

Of the polymer substrates used, both the PET and the PEN showed the best results with having the best yield and ultimate strength. This indicates that the two polymers will be able to withstand being placed under the greater amounts of force before deforming and beginning to damage the CuNWs as well as the rest of the solar cell device.

6.2 Conclusion and Future work

This research project successfully managed to synthesize CuNWs which are ideal for usage with solar cells as well as protective layers of doped ZnO nanoflakes for possible application as bottom electrodes in transparent flexible solar cells. Even though there are other alternatives to CuNWs as the main component of the electrode,

metal nanowires as a whole offer a unique potential usage. This is due to them having a limited impact on the transmittance of the substrate while improving other properties such as the roughness for better light trapping and potential conductivity as the metals used for metal nanowires are all very conductive. The usage of metal nanowires also offers the potential usage for flexible devices which is important as it allows the technology developed to be more widely implemented and used in different aspects. Furthermore, the flexibility of a device also improves the potential protective capabilities of a device allowing the substrate to absorb more of the impact.

From this work, it is possible to see that the PET and PEN polymer substrates offered the potential uses as transparent flexible substrate as both substrates possess excellent transmittance even when they have been coated with a thin layer of CuNWs and doped ZnO nanoflakes. The implementation of nanoflakes also opens additional avenues and potential for the electrodes as the nanoflakes layering increases the roughness of the film which increases the light trapping capabilities of the thin film which is ideal for solar cell-based devices. Additionally, the layering also has the beneficial impact of improving the tensile strength of the films making them more robust and resilient to external forces that would be applied to them and potentially damage other parts of the cell. This would allow the solar cell that was made with this protective layer to be implemented in various ways.

Part of this work was also featured in a local conference South African institute of Physics (SAIP) where the given presentation won an award in the submitted category of Physics of Condensed Matter and Materials. This work has since been accepted to be published as part of the conference's journals. A second paper is in the final stages of preparation to be submitted to another journal within due course.

For future work, fabrication of a perovskite-based solar cell and/or organic-based solar cells to test the performance of the device could be studied if the addition of the CuNWs and NFs are beneficial to the final solar cell device. Further protection for the perovskite will also be considered with an entrapment layer of hydroxyapatite. Graphene could also be potentially examined and used in the place of the AZO-NFs layer as it has previously been found to have excellent conductive properties making it ideal for the bottom electrode. Lastly, long term tests should be considered to test - the viability of using such a device to generate solar power.